AD-A188 390 RESEARCH AND DEVELOPMENT TO ACQUIRE AND REDUCE MELTING LAYER CLOUD PHYSIC..(U) COLORADO INTERNATIONAL CORP BOULDER L G DAVIS ET AL. MAY 87 AFGL-TR-87-0161 1/1

UNCLASSIFIED F19628-86-C-0009 F/G 4/2 NL

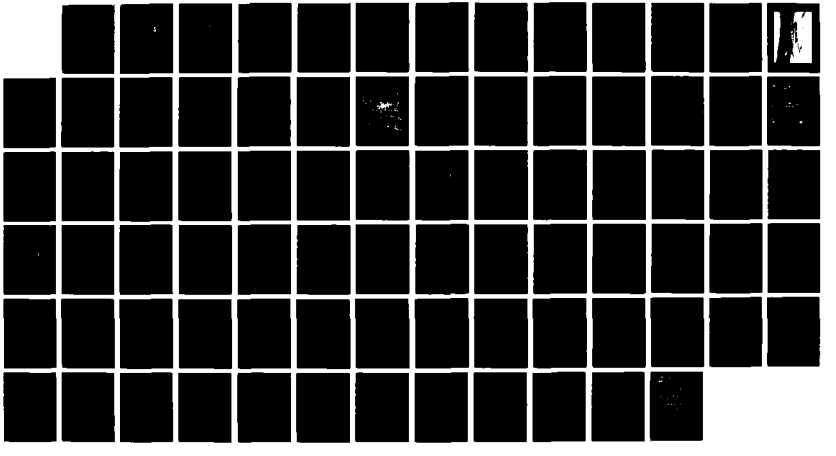

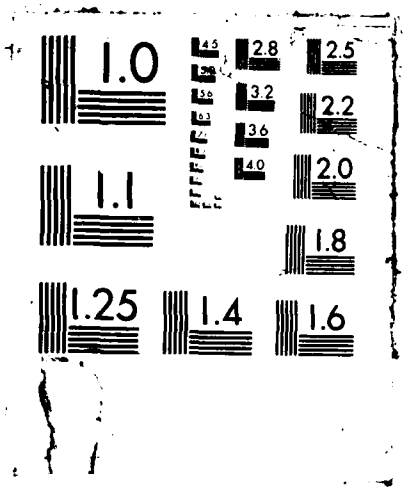
1.0
1.1
1.25
1.4
1.6
1.8
2.0
2.2
2.5
2.8
3.2
3.6
4.0
4.5

AFGL-TR-87-0161

# Research and Development to Acquire and Reduce Melting Layer Cloud Physics and Evaluate a Prototype M-Meter



Larry G. Davis
R. Paul Lawson

Colorado International Corporation
Boulder Municipal Airport
P.O. Box 3007
Boulder, CO 80307



MAY 1987

FINAL REPORT
December 1985 - May 1987

Approved for Public Release; Distribution Unlimited

AIR FORCE GEOPHYSICS LABORATORY
AIR FORCE SYSTEMS COMMAND
UNITED STATES AIR FORCE
HANSCOM AIR FORCE BASE, MASSACHUSETTS 01731-5000

"This technical report has been reviewed and is approved for publication"

Morton Glass
MORTON GLASS
Contract Manager

Arnold A. Barnes Jr.
ARNOLD A. BARNES, JR., Chief
Cloud Physics Branch

FOR THE COMMANDER

Robert A. McClatchey
ROBERT A. McCLATCHEY, Director
Atmospheric Sciences Division

This report has been reviewed by the ESD Public Affairs Office (PA) and is releasable to the National Technical Information Service (NTIS).

Qualified requestors may obtain additional copies from the Defense Technical Information Center. All others should apply to the National Technical Information Service.

If your address has changed, or if you wish to be removed from the mailing list, or if the addressee is no longer employed by your organization, please notify AFGL/DAA/LYC, Hanscom AFB, MA 01731-5000. This will assist us in maintaining a current mailing list.

Do not return copies of this report unless contractual obligations or notices on a specific document requires that it be returned.

Unclassified
SECURITY CLASSIFICATION OF THIS PAGE

AD-A188390

# REPORT DOCUMENTATION PAGE

| | |
|---|---|
| 1a. REPORT SECURITY CLASSIFICATION<br>Unclassified | 1b. RESTRICTIVE MARKINGS |
| 2a. SECURITY CLASSIFICATION AUTHORITY | 3. DISTRIBUTION/AVAILABILITY OF REPORT<br>Approved for public release<br>Distribution unlimited |
| 2b. DECLASSIFICATION/DOWNGRADING SCHEDULE | |
| 4. PERFORMING ORGANIZATION REPORT NUMBER(S) | 5. MONITORING ORGANIZATION REPORT NUMBER(S)<br>AFGL-TR-87-0161 |
| 6a. NAME OF PERFORMING ORGANIZATION<br>Colorado International Corp<br>6b. OFFICE SYMBOL (If applicable) | 7a. NAME OF MONITORING ORGANIZATION<br>Air Force Geophysics Laboratory |
| 6c. ADDRESS (City, State, and ZIP Code)<br>Boulder Municipal Airport<br>P.O. Box 3007<br>Boulder, CO 80307 | 7b. ADDRESS (City, State, and ZIP Code)<br>Hanscom AFB, AFGL/LYC<br>Massachusetts 01731-5000 |
| 8a. NAME OF FUNDING/SPONSORING ORGANIZATION<br>8b. OFFICE SYMBOL (If applicable) | 9. PROCUREMENT INSTRUMENT IDENTIFICATION NUMBER<br>F19628-86-C-0009 |
| 8c. ADDRESS (City, State, and ZIP Code) | 10. SOURCE OF FUNDING NUMBERS |

| PROGRAM ELEMENT NO. | PROJECT NO. | TASK NO. | WORK UNIT ACCESSION NO. |
|---|---|---|---|
| 62101F | 6670 | 12 | AE |

11. TITLE (Include Security Classification) Research and Development to Acquire and Reduce Melting Layer Cloud Physics and Evaluate a Prototype M-Meter

12. PERSONAL AUTHOR(S)
Larry G. Davis, R. Paul Lawson

| 13a. TYPE OF REPORT | 13b. TIME COVERED | 14. DATE OF REPORT (Year, Month, Day) | 15. PAGE COUNT |
|---|---|---|---|
| FINAL REPORT | FROM Dec 1985 TO May 1987 | 1987 May | 78 |

16. SUPPLEMENTARY NOTATION

| 17. COSATI CODES | | | 18. SUBJECT TERMS (Continue on reverse if necessary and identify by block number) |
|---|---|---|---|
| FIELD | GROUP | SUB-GROUP | Cloud Physics; Melting Layer; Microwave Attenuation; Brightband; Airborne Radar; Ka-band Radar; Aggregation; Precipitation; Airborne Instrumentation. |
| | | | |
| | | | |

19. ABSTRACT (Continue on reverse if necessary and identify by block number)

A Beech Baron research aircraft was equipped with PMS imaging probes and an airborne Ka-Band radar, along with the standard compliment of cloud physics instrumentation, and was flown in the melting layer of stratiform clouds near Hanscom AFB during the period March - May 1986. Thirteen flights were conducted with ten flights available for data analysis; of these, data from five case studies are presented in this report.

Heavy precipitation events during the research period were scarce, and the data presented here reflect analysis of precipitation from storms of light to occasionally moderate intensity. The dearth of strong precipitation events did not favor the formation of a deep melting layer with strong microwave attenuation characteristics, and this inhibited attempts to correlate observed attenuation of microwave signals with in situ cloud physics measurements.

Results of comparisons between the airborne Ka-band radar and the PMS imaging probes show a considerable variation in the echo returns as well as the cloud hydrometeor characteristics. Thus the microwave scattering properties through the melting layer are also highly variable.

The observed vertical profiles of the evolution of precipitation particles shows that rapid aggregation occurs near the -2 °C level, and that some large aggregates fall to temperatures as warm as +4 °C before melting. Thus there is a region of approximately 800 m where partially melted aggregates can substantially influence the propagation of microwaves.

| 20. DISTRIBUTION/AVAILABILITY OF ABSTRACT | 21. ABSTRACT SECURITY CLASSIFICATION | |
|---|---|---|
| ☐ UNCLASSIFIED/UNLIMITED ☐ SAME AS RPT ☐ DTIC USERS | Unclassified | |
| 22a. NAME OF RESPONSIBLE INDIVIDUAL<br>Morton Glass | 22b. TELEPHONE (Include Area Code)<br>617-377-2946 | 22c. OFFICE SYMBOL<br>AFGL/LYC |

DD FORM 1473, 84 MAR — 83 APR edition may be used until exhausted. All other editions are obsolete.

SECURITY CLASSIFICATION OF THIS PAGE
Unclassified

TABLE OF CONTENTS

# LIST OF FIGURES

# LIST OF TABLES

# 1.0 TECHNICAL BACKGROUND

Following the development of radar in the mid-1940's, investigators began to notice a pattern of enhanced radar reflectivity near the melting level in some precipitating clouds. This phenomenon was labeled the "bright band" and was the subject of several earlier theoretical and observational investigations (for example, see Ryde, 1946; Cunningham, 1947; Austin and Bemis, 1950; Marshall and Gunn, 1952; Wexler, 1955; Lhermitte and Atlas, 1963). Battan (1973) summarizes these earlier works which concluded that the bright band occurred in conjunction with the melting of snowflakes or an ice crystal aggregation process (as opposed to the accretional process which forms graupel and hail in convective clouds). However, these inferences were drawn without the benefit of in-situ observations and therefore did not explain the physics of the process.

The advent of PMS two-dimensional imaging probes (Knollenberg, 1976) facilitated the determination of in-situ hydrometer size distribution from airborne measurements (Gordon and Marwitz, 1984). This has led to the recent evaluation of the physical processes associated with bright bands using observations from aircraft by Stewart et. al. (1984). This work presented a comprehensive picture of thermodynamic and microphysical processes associated with the bright bands near the Sierra Nevada mountains in California. This report also presents some in situ airborne observations with concurrent radar observations to help identify the physical processes associated with the melting layer.

## 1.1 Physical Processes in the Melting Layer.

Radar observations typically show an enhanced reflectivity (in bright band) on the order of 10-15 dBZ increase in reflectivity, located about 300 m below the $0^{o}$C isothermal layer. Several physical factors have been proposed which could theoretically increase radar reflectivity in the bright band (see Battan, 1973 and Cohen and Sweeney, 1983 for a review); however, an evaluation of the most recent data strongly suggests that a shift in particle size distribution toward larger sizes is the most probable explanation. Since the aggregation efficiency is directly related to temperature until melting occurs, and since recent observations by Stewart et al. (1984) show a strong correlation between aggregation and the bright band effect, there is strong evidence that the bright band is associated with aggregation. Figure 1.1 is a reproduction from Stewart et al. (1984) showing the correlation between ice particle size (measured by the PMS 2-D probes) and radar reflectivity. They also point out that another factor which may support the aggregation process is an ice multiplication process active at $-5^{o}$C (Hallett and Mossop, 1974). As shown in Figure 1.1, there exists a threefold increase in ice crystals (needle shaped) near $-5^{o}$C. These needles may form aggregates or combine with existing dendritic crystals to form large lacy aggregates. These large aggregates would presumably tend to clump together near the

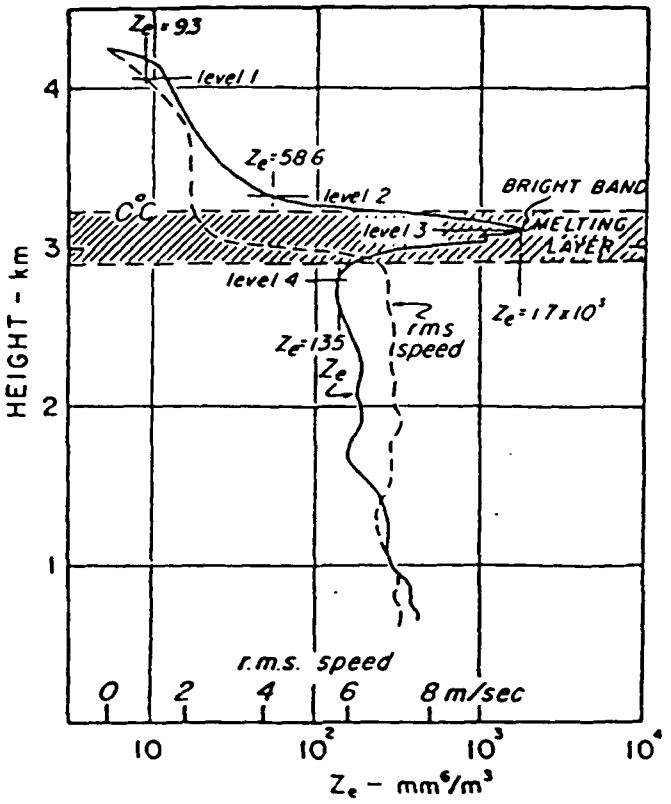


Simultaneous profiles of reflectivity factor $Z$ and root-mean-square particle-fall speed in light (1 mm/hr), steady precipitation with a bright band. From Lhermitte and Atlas (1963).

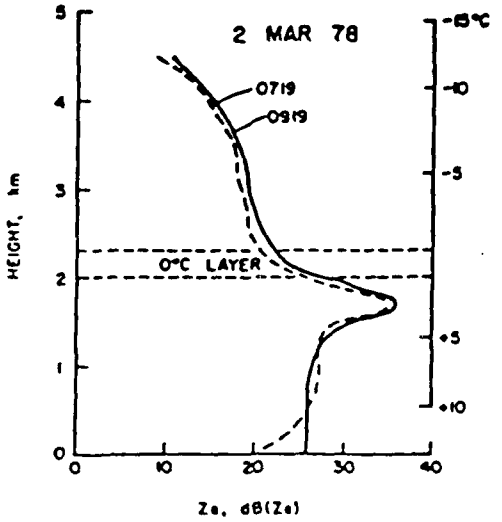


Vertical profile of radar reflectivity, and the cross section of the King Air flight track from 0711 PST (takeoff) to 0725 PST on 2 March 1978. The radar data were computed from a 7.5° elevation scan of the CP-3 radar at 0719 PST and from a 12.5° elevation angle scan at 0919 PST. (From Stewart et al.(1984)

Figure 1.1 Examples of Bright Band Radar Reflectivity

melting layer and melt into large drops which enhance radar reflectivity.

The effect of water-coated ice particles on radar reflectivity has been studied, and, according to Ekpenyong and Srivastava, (1970), when one-third of the original volume of ice has melted into a water film surrounding the ice, the index of refraction will have changed from ice to that of water. Cohen and Sweeney estimate that this would result in a 33 dBZ increase in radar reflectivity (much larger than the observed effect). However, Knight (1979) found that a circular shell of water only forms in the advanced stage of melting. Consequently, the possibility exists that an effective increase in hydrometeor diameter resulting from a less dense ice center could enhance radar reflectivity. This process is difficult to ascertain from aircraft observations.

Another feature associated with bright bands is the relative decrease in radar reflectivity below the melting layer. The increase in fall speed of the rain drops below the melting layer (see Figure 1.2) will create an effective decrease in number concentration. Lhermitte and Atlas (1963) found that this accounted for about one-third of the observed decrease in reflectivity below the melting layer (about 8 dBZ) was accounted for by the increase in fall velocity (4 dBZ) and the change in shape factor to spherical (about 3 dBZ). Stewart et. al. also concluded that raindrop collisional breakup below the melting layer was significant and tended to shift the drop size spectra toward a Marshall-Palmer distribution with the increasing temperature. The decrease in observed radar reflectivity was in agreement with the shift in the size spectra toward smaller diameters.

The aforementioned observations discussed in the literature suggest that several physical processes which affect the melting level (and the ensuing bright band) are complex and interactive. It is also apparent that the physical processes which affect the melting layer have their origins at colder temperatures (i.e., ice multiplication and aggregation) and extend well below the bright band (i.e., increased terminal velocity and collision breakup). In the present work we discuss airborne measurements in the melting layer in terms of this chain of events.

## 1.2 Overview of Airborne Measurement Systems.

For this study of the melting layer CIC provided the PMS twin engine turbo-charged Beech Baron (Figure 1.3) which is fully de-iced and has a good performance capability at the altitudes covered in this project. (See Section 1.3 for the Beech Baron aircraft specifications.)

The Baron carries, in standard research configuration, a full compliment of PMS particle sizing and imaging probes, a gust boom and the conventional state parameter sensors. A multiple

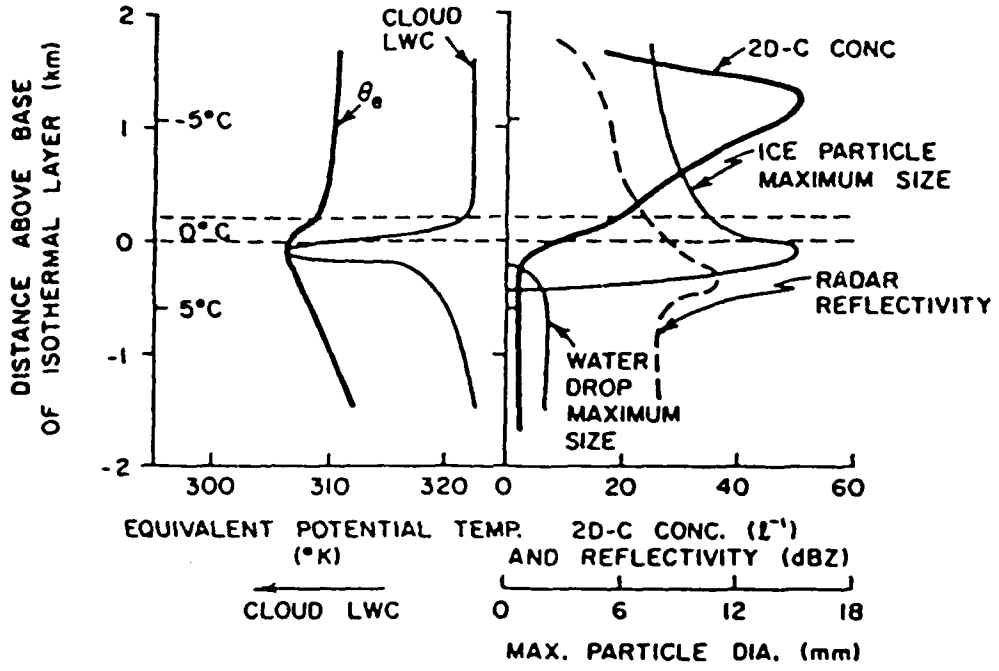


Schematic profile illustrating significant trends of various microphysical and state parameters through a typical melting layer as deduced by synthesizing the observations of all the case studies.

Figure 1.2 Profile Illustrating Trends of Microphysical and State Parameters at the Melting Layer (from Stewart et al., 1984).

Figure 1.3 Beechcraft Baron research aircraft used in the AFGL Melting Layer Studies.

DME position keeping system was installed which cycles through six VORTAC stations every six seconds, and provides position accuracy of better than 0.5 km in straight flight. A forward looking Ka band radar was installed in the nose of the Beechcraft Baron (in place of the standard radar). The return video was processed by fifteen range gates, displayed in real time on the cockpit display, and recorded on magnetic tape.

The data were recorded on computer-compatible nine track magnetic tape. A CRT display presented real-time data in engineering units to the scientist in the cockpit. A hard-copy printer output of the data was also available to the scientist in flight.

The post flight data processing was done on the CIC IBM-XT and the AFGL Vax systems. The AFGL system also benefitted from the use of several man-years of data analysis software developed by CIC and the University of Wyoming during the HIPLEX project (see Appendix B). Examples of the computer products are given in Section 3.0.

### 1.3 Performance of Beech Baron Aircraft

The performance characteristics of the Beech Baron research aircraft are shown in Table 1.1.

**Table 1.1**

TURBOCHARGED BEECHCRAFT BARON MODEL 58-TC, N23712

| | |
|---|---|
| Power, each engine | 310 hp |
| Maximum speed | 235 kts. |
| Fuel capacity | 175 gal |
| Service ceiling | 25,000 ft |
| Single engine service ceiling | 13,000 ft |
| Climb at gross wt | 1500 ft/min |
| Maximum endurance | 5 hrs |
| Maximum range | 900 nm |
| Take-off distance | 2400 ft |
| Landing distance | 2500 ft |
| Gross weight | 6100 |
| Empty weight | 4570 |
| Seating (Restricted Catagory) | 3 crew |
| Length | 30 ft |
| Wing span | 38 ft |

## 1.4 Cloud Physics Instrumentation.

### 1.4.1 Particle Spectrometers.

The PMS research aircraft is equipped with a Forward Scattering Spectrometer Probe (FSSP), Optical Array Two Dimensional Cloud Particle Imaging Probe (2D-C) and a Two Dimensional Precipitation Imaging Probe (2D-P). The FSSP sizes and counts particles from 0.5 to 45 microns, the 2D-C sizes and counts particles from 25-200 microns and the 2D-P operates in the range from 200-6400 microns. Figure 1.3 shows the PMS particle spectrometer probes mounted on the wing tips of the Baron. CIC has previously developed copious software to process PMS spectrometer probe data; samples of computer products are shown in Section 3.

The PMS 2D-C probe is equipped with a depolarization option which helps to discriminate ice and water particles. The depolarization feature works on the principle that a birefringent substance such as ice will change the polarization vector of incident polarized light, whereas water drops will not significantly affect the polarization vector. Although the discrimination is not absolute in all cases (i.e., large asymmetrical drops can cause a change in the polarization vector) the signal is a good indication of the relative phase of hydrometeors (Lawson and Stewart, 1983).

### 1.4.2 State Parameter and Air Motion Sensing Instrumentation.

Table 1.2 lists the performance characteristics of the research instrumentation used by CIC. All sensors and systems were calibrated at the CIC/PMS facility prior to the field season. A tower fly-by was conducted at the instrumented BAO/NOAA tower located 10 miles east of the Boulder Airport to verify the dynamic calibration of pressure, temperature and dew point temperature prior to the field season.

## 1.5 Ka Band Weather Radar.

CIC provided a Westinghouse AN/APD-7 Ka band radar for use on this project (see Table 1.3 for radar characteristics). The existing X-Band radar was removed and the APD-7 radar was located in its place.

Radar signal processing was accomplished using an integrating sample and hold circuit (referred to as a video

TABLE 1.2

Aircraft Instrumentation Specifications

| Parameter Measured | Instrument Type | Manufacturer and Model Number | Range | Combined Performance of Transducer, Signal Conditioning and Conversion: Accuracy | Time Constant | Sample Rate | Useable Resolution |
|---|---|---|---|---|---|---|---|
| Time | Crystal osc | PMS | 12 mo | 1s | N/A | 0.1s | 0.1s |
| Temperature | Platinum resistance | Rosemount Eng. Co. 510BF9 Bridge Model 102 Probe | ±50/°C | 0.5°C | 1 | 1Hz | 0.1°C |
| Temperature | Platinum resistance, reverse flow | NCAR - Probe Minco Inc - element | ±50°C | 0.5°C | 0.1 | 10Hz | 0.1°C |
| Dew Point | Peltier cooled mirror | Cambridge Systems Inc. Model 137-C3 | ±50°C | 1°C | 1-5 s | 1Hz | 0.3° |
| Liquid Water | Hot wire | Cloud Technology Model LWH | 0-3 gm/$m^3$ | 0.2 gm/$m^3$ | 1 | 1Hz | 0.01 gm/$m^3$ |
| Altitude | Total pressure | Rosemount Eng. Co. Model 1201 | 0-15 psia | 0.015 psia | 1 | 1Hz | 0.007 psia |
| Indicated Airspeed | Differential pressure | Rosemount Eng. Co. Model 1332B1 | ±2.5 psid | 0.0025 | 0.1 | 1Hz | 0.0025 psid |
| Heading | Gyro | Bendix | 0-360° | ±2° | 0.1 | 1Hz | 0.1° |
| Radar | KA Band | Westinghouse AN/APD/7 | (4) 600m Range bins | | 1 s | 1Hz | 600 m |
| Radar Elevation angle | Synchro | ILC Corp. | ±15° | 0.50° | 0.1 | 1Hz | 0.1° |

TABLE 1.2 cont'd

| Parameter Measured | Instrument Type | Manufacturer and Model Number | Combined Performance of Transducer, Signal Conditioning and Conversion | | | | |
|---|---|---|---|---|---|---|---|
| | | | Range | Accuracy | Time Constant | Sample Rate | Useable Resolution |
| Position (azimuth) | VOR | King Radio | 0-360° | ±1° | 0.1 | 1Hz | 0.1° |
| Position (distance) | DME | King Radio | 0-300km | 0.2km | 1 | 1Hz | 0.1km |
| Position | Multi-DME | King Radio Corp. Model KDM 7000 | 0-400km | 0.07km | 1 | 1Hz | 0.02km |
| Angle of Attack | Differential pressure | Rosemount Model 858 | ±20° | 0.25° | 0.1 | 10Hz | 0.1° |
| Slide Slip | Differential pressure | Rosemount Model 858 | ±20° | 0.25° | 0.1 | 10Hz | 0.1° |
| Cloud particle size Concentration | Optical Scattering | PMS FSSP | 1-45μ .1-1500cm$^{-3}$ | 3μ 10% | Discrete Event | Continuous | 1μ .1 cm$^{-3}$ |
| Cloud Size & Concentration | Optical array | PMS 2-dC | 25-800μ 0.1 -10,000L$^{-1}$ | | Discrete Event | Continuous | 25μ 0.1L$^{-1}$ |
| Cloud precip & concentration | Optical array | PMS 2-dP | 200-6400 μ 0.1-10,000L$^{-1}$ | | Discrete event | Continuous | 200μ 0.02L$^{-1}$ |
| Events | Digital latch | PMS | 4 events | 1s | Discrete | Continuous | 1s |

TABLE 1.3

WESTINGHOUSE AN/APD-7 Ka BAND WEATHER RADAR SPECIFICATIONS

| | |
|---|---|
| R-F Operating Frequency | 34.9 GHz |
| Peak Power Output | 100 KW |
| Average Power Output | 14 watts |
| Pulse Repetition Frequency | 1845 prf |
| Pulse Width | 0.1 usec |
| Antenna size | 12" dia. |
| Beam width | $1.5^{o}$ |
| Minimum detectable signal | 8 dBZ at 1 km |
| Range gate size | 15 gates: 600, 1800, 3000,4200,5400m; 6.6, 7.8, 10.2, 12.6, 15, 17.4, 19.8, 22.2, 27.4, 36.6 km |

integrating processor or VIP) which had previously been used by CIC on several of its ground based radar systems.

The radar transmitter generated a 0.1 micro second pulse and the return video was integrated and recorded every 1.0 seconds. A series of range gates were recorded with the first gate set at 600m ahead of the aircraft, and subsequent gates spaced as shown in Table 1.3.

## 1.6 Navigation Systems.

### 1.6.1 Multi-DME Position System.

CIC developed a multi-DME position system for use in positioning the research aircraft. The system recorded distance data from up to six different ground-based VORTAC stations at a rate of one station per second. The KDM-7000 DME used in this system has a resolution of 20 m. and the system accuracy is on the order of 200 m. when four or more stations are received (Lawson et. al., 1980). An additional advantage was that there is no drift with time (as in INS positioning systems) since the absolute data are refreshed every six seconds. The area around Hanscom AFB is densely populated with VORTAC stations as shown in Figure 1.4. At normal flight levels around Hanscom AFB DME signal reception was adaquate and gave good positions for this melting layer project.

### 1.6.2 VOR/DME.

The CIC data system routinely recorded aircraft VOR and DME data on the research data system, as well as multi-DME. Position from VOR/DME is only accurate to about 1 km., but the data are very reliable and provided useful redundancy (the multi DME system failed on some days).

## 1.7 Post Season Data Processing.

CIC copied all the raw data tapes onto 9-track 1600 bpi computer compatible magnetic tape and delivered these tapes, along with all data reduction programs (written in Fortran and formatted in ASC II on 9-track computer compatible magnetic tape) to AFGL personnel. All notes recorded by the on-board scientist were delivered to AFGL. CIC and OPHIR personnel then continued to work with AFGL personnel to develop analysis software and techniques to elucidate the microphysical and thermodynamic processes operating within and near the melting layer.

## 1.8 AFGL M-meter.

The AFGL M-meter estimates the integrated mass of hydrometeors which are impacted on a rapidly spinning disk by measuring the change in angular momentum of the disk. The M meter was installed on the starboard wing pylon which also carries the PMS FSSP probe (see Figure 1.3). Proper wiring was

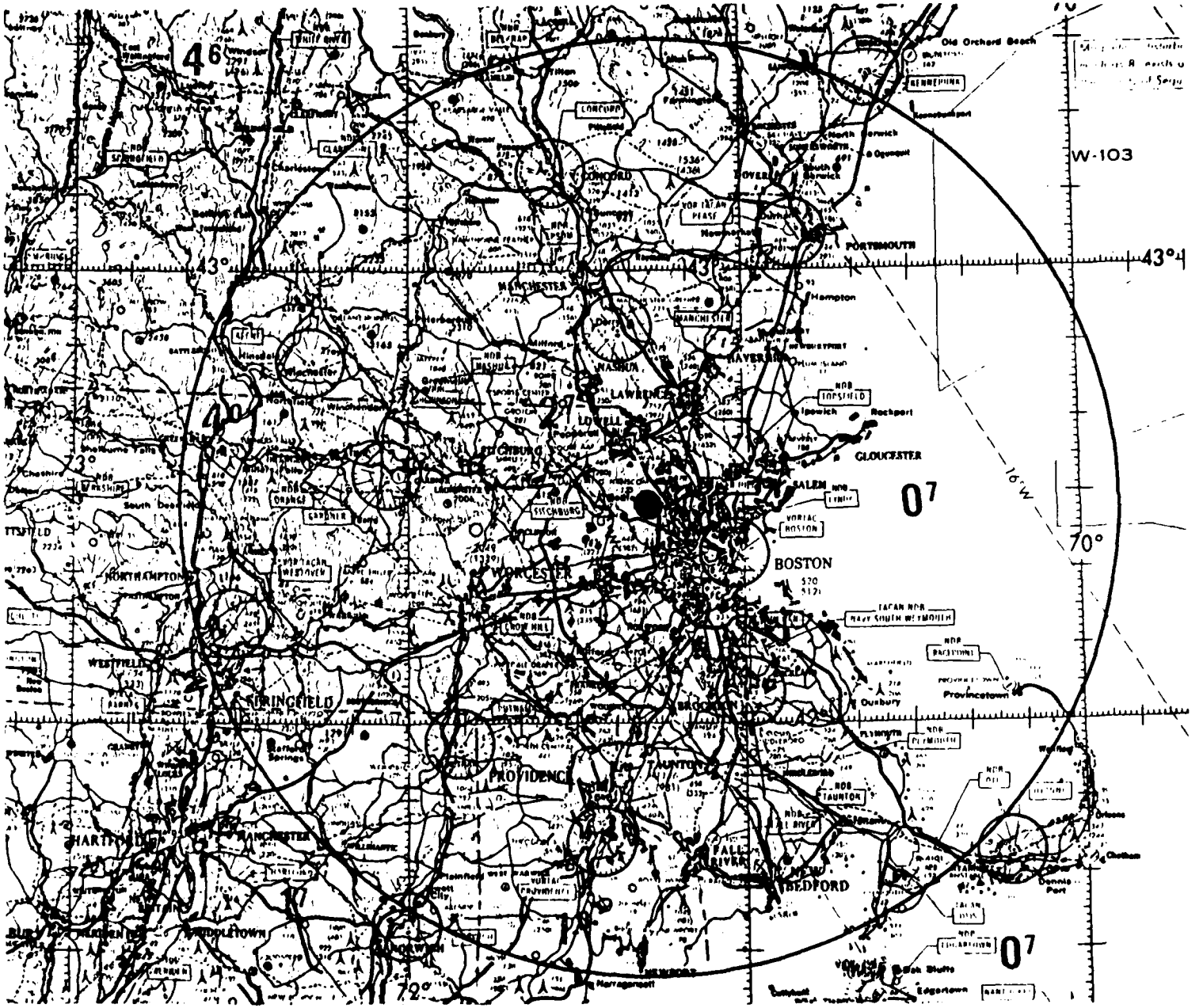


Figure 1.4 VORTAC Stations within a 60 nmi radius of Hanscom AFB

already available to provide electrical power and to transfer the output signal directly to the PMS Data Acquisition System (DAS).

In-flight data were available on the cockpit CRT and the real-time printer. Thus, field evaluation of the unit was conducted on a flight-by-flight basis. The primary evaluation tool was comparison of the unit output with the PMS probes, however, lack of sufficient funding preempted any detailed analysis, and inquiries on this matter should be directed to Mr. Vern Plank of the AFGL.

## 2.0 FIELD OPERATIONS.

### 2.1 Period of Operations.

The aircraft operated from Hanscom Field from March 17, 1986 through May 22, 1986. The aircraft was stationed at the Piper fixed base operator at Hanscom Field.

### 2.2 Air Traffic Control Procedures.

Prior to the field program CIC's pilot visited the Boston ATC center in order to explain the proposed flight operations and to obtain their cooperation in filing flight plans. The aircraft was given a code name "Cloudy I." This code name helped to identify to the FAA controllers the special aspects of this flight operation.

### 2.3 Flight Operations.

Table 2.1 is the flight summary for this project. A total of 53.5 hours were flown on test flights, ferry to and from Hanscom and on observational flights.

A standard flight profile was established for the purpose of measuring the chain of events of the cloud physical passes as they occur above, through, and below the $0^{o}C$ level. Figure 2.1 shows an example of the profile chosen. After take-off the aircraft ascended to the $-4^{o}C$ level. Then, in a series of passes, the aircraft would alter its altitude to pass through the vertical depth of the melting layer.

The horizontal tracks were designed such that the center of the vertical profile would occur over Sudbury where ground-based precipitation sensors and weather radars were stationed. However, due to air traffic control problems, not all profiles could be accomplished as planned.

### 2.4 Data Tapes.

All data tapes were copied and given to the Air Force personnel within 48 hours after each flight. The observer flight notes were also provided. Copies of these notes were also retained by CIC for further post field analysis.

TABLE 2.1

CIC FLIGHT SUMMARY

| Fl# | Date | Clock hrs | Pros Total | Type |
|---|---|---|---|---|
| PRE 1 | 3-15 | 1.2 | 1.2 | CA1-IU5 |
| PRE 2 | 3-19 | 0.5 | 1.7 | CAL-KC |
| FERRY | 3-16-20 | 10.3 | 13.0 | IV5-BED |
| 01 | 3-22 | 0.7 | 13.7 | FAM-BED |
| 02* | 3-27 | 0.8 | 14.5 | TEST-ABORT |
| 03* | 3-27 | 1.6 | 16.1 | TEST-DATA |
| 04* | 4-7 | 2.5 | 18.6 | DATA |
| 05 | 4-8 | 2.3 | 20.9 | DATA |
| 06* | 4-17 | 3.4 | 24.3 | DATA |
| 07 | 4-21 | 1.5 | 25.8 | DATA/ABORT |
| 08* | 4-26 | 3.6 | 29.4 | DATA |
| 09* | 4-27 | 3.6 | 33.0 | DATA |
| 10 | 5-2 | 0.6 | 33.6 | M-M TEST |
| 11* | 5-12 | 2.3 | 35.9 | DATA |
| 12 | 5-14 | 0.9 | 36.8 | M-M TEST |
| 13 | 5-14 | 1.5 | 38.3 | M-M TEST |
| 14* | 5-17 | 2.2 | 40.5 | DATA |
| 15* | 5-22 | 2.1 | 42.6 | DATA |
| 16 | 5-22 | 1.7 | 47.3 | FERRY |
| 17 | 5-23 | 3.5 | 50.8 | FERRY/DATA M-M |
| 18 | 5-23 | 2.7 | 53.5 | FERRY |

* Flights which provided data of particular interest

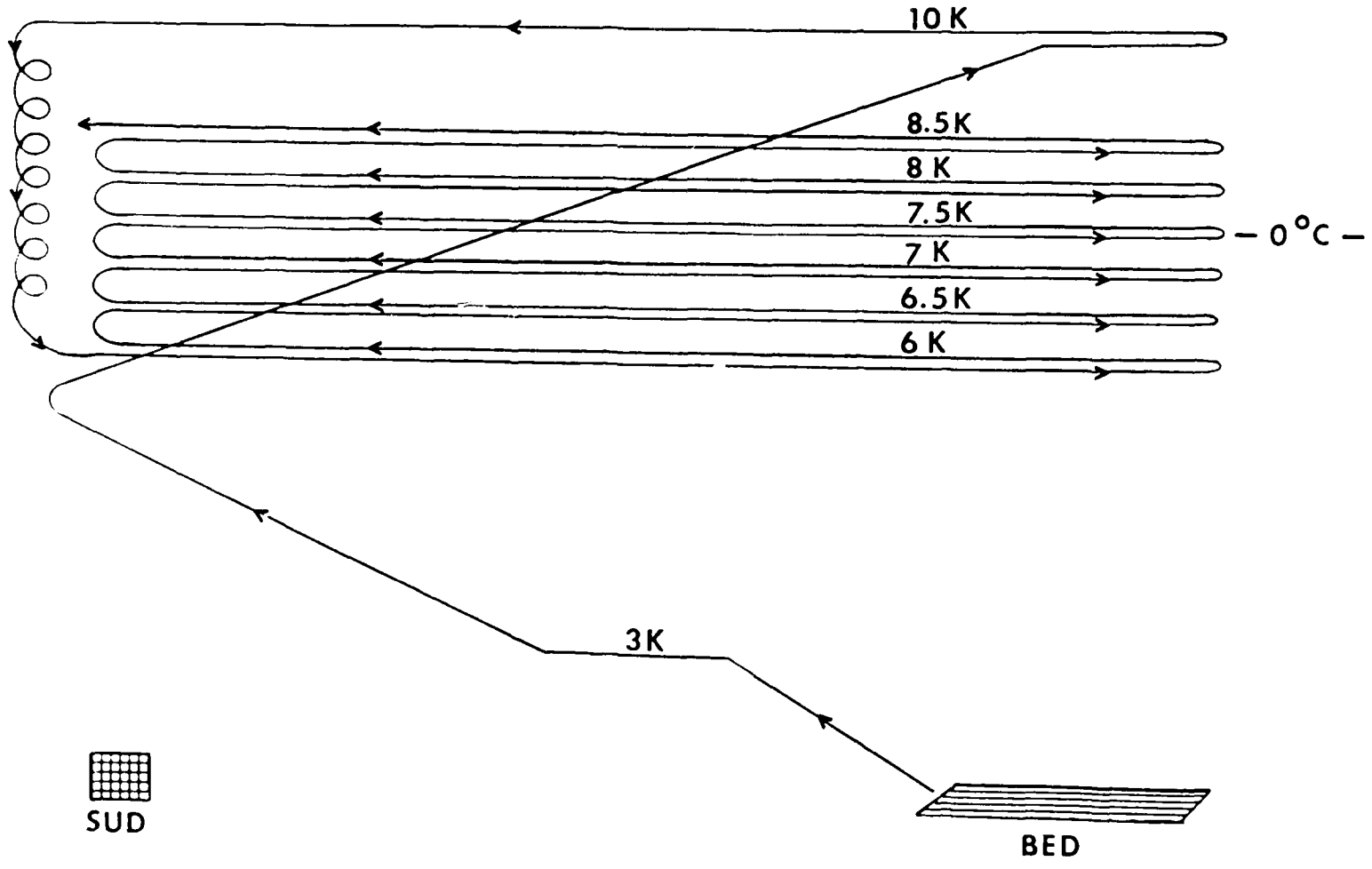


Figure 2.1 Typical flight profile for AFGL Melting Layer Studies.

# 3.0 SOFTWARE FOR DATA REDUCTION AND ANALYSIS.

## 3.1 Background.

The instrumented aircraft collected data on magnetic tape which was transcribed to hardcopy computer products after each flight. These computer products provided the AFGL with a quick-turnaround evaluation of the mission performance (for example see Figure 3.1).

During a meeting on 13 May 1986 with AFGL and CIC personnel, it was agreed that CIC personnel would pursue the analysis of data after the close of the field season (an extension of the field season by the AFGL due to lack of suitable weather reduced the original estimate of funds available for data analysis). AGFL personnel recommended that CIC develop software to produce the following computer products:

1. Plan view of aircraft position as a function of time.

2. Integrated total water content and equivalent radar reflectivity including artifact rejection from the PMS FSSP, 2DC and 2DP particle imaging data.

3. Time series plots of the airborne Ka-band radar reflectivity data which have been time-correlated for distance from the aircraft.

4. Spectral analysis of correlation between the airborne Ka-band radar data with particle image data.

It was further agreed that CIC would use these software tools to produce plan-view and vertical cross-section analyses of the melting layer data identifying the location and type of hydrometeors, the depth of the melting layer and the precipitation processes which were active. These in-situ data were intended to be correlated with remote-sensing data from ground-based radars and satellite beacons.

## 3.2 Computer Software Products.

### 3.2.1 PMS 2D Images.

Figure 3.2 is an example of PMS 2DC and 2DP image data collected on 27 March 1986. The images are underscored by lines of meteorological data collected by the aircraft at the same time.

### 3.2.2 Aircraft Track.

Figure 3.3 is an example of a plot of aircraft track from the multiple DME system as a function of time. Since the aircraft flew repeated legs over the same location on the ground, it is necessary to separate a mission into several time periods for the sake of clarity. Appendix A contains the flight tracks

AIR FORCE GEOPHYSICS LABORATORY MELTING LAYER DATA COLLECTED ON 3/27/86 BY CIC CLOUD PHYSICS AIRCRAFT N23712

| TIME | PRES | ALT | VOR/DME | M-DME | STA | PITCH | HDG | IAS | TAS | RSMT | RFT | DEW | Q | THETA | TH-E | LWC | FWC | MM | CONC | DBAR | 2DC | 2DP | EVT |
|---|---|---|---|---|---|---|---|---|---|---|---|---|---|---|---|---|---|---|---|---|---|---|---|
| 1034 0 | 929 | 721 | 313/ | 0 | -1.0 | 6 | 7.7 | 321 | 125 | 66.9 | 9.5 | 8.8 | 7.7 | 7.1 | 288.6 | 309.1 | 0.00 | 0.01 | 3187 | 1.4 | 18 | 2.1 | 1.3 | 0. |
| 1034 1 | 929 | 721 | 313/ | 0 | 19.7 | 1 | 8.2 | 321 | 125 | 66.5 | 9.4 | 8.8 | 7.5 | 7.0 | 288.5 | 308.7 | 0.00 | 0.01 | 3123 | 2.7 | 15 | 0.7 | 1.4 | 0. |
| 1034 2 | 927 | 736 | 313/ | 0 | 18.8 | 2 | 7.0 | 318 | 123 | 65.8 | 9.7 | 8.9 | 7.1 | 6.8 | 288.9 | 308.6 | 0.00 | 0.01 | 3080 | 1.2 | 19 | 0.7 | 1.4 | 0. |
| 1034 3 | 924 | 767 | 313/ | 0 | 21.5 | 3 | 7.0 | 317 | 120 | 64.4 | 9.8 | 9.0 | 6.9 | 6.7 | 289.3 | 308.8 | 0.00 | 0.01 | 2993 | 1.6 | 18 | 1.1 | 1.5 | 0. |
| 1034 4 | 926 | 752 | 315/ | 0 | 30.1 | 4 | 7.0 | 317 | 117 | 62.6 | 9.8 | 8.9 | 6.7 | 6.6 | 289.2 | 308.4 | 0.00 | 0.01 | 2912 | 2.1 | 14 | 2.6 | 2.1 | 0. |
| 1034 5 | 922 | 783 | 313/ | 0 | 39.3 | 5 | 6.7 | 318 | 115 | 61.7 | 9.6 | 9.0 | 6.9 | 6.7 | 289.4 | 308.9 | 0.00 | 0.01 | 2842 | 2.2 | 17 | 0.8 | 2.2 | 0. |
| 1034 6 | 922 | 783 | 313/ | 0 | 38.7 | 6 | 6.5 | 319 | 116 | 62.1 | 9.5 | 8.8 | 6.9 | 6.7 | 289.2 | 308.7 | 0.00 | 0.01 | 2805 | 1.7 | 20 | 3.0 | 1.8 | 0. |
| 1034 7 | 920 | 798 | 311/ | 0 | 19.9 | 1 | 7.0 | 319 | 111 | 59.4 | 9.4 | 8.7 | 6.7 | 6.7 | 289.2 | 308.6 | 0.00 | 0.02 | 2743 | 3.0 | 18 | 0.0 | 3.3 | 0. |
| 1034 8 | 922 | 783 | 311/ | 0 | 18.8 | 2 | 6.0 | 322 | 113 | 60.3 | 9.0 | 8.5 | 7.0 | 6.8 | 288.7 | 308.3 | 0.00 | 0.01 | 2651 | 2.6 | 16 | 1.9 | 1.3 | 0. |
| 1034 9 | 920 | 798 | 311/ | 0 | 21.3 | 3 | 4.3 | 326 | 116 | 62.2 | 8.7 | 8.3 | 7.2 | 6.9 | 288.6 | 308.5 | 0.00 | 0.01 | 2765 | 2.1 | 17 | 2.2 | 2.2 | 0. |
| 103410 | 920 | 798 | 312/ | 0 | 29.9 | 4 | 5.3 | 327 | 115 | 61.5 | 8.6 | 8.4 | 7.2 | 6.9 | 288.5 | 308.5 | 0.01 | 0.02 | 2789 | 2.9 | 18 | 0.8 | 2.3 | 0. |
| 103411 | 919 | 814 | 311/ | 0 | 39.4 | 5 | 6.5 | 327 | 117 | 62.9 | 8.3 | 8.2 | 7.1 | 6.9 | 288.4 | 308.2 | 0.00 | 0.01 | 2787 | 3.1 | 17 | 0.7 | 1.6 | 0. |
| 103412 | 920 | 798 | 311/ | 0 | 39.0 | 6 | 6.2 | 324 | 114 | 61.2 | 8.7 | 8.3 | 6.9 | 6.7 | 288.5 | 308.0 | 0.00 | 0.01 | 2785 | 2.3 | 18 | 2.6 | 3.6 | 0. |
| 103413 | 919 | 814 | 312/ | 0 | 20.1 | 1 | 6.5 | 324 | 112 | 60.2 | 8.5 | 8.2 | 7.1 | 6.9 | 288.5 | 308.4 | 0.01 | 0.01 | 2727 | 1.9 | 15 | 3.5 | 1.8 | 0. |
| 103414 | 919 | 814 | 312/ | 0 | 18.8 | 2 | 6.7 | 325 | 113 | 60.5 | 8.4 | 8.0 | 7.1 | 6.9 | 288.4 | 308.2 | 0.00 | 0.01 | 2698 | 1.5 | 18 | 0.8 | 2.5 | 0. |
| 103415 | 917 | 829 | 312/ | 0 | 21.2 | 3 | 6.7 | 324 | 109 | 58.3 | 8.3 | 8.0 | 7.1 | 6.9 | 288.5 | 308.4 | 0.00 | 0.01 | 2632 | 2.2 | 17 | 0.8 | 2.4 | 0. |
| 103416 | 917 | 829 | 311/ | 0 | 29.8 | 4 | 6.0 | 324 | 111 | 59.3 | 8.1 | 7.8 | 7.1 | 6.9 | 288.2 | 308.1 | 0.00 | 0.01 | 2645 | 1.8 | 18 | 2.0 | 1.8 | 0. |
| 103417 | 917 | 829 | 311/ | 0 | 39.4 | 5 | 6.7 | 321 | 108 | 58.0 | 8.1 | 7.9 | 7.2 | 6.9 | 288.3 | 308.3 | 0.00 | 0.01 | 2601 | 0.9 | 16 | 1.2 | 2.2 | 0. |
| 103418 | 915 | 845 | 311/ | 0 | -1.0 | 6 | 6.2 | 321 | 105 | 56.5 | 8.0 | 7.8 | 7.1 | 6.9 | 288.3 | 308.2 | 0.00 | 0.01 | 2558 | 2.6 | 16 | 0.8 | 1.3 | 0. |
| 103419 | 915 | 845 | 312/ | 0 | 20.3 | 1 | 6.7 | 319 | 105 | 56.2 | 8.0 | 7.8 | 7.0 | 6.8 | 288.4 | 308.1 | 0.00 | 0.01 | 2520 | 2.1 | 15 | 1.2 | 2.7 | 0. |
| 103420 | 915 | 845 | 312/ | 0 | 18.8 | 2 | 6.2 | 316 | 104 | 55.7 | 8.0 | 7.8 | 7.0 | 6.8 | 288.3 | 308.0 | 0.00 | 0.01 | 2491 | 1.3 | 21 | 0.8 | 2.5 | 0. |
| 103421 | 914 | 861 | 313/ | 0 | 21.0 | 3 | 6.0 | 315 | 103 | 55.4 | 8.0 | 7.7 | 7.1 | 6.9 | 288.5 | 308.4 | 0.00 | 0.02 | 2465 | 3.7 | 18 | 2.5 | 2.8 | 0. |
| 103422 | 914 | 861 | 311/ | 0 | 29.7 | 4 | 6.0 | 313 | 103 | 55.4 | 7.8 | 7.6 | 7.1 | 6.9 | 288.3 | 308.2 | 0.00 | 0.01 | 2438 | 2.6 | 15 | 0.8 | 2.4 | 0. |
| 103423 | 912 | 876 | 311/ | 0 | 39.4 | 5 | 5.8 | 313 | 103 | 55.4 | 7.7 | 7.6 | 6.9 | 6.8 | 288.3 | 307.9 | 0.00 | 0.01 | 2435 | 1.8 | 19 | 3.8 | 2.0 | 0. |
| 103424 | 912 | 876 | 315/ | 0 | 39.3 | 6 | 5.3 | 314 | 104 | 55.7 | 7.7 | 7.6 | 6.9 | 6.8 | 288.3 | 307.9 | 0.00 | 0.00 | 2435 | 1.5 | 13 | 2.1 | 1.5 | 0. |
| 103425 | 910 | 892 | 311/ | 0 | 20.4 | 1 | 5.0 | 315 | 107 | 57.4 | 7.5 | 7.3 | 7.1 | 6.9 | 288.2 | 308.2 | 0.00 | 0.01 | 2459 | 1.6 | 18 | 3.4 | 1.8 | 0. |
| 103426 | 910 | 892 | 311/ | 0 | 18.8 | 2 | 4.3 | 316 | 109 | 58.5 | 7.6 | 7.3 | 7.2 | 7.0 | 288.4 | 308.6 | 0.00 | 0.01 | 248[illegible] | 1.1 | 16 | 0.4 | 1.9 | 0. |
| 103427 | 912 | 876 | 314/ | 0 | 20.9 | 3 | 3.4 | 320 | 111 | 59.8 | 7.5 | 7.3 | 7.0 | 6.9 | 288.2 | 307.9 | 0.00 | 0.01 | 2534 | 1.6 | 20 | 0.0 | 1.9 | 0. |
| 103428 | 910 | 892 | 314/ | 0 | 29.5 | 4 | 2.9 | 324 | 113 | 60.6 | 7.7 | 7.4 | 6.6 | 6.7 | 288.5 | 307.8 | 0.00 | 0.01 | 2583 | 1.5 | 16 | 0.8 | 2.3 | 0. |
| 103429 | 910 | 892 | 314/ | 0 | 39.5 | 5 | 2.4 | 327 | 114 | 61.3 | 7.8 | 7.4 | 6.4 | 6.6 | 288.6 | 307.6 | 0.00 | 0.01 | 2629 | 0.7 | 19 | 3.8 | 1.5 | 0. |
| 103430 | 910 | 892 | 313/ | 0 | 39.5 | 6 | 2.2 | 331 | 116 | 62.3 | 7.8 | 7.3 | 6.4 | 6.6 | 288.6 | 307.5 | 0.00 | 0.02 | 2681 | 2.2 | 20 | 0.0 | 2.9 | 0. |
| 103431 | 912 | 876 | 313/ | 0 | 20.6 | 1 | 2.2 | 334 | 116 | 62.4 | 7.8 | 7.3 | 6.6 | 6.7 | 288.4 | 307.7 | 0.00 | 0.02 | 2694 | 2.7 | 19 | 2.2 | 1.9 | 0. |
| 103432 | 910 | 892 | 313/ | 0 | 18.7 | 2 | 2.2 | 337 | 117 | 62.7 | 7.8 | 7.3 | 6.9 | 6.8 | 288.5 | 308.2 | 0.00 | 0.01 | 2723 | 2.2 | 16 | 3.7 | 2.9 | 0. |
| 103433 | 912 | 876 | 312/ | 0 | 20.7 | 3 | 2.6 | 340 | 117 | 63.0 | 7.7 | 7.3 | 6.9 | 6.8 | 288.4 | 308.0 | 0.00 | 0.01 | 2758 | 2.1 | 15 | 0.7 | 2.9 | 0. |
| 103434 | 912 | 876 | 313/ | 0 | 29.4 | 4 | 3.1 | 343 | 119 | 64.1 | 7.7 | 7.3 | 6.6 | 6.7 | 288.3 | 307.6 | 0.00 | 0.00 | 2751 | 1.1 | 16 | 1.4 | 1.7 | 0. |
| 103435 | 910 | 892 | 313/ | 0 | 39.6 | 5 | 2.6 | 348 | 121 | 65.0 | 7.7 | 7.2 | 6.5 | 6.6 | 288.5 | 307.6 | 0.00 | 0.01 | 2803 | 1.7 | 16 | 1.4 | 2.6 | 0. |
| 103436 | 910 | 892 | 312/ | 0 | 39.7 | 6 | 3.1 | 351 | 121 | 65.3 | 7.7 | 7.2 | 6.7 | 6.8 | 288.5 | 308.0 | 0.00 | 0.01 | 2873 | 1.5 | 16 | 2.1 | 2.5 | 0. |
| 103437 | 910 | 892 | 313/ | 0 | 20.8 | 1 | 3.8 | 352 | 122 | 65.4 | 7.7 | 7.1 | 7.0 | 6.9 | 288.5 | 308.3 | 0.17 | 0.02 | 2890 | 3.4 | 18 | 1.1 | 3.6 | 0. |
| 103438 | 910 | 892 | 313/ | 0 | 18.7 | 2 | 4.6 | 354 | 120 | 64.7 | 7.6 | 7.2 | 7.0 | 6.9 | 288.4 | 308.2 | 0.17 | 0.04 | 2868 | 5.1 | 20 | 1.4 | 2.9 | 0. |
| 103439 | 910 | 892 | 313/ | 0 | 20.5 | 3 | 5.3 | 357 | 121 | 65.2 | 7.6 | 7.1 | 6.6 | 6.7 | 288.4 | 307.7 | 0.06 | 0.02 | 2854 | 3.0 | 17 | 0.4 | 3.7 | 0. |
| 103440 | 908 | 907 | 315/ | 0 | 29.4 | 4 | 5.3 | 0 | 121 | 65.3 | 7.6 | 7.1 | 6.7 | 6.8 | 288.5 | 308.1 | 0.00 | 0.01 | 2884 | 1.9 | 16 | 0.0 | 2.0 | 0. |
| 103441 | 908 | 907 | 315/ | 0 | 39.8 | 5 | 5.5 | 1 | 120 | 64.5 | 7.7 | 7.2 | 6.9 | 6.8 | 288.7 | 308.4 | 0.00 | 0.01 | 2874 | 2.7 | 15 | 0.0 | 3.3 | 0. |
| 103442 | 908 | 907 | 316/ | 0 | -1.0 | 6 | 6.0 | 2 | 119 | 64.1 | 7.7 | 7.3 | 7.0 | 6.9 | 288.6 | 308.5 | 0.07 | 0.03 | 2844 | 3.9 | 19 | 2.5 | 1.8 | 0. |
| 103443 | 907 | 923 | 316/ | 0 | 20.9 | 1 | 6.0 | 5 | 118 | 63.3 | 7.7 | 7.1 | 6.7 | 6.8 | 288.8 | 308.4 | 0.01 | 0.01 | 2827 | 2.6 | 16 | 1.5 | 3.4 | 0. |
| 103444 | 907 | 923 | 317/ | 0 | 18.5 | 2 | 6.0 | 8 | 116 | 62.2 | 7.8 | 7.2 | 6.6 | 6.7 | 288.9 | 308.3 | 0.00 | 0.01 | 2793 | 2.7 | 17 | 1.5 | 1.8 | 0. |
| 103445 | 905 | 938 | 316/ | 0 | 20.3 | 3 | 6.2 | 10 | 114 | 61.6 | 7.8 | 7.3 | 6.6 | 6.7 | 289.1 | 308.5 | 0.02 | 0.01 | 2749 | 2.4 | 18 | 1.5 | 3.2 | 0. |
| 103446 | 903 | 954 | 316/ | 0 | 29.4 | 4 | 6.5 | 11 | 114 | 61.6 | 7.8 | 7.3 | 6.6 | 6.7 | 289.2 | 308.8 | 0.00 | 0.02 | 2729 | 2.9 | 18 | 0.4 | 1.7 | 0. |
| 103447 | 903 | 954 | 316/ | 0 | 40.0 | 5 | 6.5 | 12 | 113 | 61.1 | 7.9 | 7.3 | 6.4 | 6.6 | 289.3 | 308.4 | 0.03 | 0.02 | 2728 | 2.1 | 20 | 0.4 | 3.4 | 0. |
| 103448 | 903 | 954 | 317/ | 0 | -1.0 | 6 | 6.7 | 14 | 113 | 61.1 | 8.0 | 7.3 | 6.2 | 6.6 | 289.4 | 308.4 | 0.00 | 0.01 | 2735 | 3.1 | 15 | 3.8 | 2.7 | 0. |
| 103449 | 902 | 969 | 317/ | 0 | 21.0 | 1 | 6.5 | 15 | 114 | 61.4 | 7.8 | 7.3 | 6.4 | 6.6 | 289.4 | 308.6 | 0.02 | 0.01 | 2745 | 2.7 | 15 | 0.4 | 3.0 | 0. |
| 103450 | 900 | 985 | 318/ | 0 | 18.3 | 2 | 6.2 | 18 | 112 | 60.5 | 7.8 | 7.2 | 6.2 | 6.6 | 289.5 | 308.6 | 0.01 | 0.03 | 2742 | 3.7 | 20 | 3.1 | 1.5 | 0. |

Figure 3.1 Example of parameter listing in engineering units.

AIR FORCE GEOPHYSICS LABORATORY MELTING LAYER DATA COLLECTED ON 3/27/86 BY CIC CLOUD PHYSICS AIRCRAFT N23712

| TIME | PRES | VOR/DME | HDG | TAS | RSMT | RFT | DEW | Q | THETA | TH-E | LWC | FWC | MM | CONC | DBAR | 2DC | 2DP | RAD1 | RAD2 | RAD3 | RAD4 |
|---|---|---|---|---|---|---|---|---|---|---|---|---|---|---|---|---|---|---|---|---|---|
| 1034 0 | 929 | 313/ 0 | 321 | 66.9 | 9.5 | 9.3 | 7.7 | 7.1 | 288.6 | 309.1 | 0.00 | 0.01 | 3187 | 1.4 | 18 | 2.1 | 1.3 | -103 | -103 | -103 | -103 |

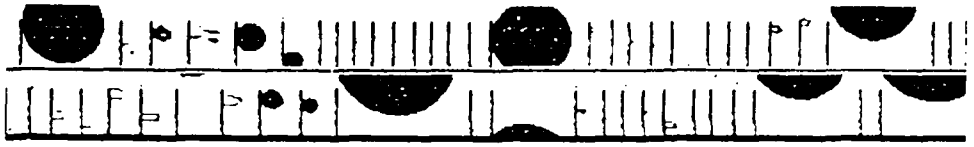

| TIME | PRES | VOR/DME | HDG | TAS | RSMT | RFT | DEW | Q | THETA | TH-E | LWC | FWC | MM | CONC | DBAR | 2DC | 2DP | RAD1 | RAD2 | RAD3 | RAD4 |
|---|---|---|---|---|---|---|---|---|---|---|---|---|---|---|---|---|---|---|---|---|---|
| 1034 1 | 929 | 313/ 0 | 321 | 66.5 | 9.4 | 9.3 | 7.5 | 7.0 | 288.5 | 308.7 | 0.00 | 0.01 | 3123 | 2.7 | 15 | 0.7 | 1.4 | -103 | -103 | -103 | -103 |

| TIME | PRES | VOR/DME | HDG | TAS | RSMT | RFT | DEW | Q | THETA | TH-E | LWC | FWC | MM | CONC | DBAR | 2DC | 2DP | RAD1 | RAD2 | RAD3 | RAD4 |
|---|---|---|---|---|---|---|---|---|---|---|---|---|---|---|---|---|---|---|---|---|---|
| 1034 2 | 927 | 313/ 0 | 318 | 65.8 | 9.7 | 9.4 | 7.1 | 6.8 | 288.9 | 308.6 | 0.00 | 0.01 | 3080 | 1.2 | 19 | 0.7 | 1.4 | -103 | -103 | -103 | -103 |
| 1034 3 | 924 | 313/ 0 | 317 | 64.4 | 9.8 | 9.5 | 6.9 | 6.7 | 289.3 | 308.8 | 0.00 | 0.01 | 2993 | 1.6 | 18 | 1.1 | 1.5 | -103 | -103 | -103 | -103 |

| TIME | PRES | VOR/DME | HDG | TAS | RSMT | RFT | DEW | Q | THETA | TH-E | LWC | FWC | MM | CONC | DBAR | 2DC | 2DP | RAD1 | RAD2 | RAD3 | RAD4 |
|---|---|---|---|---|---|---|---|---|---|---|---|---|---|---|---|---|---|---|---|---|---|
| 1034 4 | 926 | 315/ 0 | 317 | 62.6 | 9.8 | 9.4 | 6.7 | 6.6 | 289.2 | 308.4 | 0.00 | 0.01 | 2912 | 2.1 | 14 | 2.6 | 2.1 | -103 | -103 | -103 | -103 |

| TIME | PRES | VOR/DME | HDG | TAS | RSMT | RFT | DEW | Q | THETA | TH-E | LWC | FWC | MM | CONC | DBAR | 2DC | 2DP | RAD1 | RAD2 | RAD3 | RAD4 |
|---|---|---|---|---|---|---|---|---|---|---|---|---|---|---|---|---|---|---|---|---|---|
| 1034 5 | 922 | 313/ 0 | 318 | 61.7 | 9.6 | 9.5 | 6.9 | 6.7 | 289.4 | 308.9 | 0.00 | 0.01 | 2842 | 2.2 | 17 | 0.8 | 2.2 | -103 | -103 | -103 | -103 |

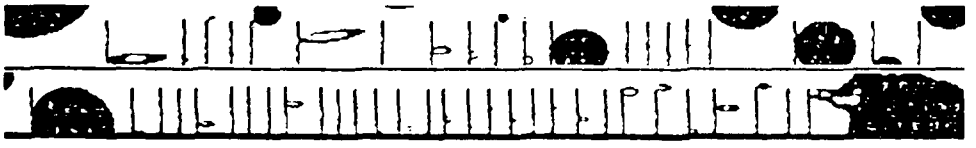

| TIME | PRES | VOR/DME | HDG | TAS | RSMT | RFT | DEW | Q | THETA | TH-E | LWC | FWC | MM | CONC | DBAR | 2DC | 2DP | RAD1 | RAD2 | RAD3 | RAD4 |
|---|---|---|---|---|---|---|---|---|---|---|---|---|---|---|---|---|---|---|---|---|---|
| 1034 6 | 922 | 313/ 0 | 319 | 62.1 | 9.5 | 9.3 | 6.9 | 6.7 | 289.2 | 308.7 | 0.00 | 0.01 | 2805 | 1.7 | 20 | 3.0 | 1.8 | -103 | -103 | -103 | -103 |

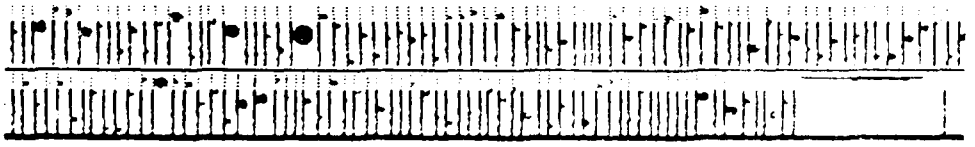

Figure 3.2 Example of images from PMS 2D-C probe (larger images with vertical scale of 800 microns) and 2D-P probe (smaller images with vertical scale of 6.4 mm).

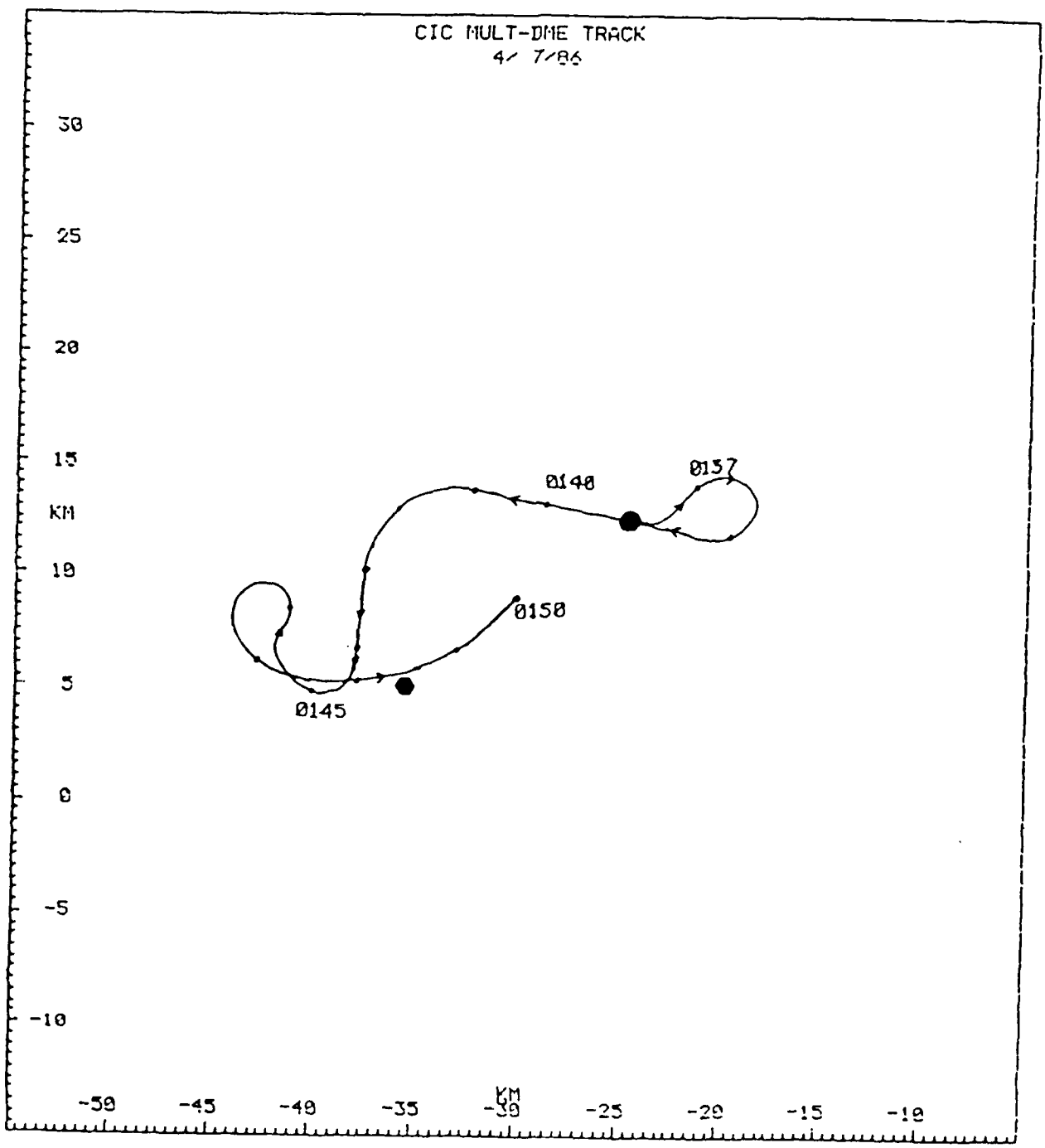


Figure 3.3 Sample plot of aircraft position from the CIC multiple DME system.

for the priority days.

### 3.2.3 PMS Hydrometeor & Ka-band Radar Data Comparison.

Figures 3.4 - 3.5 are examples of the correlation between the reflectivities from the airborne Ka-band radar and the equivalent radar reflectivity integrated from the PMS hydrometeor spectra. The hydrometeor data are corrected for artifact rejection (artifacts created by particles colliding with the probe tips, cloud water streaking across the mirrors, etc.) using the algorithm reported by Cooper (1978). The airborne Ka-band radar sees hydrometeors well ahead of the aircraft (from 0.6 to 36 km), and these data are adjusted in time using the recorded true airspeed to correspond with the PMS particle imaging data. The data in Figures 3.4 & 3.5 show a casual correlation between equivalent reflectivity from the integrated hydrometeor spectra and the first range bin of the airborne data, but we fail to see any correlation extending beyond the first range gate. We feel that this is due to the very light precipitation (maximum of 2 mm diameter drops), and that the reflected radar signal was lost in the noise past the first range gate.

Figure 3.6 shows an ensemble plot of equivalent radar reflectivity from the 2DP probe versus the first range gate of the airborne radar, and indicates that the data contain a large degree of variance.

### 3.2.4 Spectral Analysis.

The correlation between two variables can be examined in the frequency domain using FFT analysis techniques. Figures 3.7a, b and c show the correlation between the first range gate from the airborne Ka-band radar reflectivity (adjusted in time) and the equivalent reflectivity from the integrated spectra seen by the 2DP probe. The coherence plot shows significant correlation out to about 0.05 Hz, which corresponds to 1.6 km at a true airspeed of 80 m/s. This is some indication of the degree of stationarity in the precipitation field during this mission.

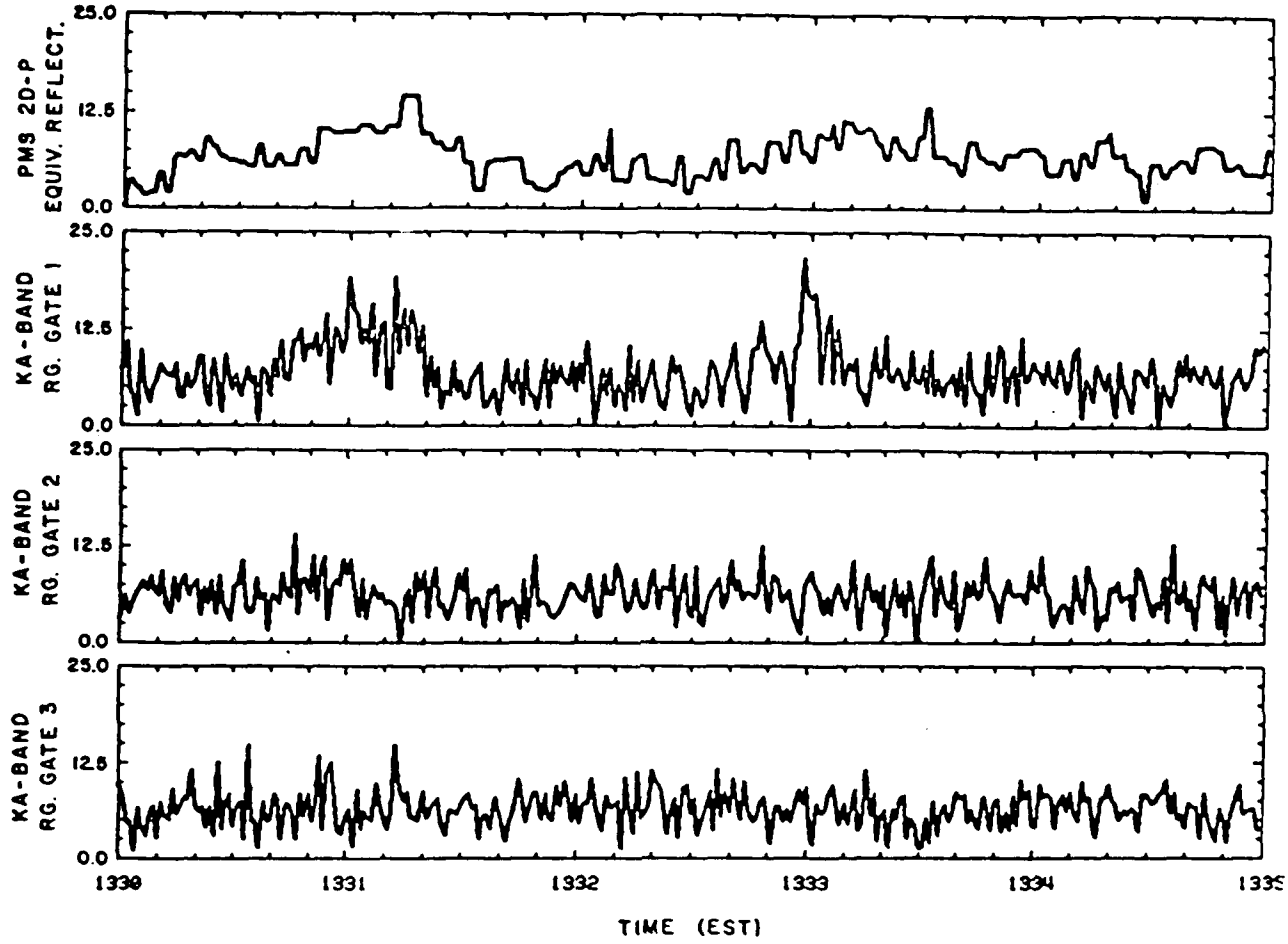


Figure 3.4 Example of time series data showing equivalent reflectivity from PMS 2D-P image data (top) and reflectivities from the first three range gates of the airborne Ka-band radar which have been shifted in time to correspond with the position in space of the image data collected on 5/12/86.

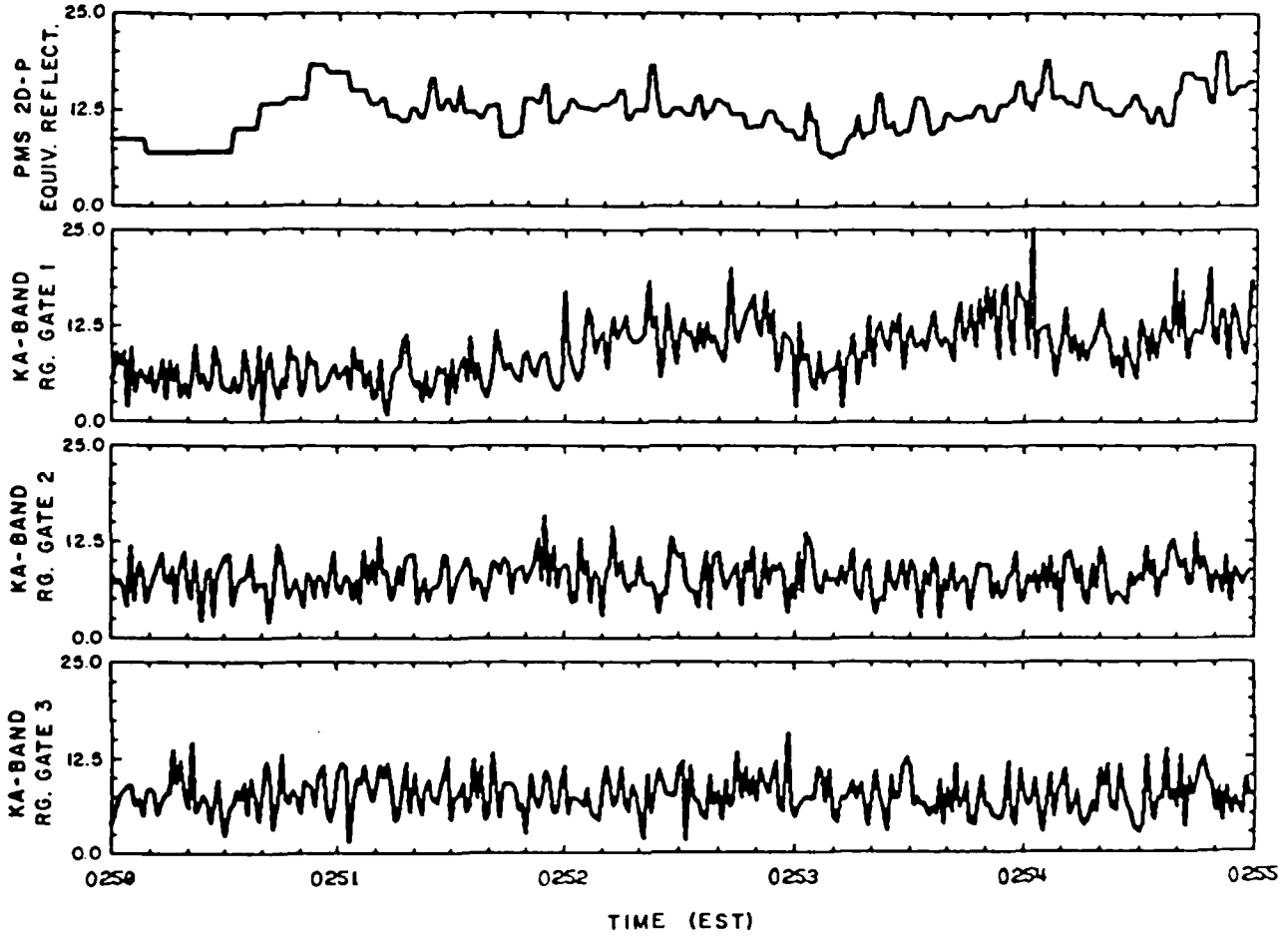


Figure 3.5 As in Figure 3.4 except for data collected on 5/17/86.

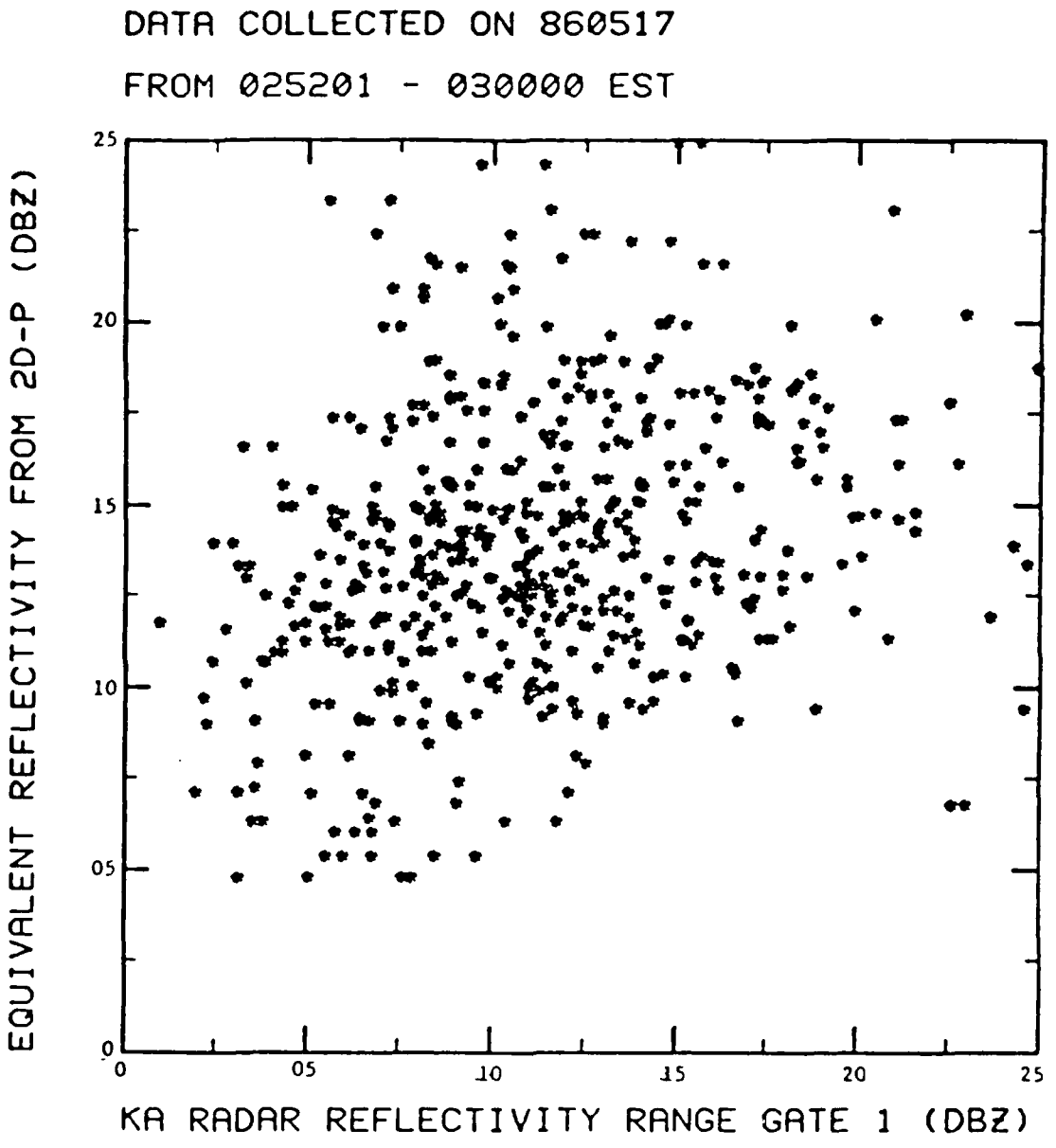


Figure 3.6 Scatterplot of the equivalent reflectivity from the PMS 2D-P probe plotted against the (time adjusted) reflectivity from the first range gate of the airborne Ka-band radar.

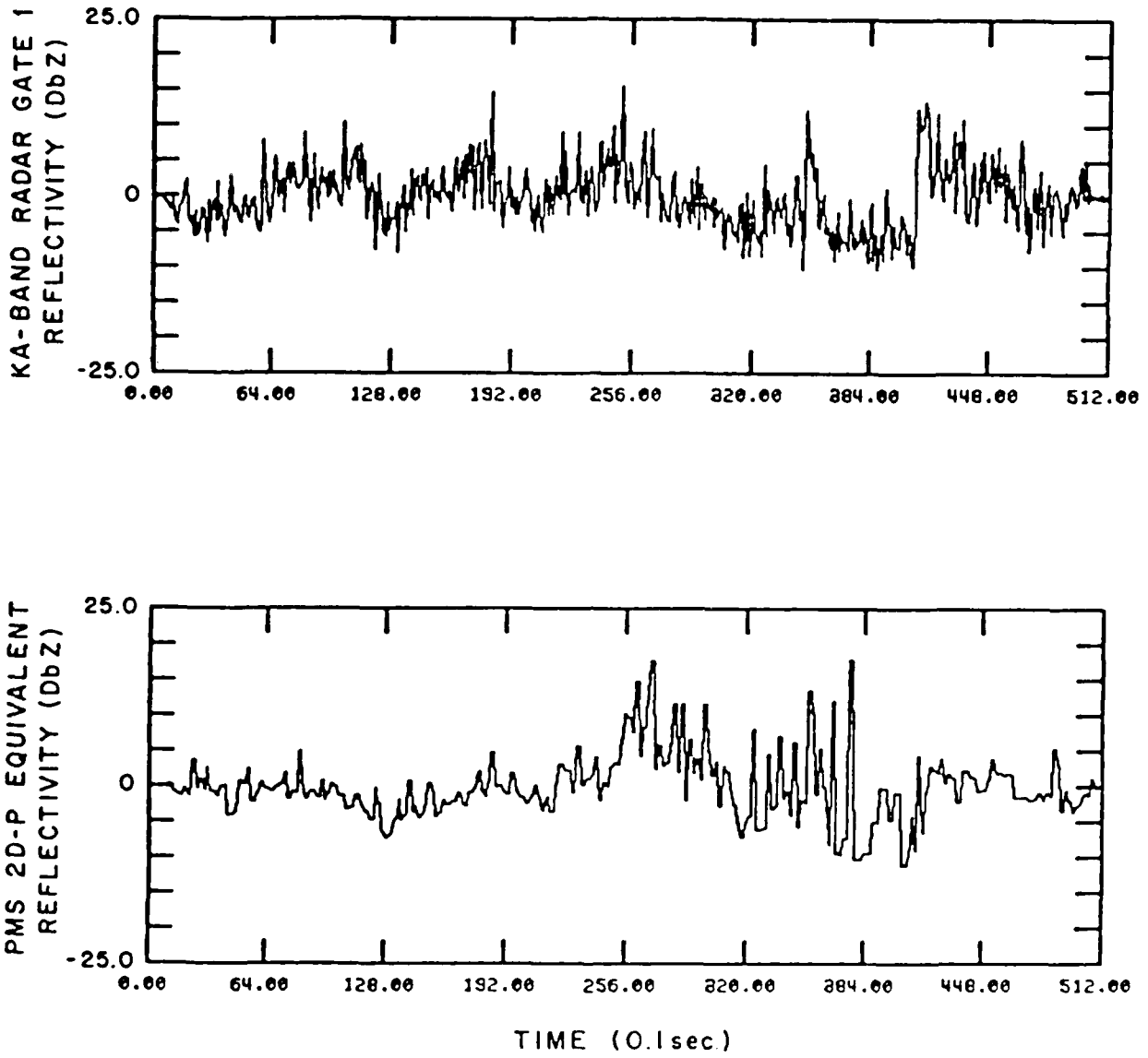


Figure 3.7a Time series data with mean and trend removed for aircraft Ka-band radar reflectivity from (time adjusted) range gate 1 and cloud water content from integrated PMS 2D-P image data.

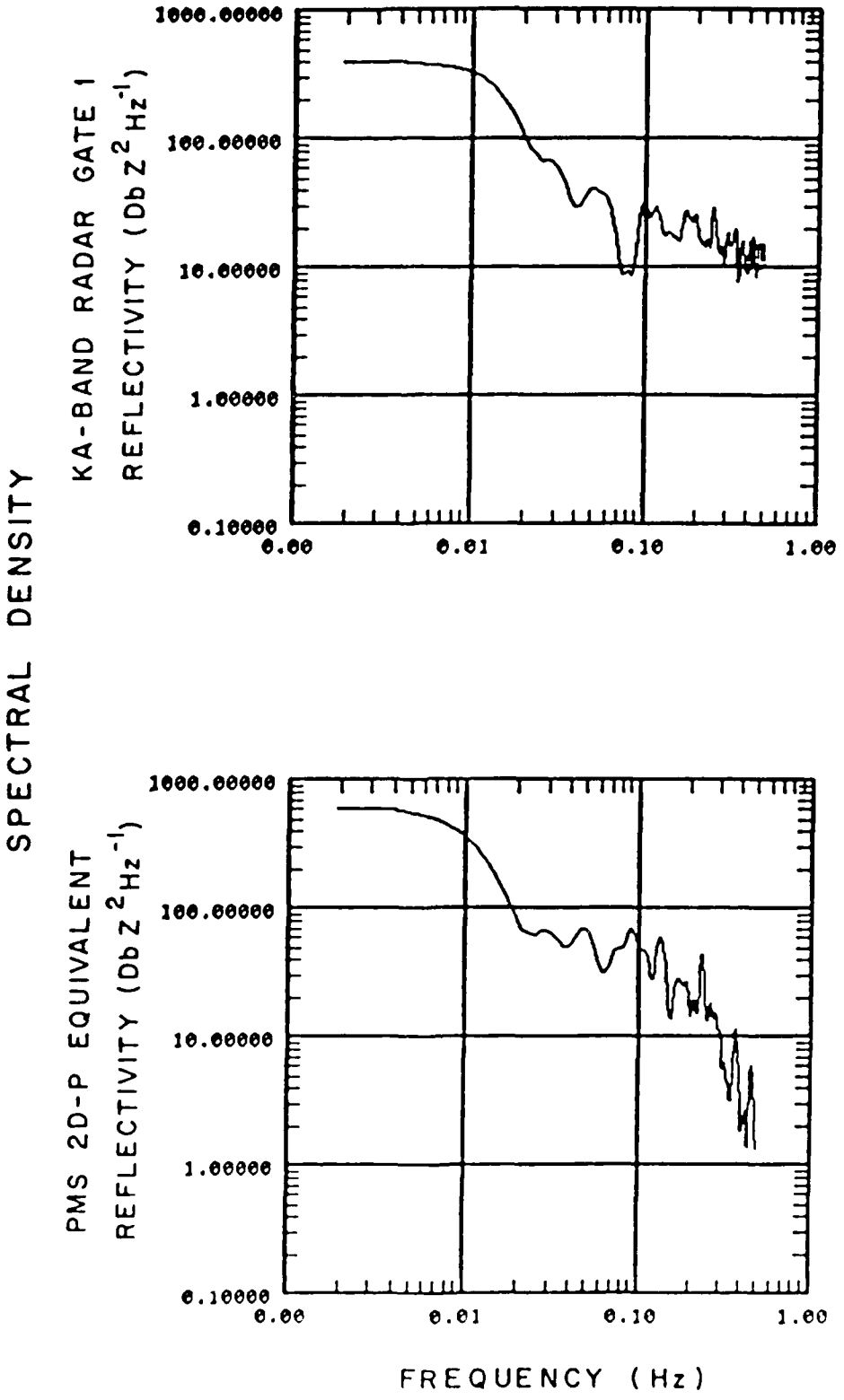


Figure 3.7b Spectral densities for time series data shown in Figure 3.7a

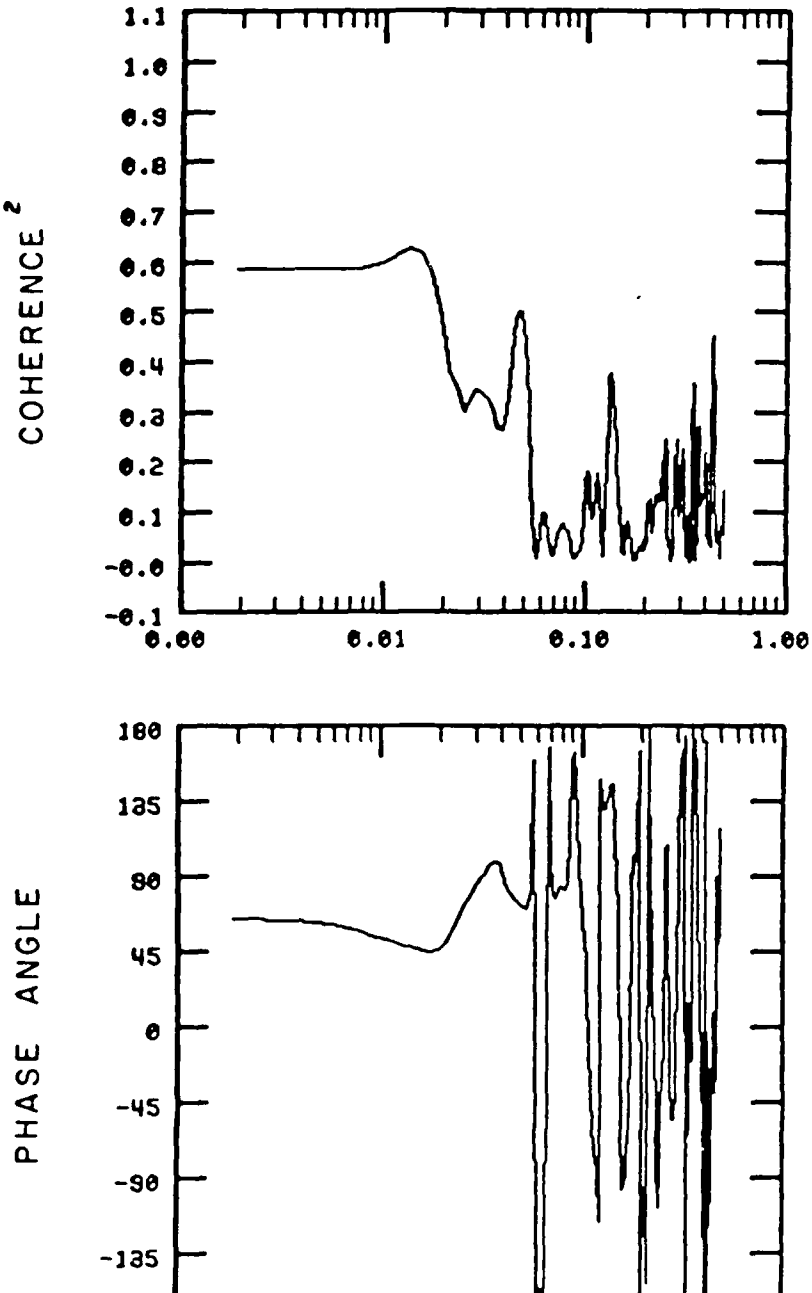


Figure 3.7c Coherence and phase angle plots of Ka-band radar reflectivity from first range gate and equivalent reflectivity calculated from PMS 2D-P image data.

## 4.0 CASE STUDIES.

### 4.1 Overview.

As pointed out in Section 1.0, understanding the physical chain of events leading to the formation of precipitation is the major concern in describing characteristics of the melting layer. During the field observational period the Baron research aircraft collected data at various levels above, below and near the $0^{o}C$ level. The purpose of this section is to examine the images as seen by the PMS 2D probes and correlate these observations with the formation of precipitation.

Vertical cross sections of the 2DP data have been analyzed and for each leg of the flight track the 2DP images have been studied to determine the occurrence of various types of solid precipitation and to estimate the elevation at which these hydrometeors melted. Since funding for analyses of these cases is limited, we have chosen to present a brief description of the five cases selected, with a more detailed analysis of a portion of the 27 April case. This case provided the best example of a steady state episode which allowed us to draw some generalizations. The other cases generally support the major findings of the 27 April study, and a summary of these results is presented in Section 4.6.

### 4.2 Case Study I (4.7.86)

On this day the aircraft first climbed to about 3000 m and made a NE pass over the area. The temperature at this level was $3.3^{o}C$. Along this track the PMS 2DP probe showed a mixture of graupel and needles (mostly in mutually exclusive pockets of one or the other). Near the end of this leg there were graupel particles and signs of riming. There were moderate sized 2DC images also showing evidence of riming.

Leg two was the reverse pass (westerly) at the same altitude and showed similar images. There were a few aggregates on this pass.

The aircraft then descended to about 1500 m where the temperature was $4.0^{o}C$. All along this leg the 2DP showed a uniform pattern of rain images. Next the aircraft climbed to about 1650 m where the temperature was $3.5^{o}C$. Along this leg there were mostly 1.2 mm raindrops.

Image data for the remainder of the flight are not available.

### 4.3 Case Study II (4.26.86)

The first two legs of this flight were made at about 2000 m where the temperature was $2.4^{o}C$. Image data for this portion of the flight were not available. Leg three was made in a southwesterly direction at 1900 m ($1.6^{o}C$). The images show mostly raindrops with an occasional unmelted aggregate observed.

especially near the western end of the track.

The aircraft next climbed to 2150 m (2.2$^{o}$C) and started leg four in a NE direction. On this leg there were large unmelted aggregates mixed with small raindrops. Some of the aggregates were quite large. The aircraft then ascended to about 2200 m (1.4$^{o}$C) and started leg five. Again on this leg there were large unmelted aggregates mixed with small raindrops.

Leg six was flown at 2300 m where the temperature was just about 0$^{o}$C. The images were a mixture of medium-sized aggregates and graupel particles, which did not co-exist but appeared to occur in patches, a re-occurring theme found in the data. There was a large variation in particle concentration along this leg. Leg seven was flown at 2400 m ( 0.4$^{o}$C and had images very similar to leg six (mixture of aggregates and graupel). Leg eight was a reciprocal leg of seven and showed the same types of images as did leg nine.

Leg ten started at 2500 m, then the aircraft ascended to about 2700 m (-1.2$^{o}$C). The images were a mixture of large aggregates and small graupel The 2DC malfunctioned and the image data were unusable on this leg. Next the aircraft ascended to 2800 m (-1.8$^{o}$C) and made legs eleven and twelve at this altitude. The images on these legs were mostly graupel particles with a few large aggregates, and some needles.

At 0342 EST the aircraft descended to about 1800 m (2.9$^{o}$C and conducted leg 13. On this leg there were mostly 1-3 mm raindrops with a few large, unmelted aggregates.

4.4 Case Study III (4-27-86).

This case has the most extensive set of cloud physics data with 25 legs flown in three separate vertical profiles. Table 4.1 describes the first 11 legs on this flight. The aircraft ascended from 1800 to 2700 m while making transects from Hanscom AFB to Sudbury. The principle precipitation mechanism during this profile seemed to be an aggregation process. Large aggregates (2-5 mm) were observed to form just above the 0$^{o}$C level and melted forming 1-2 mm rain after descending about 800 m. Occasional large melted aggregates were observed along with the rain drops. There were few graupel particles observed during this profile, and the accretional growth of ice into graupel particles did not appear to be a significant precipitation mechanism. This vertical profile is notably different from that observed later (0120 - 0214) which showed discrete pockets of either graupel or aggregates.

TABLE 4.1. Description of Hydrometeors Observed by the PMS Probes on the Baron Aircraft During the First Vertical Profile on 27 April 1986.

| Leg | Time(EST) | Altitude(m) | Image Characteristics |
|---|---|---|---|
| 1 | 0014-0019 | 1800 (2.0°C) | mostly rain, few large unmelted aggregates |
| 2 | 0019-0024 | 1800 (2.0°C) | same as above |
| 3 | 0025-0028 | 1800 (2.0°C) | same as above |
| 4 | 0028-0032 | 2135 (0.3°C) | mostly rain, frequent large aggregates |
| 5 | 0033-0038 | 2135(0.3°C) | same as above |
| 6 | 0038-0048 | 2275(0.4°C) | pockets of large aggregates, small stellars, small drops |
| 7 | 0048-0053 | 2275(0.4°C) | aggregates, ice particles |
| 8 | 0055-0100 | 2431(-0.6°C) | large aggregates, few small rimed ice or graupel embryos |
| 9 | 0101-0106 | 2431 (-0.6°C) | mixture aggregates, graupel embryos, stellar ice |
| 10 | 0108-0113 | 2600 (-1.3°C) | many small aggregates made of needles, ice particles |
| 11 | 0114-0119 | 2586 (-1.2°C) | few large aggregates, mostly small ice, some graupel embryos. |

Table 4.2 lists the characteristics of the next eleven legs. This profile characterizes the pattern which we have seen in several other portions of the data, in that graupel particles and aggregates appear to exist in separate pockets across the cross section. The mechanisms responsible for the generation of these inhomogeneous regions are beyond the scope of this analysis (the aircraft did not ascend above $-3^{o}C$, where the formation of the graupel and ice particles originated).

Figure 4.1 is an analysis of the vertical cross section of the data from 0120 - 0214, which suggests that there were two distinct regions of hydrometeor types. In the southwestern region (near Sudbury), relatively high concentrations (up to 30 $L^{-1}$ of ice and graupel particles were observed above the melting layer, while over the northeastern area (near Hanscom AFB), smaller concentrations of ice particles and aggregates were found above the $0^{o}C$ level. Examples of the images from these two regions are shown in Figure 4.2. The graupel particles co-existed with a significant region of supercooled liquid water, while the aggregates did not. This regime seemed to persist in a spatial relationship commensurate with the shear of the mean wind as the aircraft ascended, and therefore appears to be a quasi steady-state feature. This is substantiated by the rapid spiral descent from 2700 - 1800 m at 2115 which showed the evolution of graupel to small rain. Below the melting layer, the 2DP images suggest that the graupel melted into fairly uniform, small (1 mm) raindrops at a level very close to $0^{o}C$. On the other hand, the aggregates did not melt uniformly and some partially melted aggregates are seen down to $+3^{o}C$, where there is a larger variance in the precipitation spectrum and several larger (1-3 mm) raindrops are observed. Examples of images from these two regions below the melting layer are also shown in Figure 4.2. It thus appears that the aggregation process may have been more efficient in utilizing the available supercooled cloud water, generating larger particles which took longer to melt and subsequently produced larger raindrops. This is contrary to observations in summertime cumuli (Cooper and Lawson, 1984) and is discussed further in Section 4.6.

TABLE 4.2. Description of Hydrometeors Observed by the PMS Probes on the Baron Aircraft During the Second Vertical Profile on 27 April 1986.

| Leg | Time(EST) | Altitude(m) | Image Characteristics |
|---|---|---|---|
| 1 | 0120-0124 | 1800(3.7°C) | 1 mm rain SW; 1-2 mm rain & unmelted aggregate NE. |
| 2 | 0124-0129 | 1800(3.7°C) | same as above |
| 3 | 0130-0135 | 2130(1.8°C) | same as above |
| 4 | 0136-0141 | 2130(1.8°C) | same as above |
| 5 | 0141-0146 | 2244(0.7°C) | mixed 1 mm graupel & rain SW; mixed 1-2 mm rain & 2-5 mm aggregate NE |
| 6 | 0146-0152 | 2275 (0.3°C) | same as above |
| 7 | 0153-0158 | 2445 (0°C) | same as above |
| 8 | 0158-0204 | 2400 (-0.6°C) | ice & 0.5 1 mm graupel SW; ice and 2-5 mm aggregate NE |
| 9 | 0204-0209 | 2650 (-1.5°C) | ice and 0.5 mm graupel SW; ice and 1 mm aggregate NE |
| 10 | 0209-0214 | 2757 (-2.0°C) | same as above |
| 11 | 0215-0220(Spiral Descent over SUD) | | Graupel increasing from 0.5 to 2 mm and melting to form 1 mm rain |

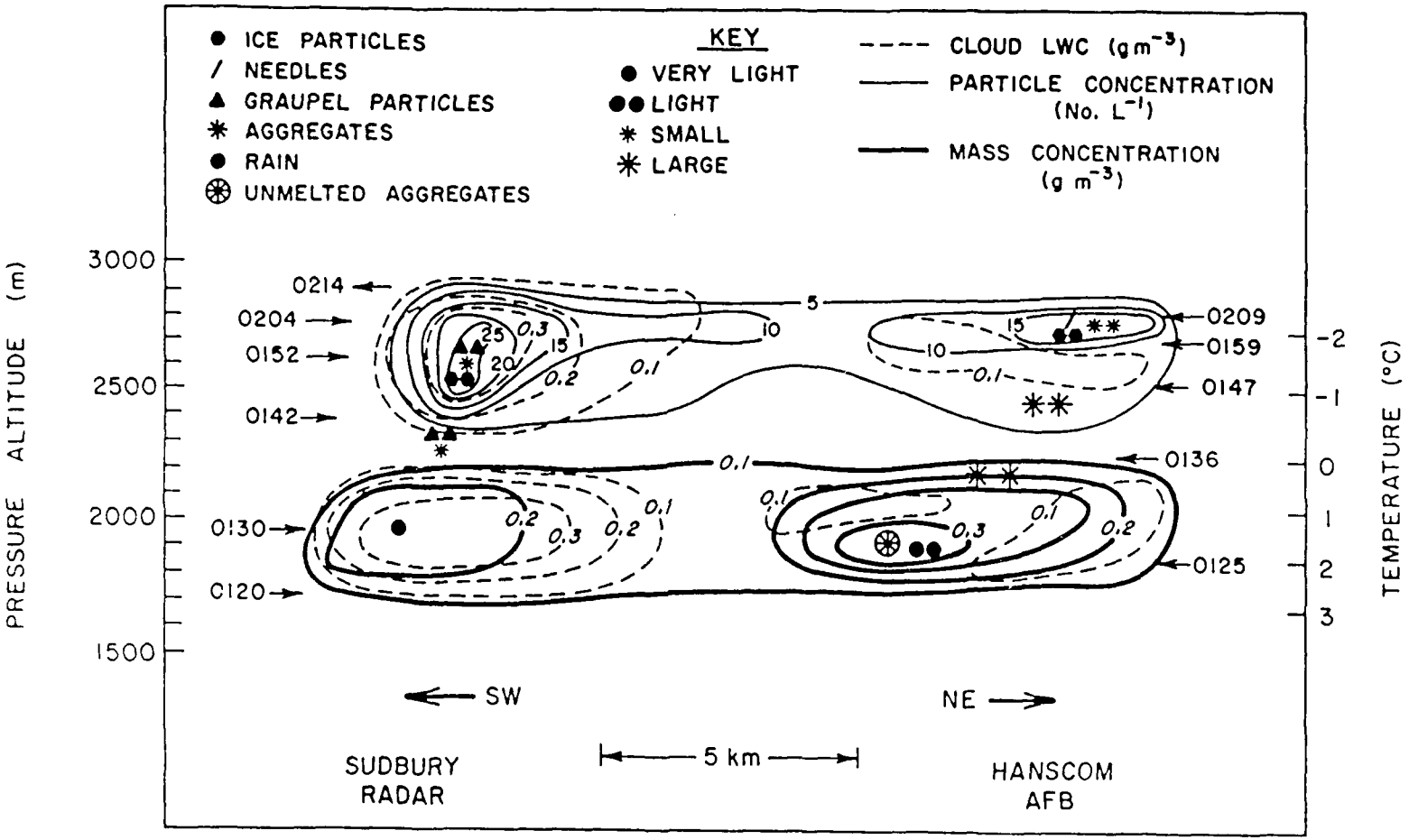


Figure 4.1 Vertical cross-section of hydrometeors and cloud liquid water content derived from data collected by the Baron research aircraft on 4/27/86.

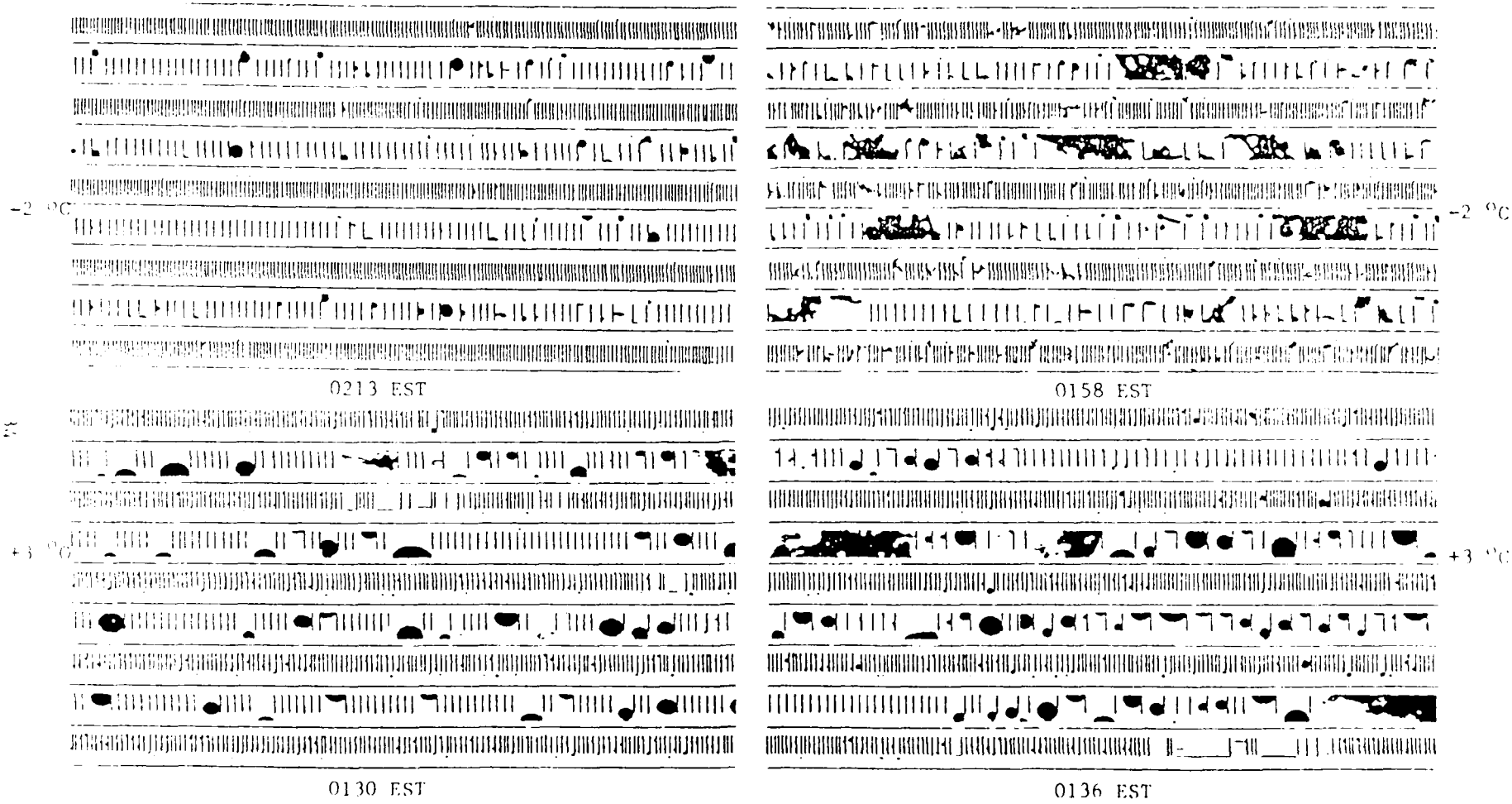


Figure 4.2 Examples of PMS images from the 2D probes obtained over the southwest portion of the flight (left side of page) and over the northeast portion of the flight track (right side of page) at -2 °C and +3 °C on 27 April 1986.

## 4.5 Case Study IV (5-17-86)

The flight profile for this case was very similar to the previous cases. There were six significant periods during this flight and they are summarized and shown in Table 4.3.

TABLE 4.3. Description of Hydrometeors Observed by the PMS Probes on the Baron Aircraft on 17 May 1986.

| Leg | Time(EST) | Temperature(m) | Image Characteristics |
|---|---|---|---|
| 1 | 0300-0310 | 0.4°C | large unmelted aggregate, small rain. |
| 2 | 0311-0318 | 0°C | large unmelted aggregate, graupel, needles |
| 3 | 0318-0320 | -0.8°C | very large aggregate, mixed graupel |
| 4 | 0325-0327 | -1.4°C | mixture aggregate, needles, ice particles |
| 5 | 0327-0338 | -2.3°C | more graupel, rimed ice, clumps of rimed particles |
| 6 | 0340-0359 | -4.4°C | needles, dendrites, clumps, rimed ice |
| | 0352-descent | | unmelted aggregate to 4.1°C |

## 4.6 Summary of Case Studies.

Figure 4.3 shows a summary of the results of the case studies. The characteristics of the images are graphically depicted as a function of temperature for each of the vertical profiles obtained, and a typical cloud liquid water content (1 - 30 micron droplet diameter) is shown. This figure clearly shows a systematic sequence of events as the cloud particles pass through the melting layers. Those events are as follows:

A. At temperatures -2°C and colder there is usually a mixture of graupel embryos (or rimed ice particles of about 0.3-0.5 mm), ice particles and small aggregates. The graupel embryos are often associated with pockets of liquid water content of a few tenths of a gram per cubic meter. These pockets are usually distinct from pockets of ice particles and small aggregates where the liquid water has been depleted. The spatial dimension of these pockets is on the order of 10 km.

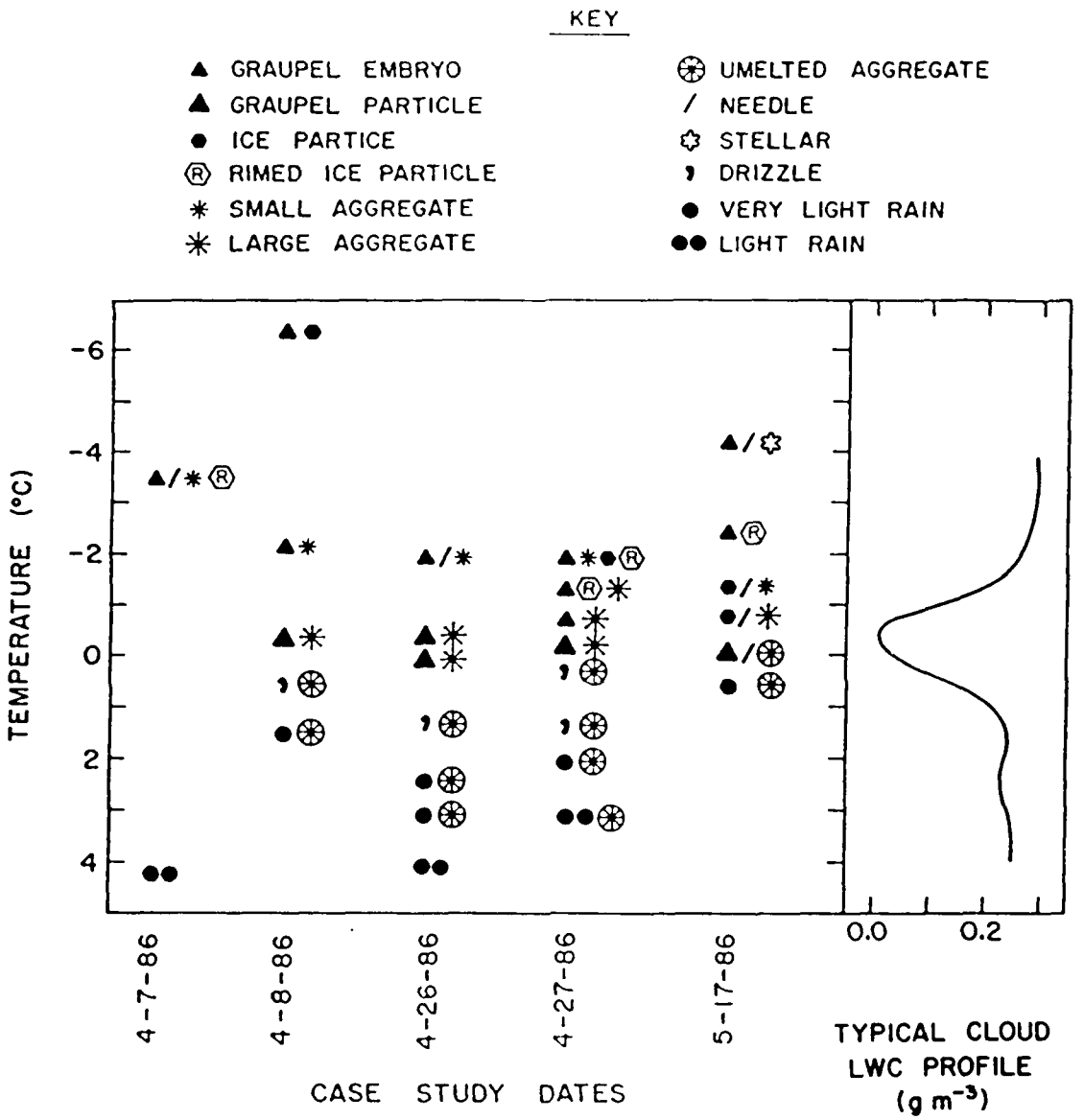


Figure 4.3 Summary of data from five case studies showing vertical profile of cloud liquid water content and evolution of hydrometeors.

B. Ice and small aggregates form large aggregates beginning at about $-2^{o}C$. This process proceeds very rapidly with large aggregates forming near the $0^{o}C$ level. When present, pockets of graupel embryos and ice grow (slowly due to the low LWC) via a wet accretional process to 1 mm graupel.

C. Near $0^{o}C$ there is a mixture of large aggregates and sometimes graupel particles, usually in discrete pockets of ~10 km across. Aggregation appears to continue through this layer while the graupel particles start to melt.

D. At about $0.3^{o}C$ small (1-2 mm) melting aggregates and large (2-5 mm) unmelted aggregates are observed. When present, melting small (1-2 mm) graupel particles and 1 mm rain drops are observed in pockets which are usually separate from the aggregates.

E. At $+2^{o}$ to $+4^{o}C$ large (2-5 mm) unmelted aggregates are mixed with smaller (1 mm) raindrops; any graupel particles all appear to have melted into 1 mm rain.

The primary precipitation mechanism appears to be through an aggregation process, starting with 0.2 - 0.5 mm ice particles (often needles) near $-3^{o}C$ and small aggregates, and leading to the formation of large (2-5 mm) aggregates near the $0^{o}C$ level. These aggregates melt to form 1 2 mm rain with occasional large (2-5 mm) unmelted aggregates falling to ~800 m below $0^{o}C$. Sometimes, a very different precipitation process is observed which starts with graupel embryos (~0.5 mm rimed ice particles) at $-3^{o}C$, and proceeding through an accretional process which leads to the formation of small (1 mm) rain. The aggregation process appears to be more efficient in the utilization of cloud liquid water, and we suspect that this is due to the long residence time of the (slowly falling) aggregates in the region above the melting layer, resulting in dry growth from vapor deposition. The graupel particles, on the other hand, have larger fall velocities and pass quickly through the region of supercooled water above the melting layer, scavenging out a small percentage of the total volume. The relative importance of the two mechanisms is the reverse of that seen in summertime convective clouds where wet accretion is the primary precipitation process, and aggregation is usually secondary (Cooper and Lawson, 1984). This is due to the much higher initial liquid water contents of convective clouds (favoring accretional growth), and the subsequent rapid depletion of cloud water via entrainment (reducing the lifetime shortens the residence time for growth via vapor deposition and subsequent aggregation).

It appears that the partially melted, large aggregates, may be an explanation for the increase in radar reflectivity. It is shown that these particles can exist up to 800m or so below the $0^{o}C$ level. The vertical profiles observed here are similar to those seen by other investigators (see Section 1.0 and Figure 1.1), and it appears that aggregation may play an important role

in the formation of bright bands in general.

The curious part of this chain of events is how these large aggregates develop so fast just above the 0°C level. The "aggregation zone" near 0°C has often been associated with rapid rates of aggregation (Rogers, 1973). Rapid aggregation rates have also been observed by Cotton et al. (1986) at much colder temperatures (-10 to -12°C) in wintertime storms over the Park Range in Colorado. Numerical simulations by Cotton et al. (1986) suggest that the major term in the aggregation process is the scavenging of smaller ice crystals by mature (large) aggregates via a sedimentation process. Figure 4.3 shows that at -3° to -4°C there are mostly single crystals and small clumps. But at about -2°C aggregation proceeds rapidly through to the 0°C level (distance of 300-400 m) with fall velocities of about 1 m/sec. That is, the aggregation process apparently took only 5-8 minutes, and the rate of aggregation appeared to accelerate rapidly near the 0°C level, which was also coincident with the formation of larger aggregates which would be required to scavenge smaller ice particles and aggregates via sedimentation.

## 5.0 EVALUATION OF THE M-METER

We have previously submitted a preliminary analysis of the M-meter in a special technical report to the AFGL. Subsequent refinement of the data reduction procedure which includes a bearing friction factor and the effects of heating of the impacted hydrometeors was suggested by Mr. Vern Plank of AFGL, however, lack of funds has prevented this new analysis from being completed. Interested parties should contact Mr. Plank for a current interpretation of the performance of the M-meter.

## 6.0 EVALUATION OF THE KA BAND RADAR AND ATTENUATION MEASUREMENTS.

At the beginning of the project it was thought that a nose-pointing Ka band radar could be used to measure radar reflectivity at various ranges and from these sequential measurements it would be possible to deduce attenuation. However, the Ka band radar installed for this project had a higher noise level then anticipated and thus it was difficult to obtain any clearcut measurements (see section 3.0 for examples). This problem was amplified by the fact that during the project we encountered only light to moderate precipitation. The reflectivity returns were, therefore, very weak and often buried in the noise.

The narrow beam and the small pulse width led to the sampling of relatively small volumes of cloud. From the PMS particle data we know there are large variations in particle sizes over small areas, hence significant reflectivity variations would also be expected on this scale.

Another problem was that the aircraft altered its heading on frequent occasions. This meant that the narrow beam was sampling different cloud volumes compared to those subsequently penetrated. Thus from a practical viewpoint, only range gates within a few kilometers of the radar could be used to correlate to measured hydrometeors.

## 7.0 PERSONNEL

The following personnel worked on this contract:

### CIC Personnel

Dr. Larry G. Davis - Contract Manager

R. Paul Lawson - Principle Investigator and On-Board Scientist
Data reduction and software

Norman Ostrander - Pilot

Brian Jesse - Airborne Technician

### Consultants

Dennis Treddenick - Detrek Engineering-Ka band radar

Dr. Loren Nelson - Ophir Corporation-software

Dave Melita - Ophir Corporation-On-board Scientist; data reduction

## 8.0 REFERENCES


Austin, P.M. and A. Bemis, 1950: A quantitative study of the bright band in radar precipitation echoes. J. Meteor., 7, 165-171.

Battan, L.J., 1973: Radar observations of the atmosphere. Univ. of Chicago Press, Chicago, Il, 324 p.

Cohen, I.D. and H.J. Sweeney, 1983: Melting layer survey final report. AFGL TR-83-0200, No. 848. ADA137911

Cooper, W. A., 1978: Cloud physics investigations by the University of Wyoming in HIPLEX 1977. Univ. of Wyoming Dept. of Atmospheric Science Report No. AS 119

Cooper, W. A. and R. P. Lawson, 1984: Physical interpretation of results from the HIPLEX 1 experiment. J. Climate and Applied Meteor., 23, 523 540.

Cotton, W.R, G.J. Tripoli, R.M. Rauber and E.A Mulvihill, 1986: Numerical simulation of the effects of varying ice crystal nucleation rates and aggregation processes on orographic snowfall. J. Climate and Applied Meteor., 25, 1658-1680.

Cunningham, R.M., 1947: A different explanation of the "bright line". J. Meteor., 4, 163.

Ekpenyong, B. and R. Srivastava, 1970: Radar characteristics of the melting layer, a theoretical study. Univ. of Chicago Dept. of Geophys. Sciences and Illinois Inst. of Tech. Dept. of Elec. Eng., Technical Report No. 16, Lab for Atmos. Probing, Chicago, Illinois.

Gordon, G. and J.D. Marwitz, 1984: An airborne comparison of three PMS probes. J. Atmos. Ocean. Technol., 1, 2227.

Hallett, J. and S.C. Mossop, 1974. Production of secondary ice particles during the riming process. Nature, 249, 2628.

Knight, C., 1979: Observations of the morphology of melting snow. J. Atmos. Sci., 36, 1123 1130.

Knollenberg, R.G., 1976: The response of optical array spectrometers to ice and snow: a study of 2D probe area to mass relationships. Final Report Air Force Geophysics Laboratory, AFGL TR 76 0273. 31 pp. ADA034731

Lawson, R.P., L.G. Davis, and D.S. Treddenick, 1980: Colorado International Corp. airborne seeding and cloud physics studies in HIPLEX 1977 1980. Final Report to U.S. Dept. of Interior.

Lawson, R.P. and R.A. Stewart, 1983: An improved optical ice particle counter. Preprints, Fifth Symposium on Meteorological Observations and Instrumentation, Toronto, 5663 pp.

Lhermitte, R. and D. Atlas, 1963: Doppler fallspeed and particle growth in stratiform precipitation. Proc. Tenth Conf. on Radar Met., Washington, D.C., 297-302.

Marshall, J.S. and K.L.S. Gunn, 1952: Measurement of snow parameters by radar. J. Meteor., 9, 332-327.

Rogers, D.C., 1973: The aggregation of natural ice crystals. M.S. thesis to the Univ. of Wyoming Dept. of Atmospheric Science, 86 pp.

Ryde, J.W., 1946: The attenuation and radar echoes produced at centimetre wavelengths by various meteorological phenomena. Meteorological Factors in Radio Wave Propagation, London, The Physical Society, 169-188.

Stewart, R.E., J.D. Marwitz, and J.C. Pace, 1984: Characteristics through the melting layer of stratiform clouds. J. Atmos. Sci., 32, 237-273.

Wexler, R., 1955: Precipitation growth in stratiform clouds. Quart. J. Roy. Meteor. Soc., 72, 363-371.

# APPENDIX A

## FLIGHT TRACKS

The following flight tracks were obtained using a combination of multi DME data, VOR/DME data, and dead reckoning (integrated heading and true airspeed). The accuracy of the multi-DME system is about 0.2 km in straight flight and 0.5 km in turns. On 4-26 and 4-27 86, the multi DME was inoperative and the position is plotted using only VOR/DME and dead reckoning. The accuracy of the position is degraded to about 1 km in straight flight and 2-3 km in turns. During tape changes when there are no position data the estimated track is shown in dashed lines. On 4-7-86, when the aircraft proceeded north of the primary target area, the position is estimated (but shown as a solid line) due to changes in the cockpit VOR and poor reception from the multi-DME. On 4-26-86 the aircraft proceeded north of the target area in search of precipitataion, but no usable data were obtained, and thus the aircraft position from 0232-0330 EST is not plotted. The heading gyro did not slave properly after 4-8-86 and the heading shown on the 48 hr print out (from the AFGL VAX) is in error. An offset has been added to correct these headings on 4-26-86 ($-135^{o}$) and 4 27 86 ($-200^{o}$). The position shown for Hanscom AFB is $296.5^{o}$ true and 27.6 km, and for the Sudbury radar is $278.5^{o}$ true and 36.1 km. It has come to our attention that the postion that we used for the Sudbury radar may be slightly in error; if this is the case, the aircraft tracks are still valid and the Sudbury radar postiion should be adjusted on the plots.

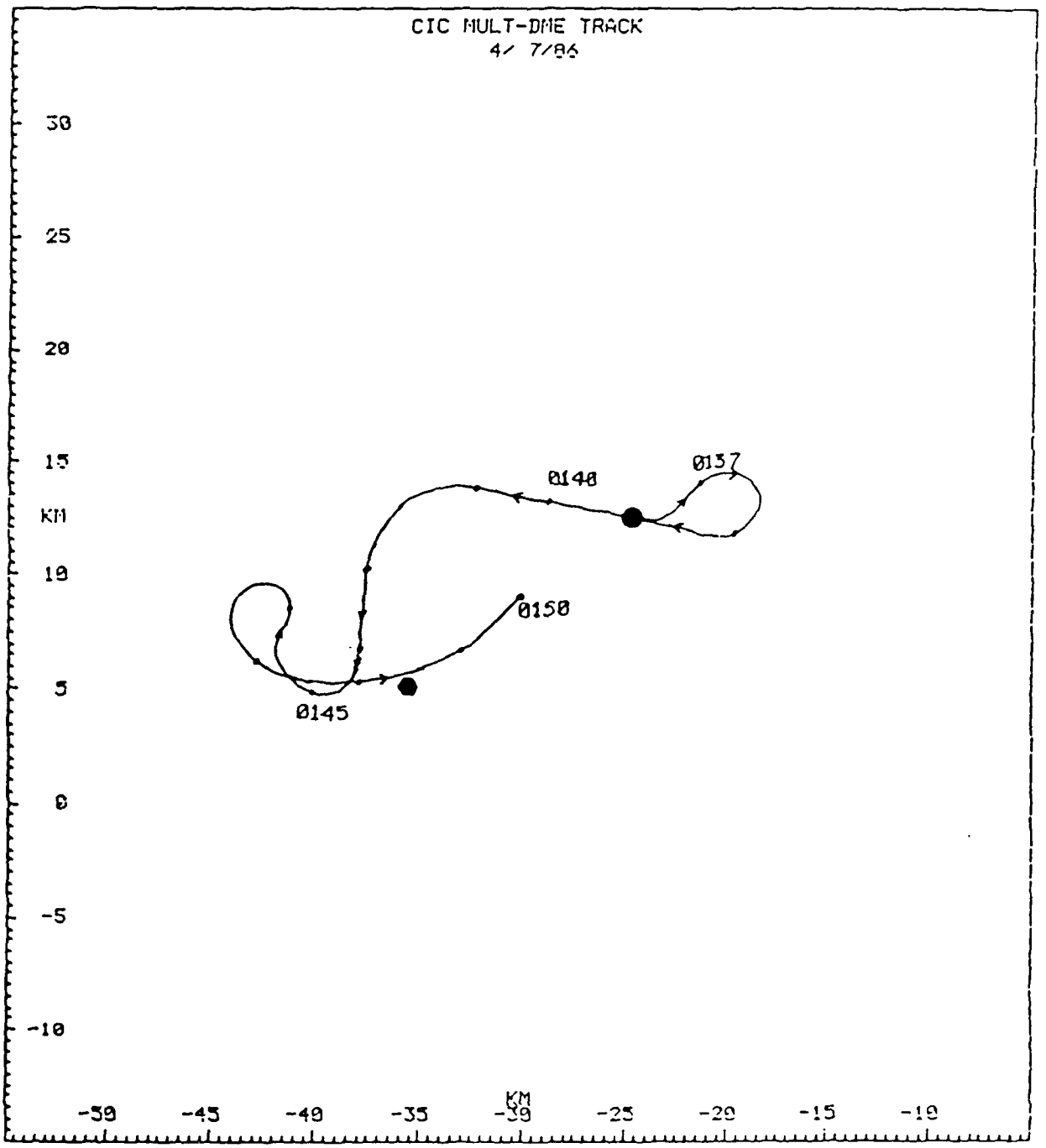
CIC MULT-DME TRACK
4/ 7/86
30
25
20
15
KM
10
5
0
-5
-10
0137
0140
0150
0145
-50
-45
-40
-35
-30
KM
-25
-20
-15
-10

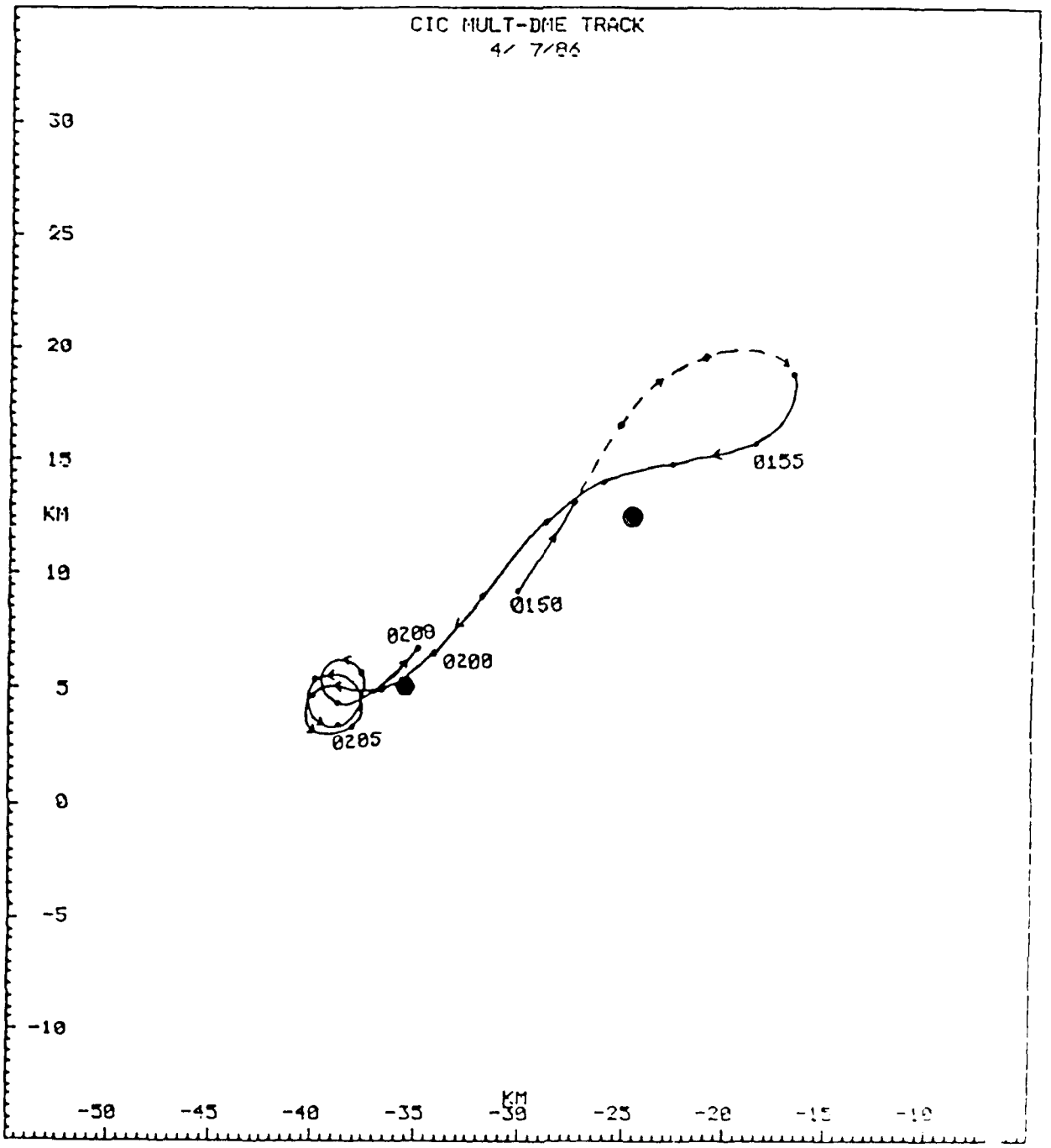
CIC MULT-DME TRACK
4/ 7/86
30
25
20
15
KM
10
5
0
-5
-10
-50
-45
-40
-35
-30
KM
-25
-20
-15
-10
0155
0150
0200
0200
0205

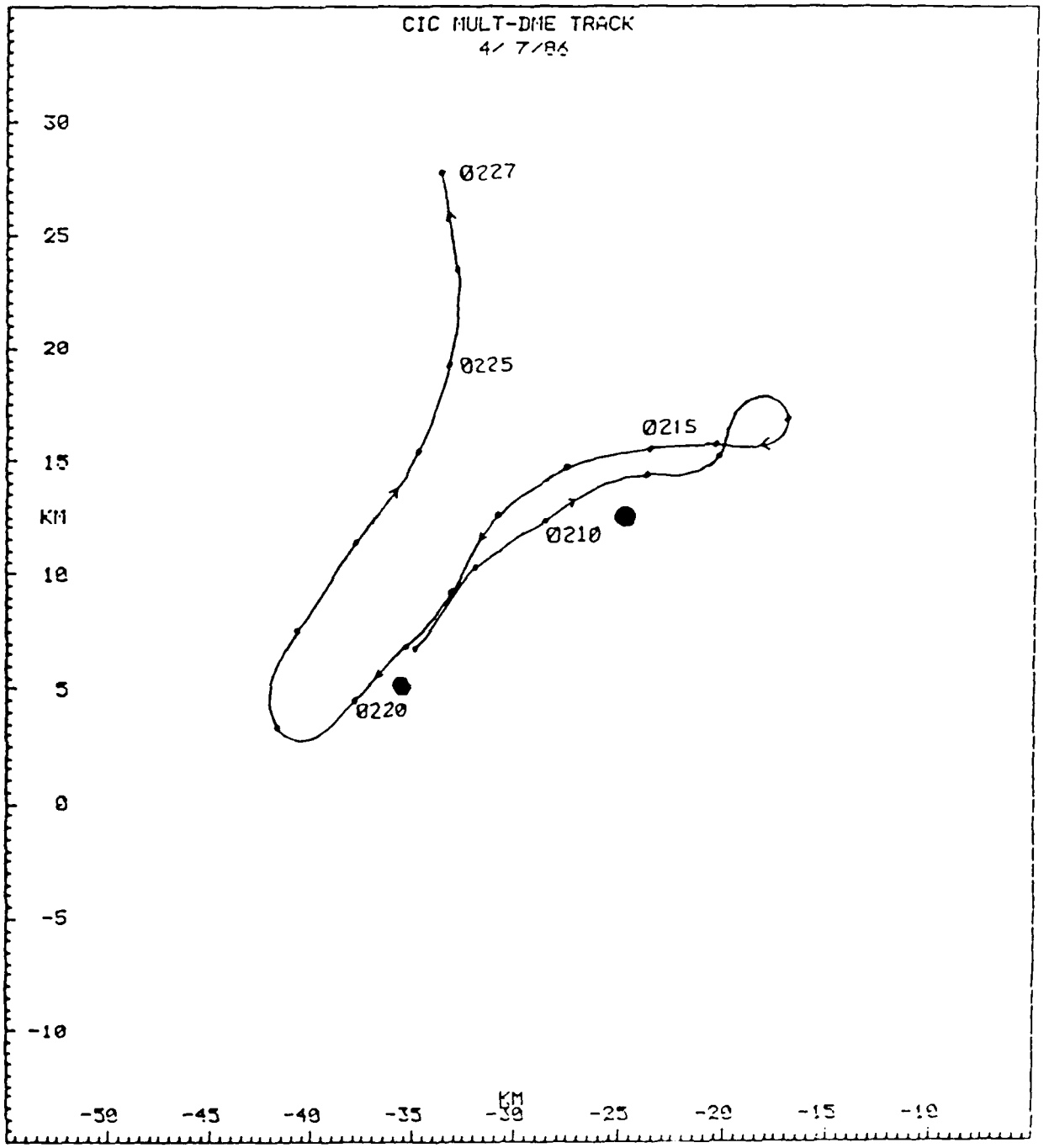
CIC MULT-DME TRACK
4/ 7/86
30
25
20
15
KM
10
5
0
-5
-10
0227
0225
0215
0210
0220
-50
-45
-40
-35
KM
-30
-25
-20
-15
-10

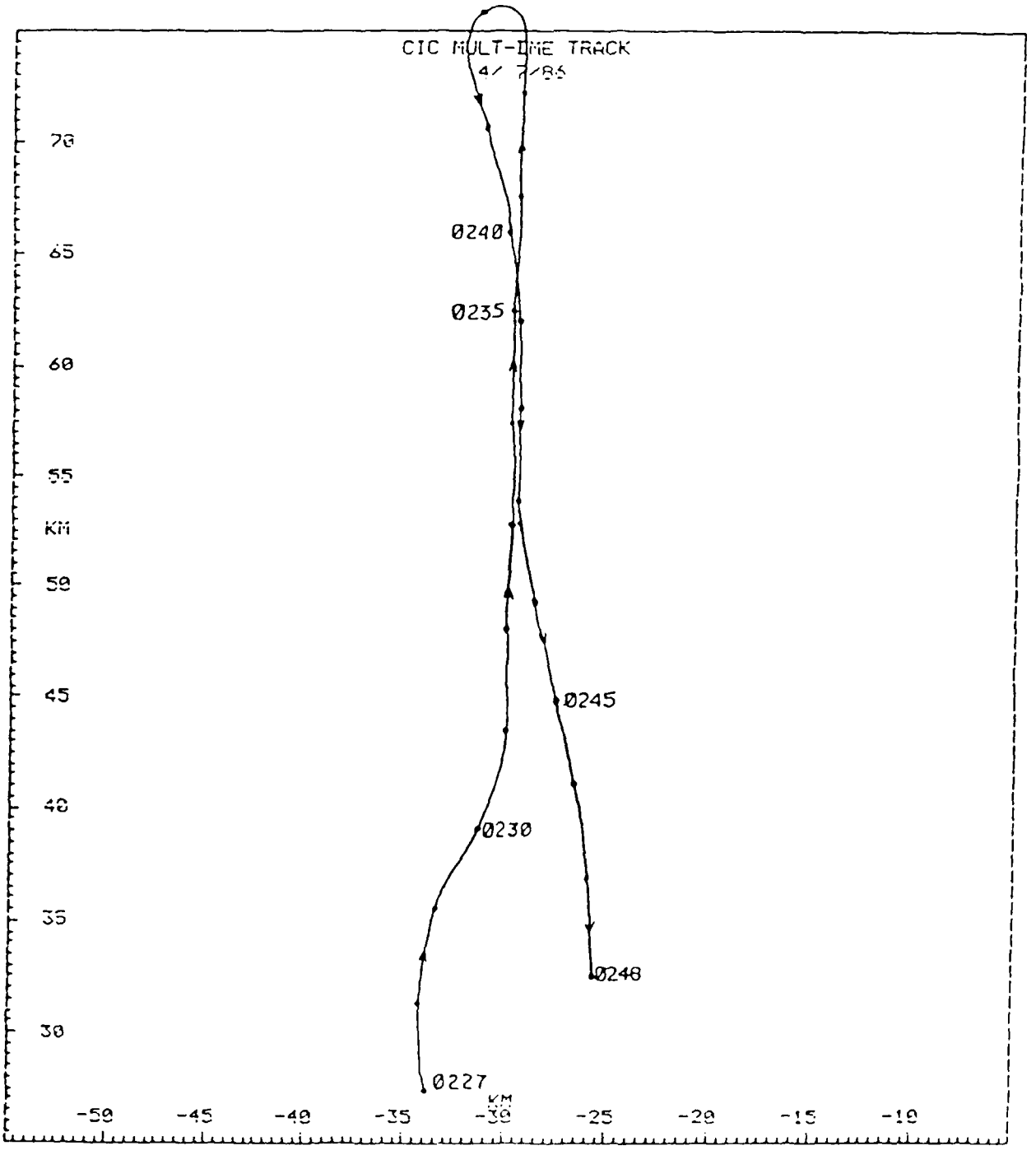
CIC MULT-DME TRACK
4/ 7/85
70
65
60
55
KM
50
45
40
35
30
0240
0235
0245
0230
0248
0227
-50
-45
-40
-35
-30
KM
-25
-20
-15
-10

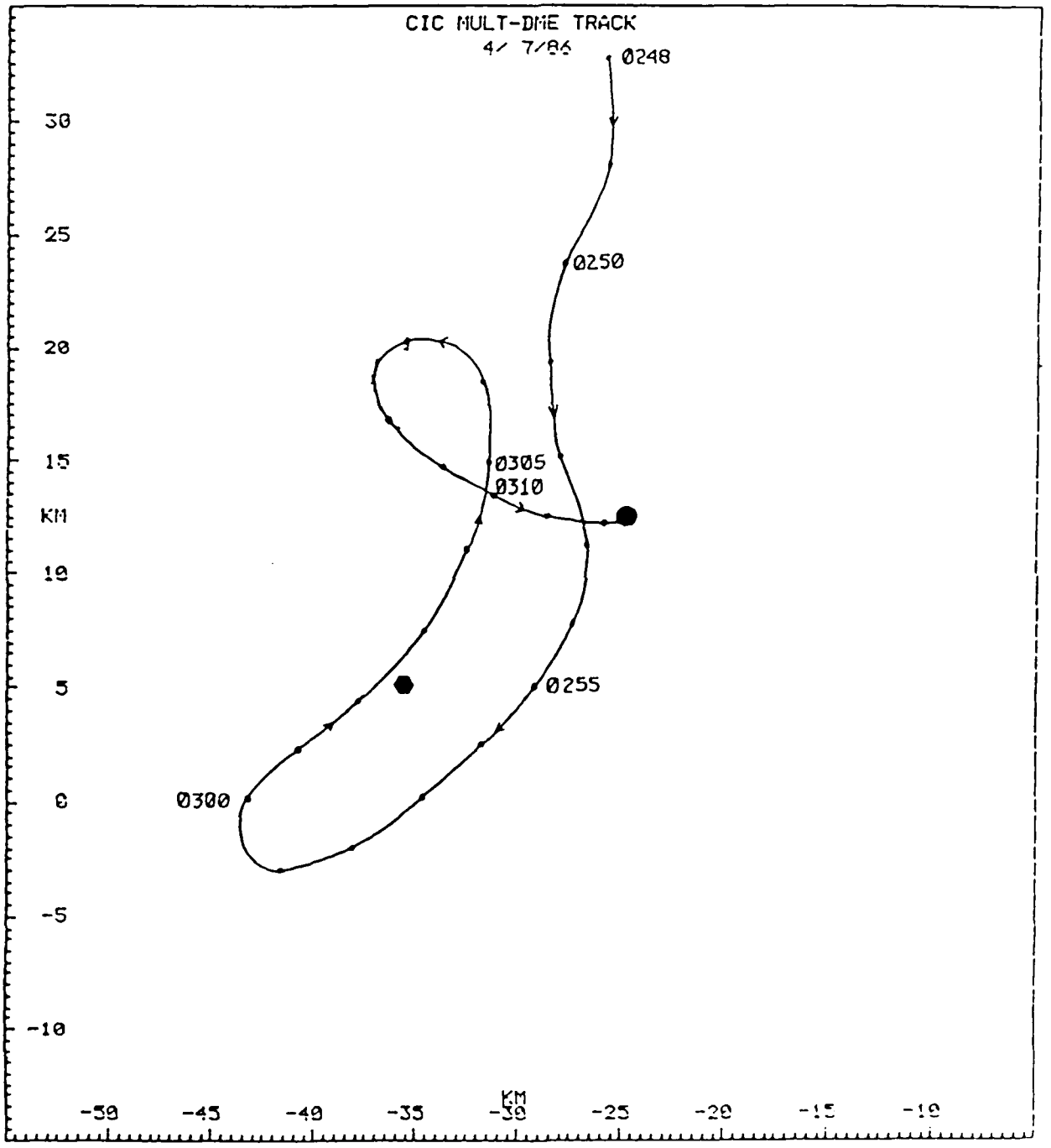
CIC MULT-DME TRACK
4/ 7/86
0248
0250
0255
0300
0305
0310
30
25
20
15
KM
10
5
0
-5
-10
-50
-45
-40
-35
-30
-25
-20
-15
-10
KM

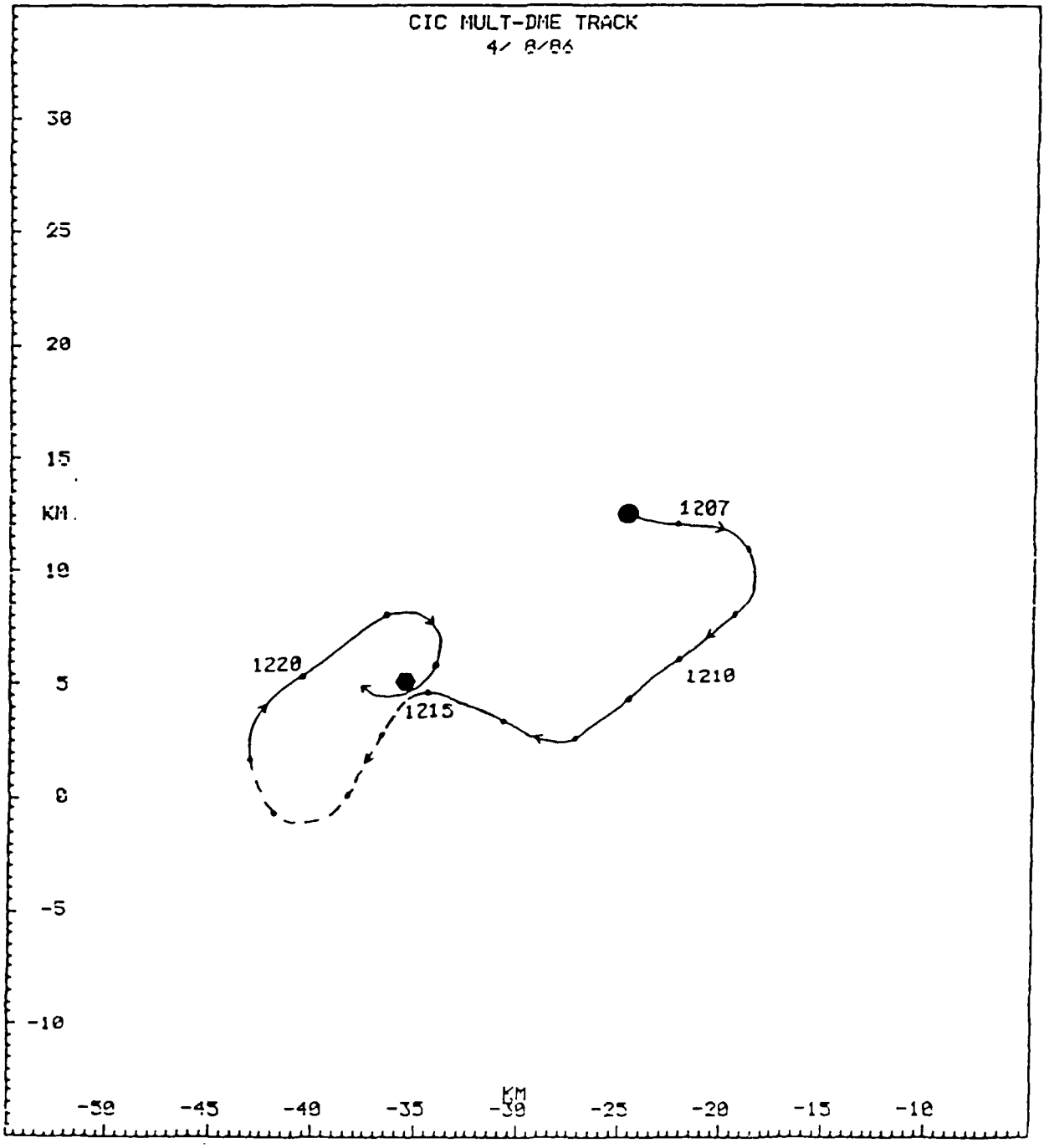
CIC MULT-DME TRACK
4/ 8/86
30
25
20
15
KM
10
5
0
-5
-10
1207
1210
1215
1220
-50
-45
-40
-35
-30
KM
-25
-20
-15
-10

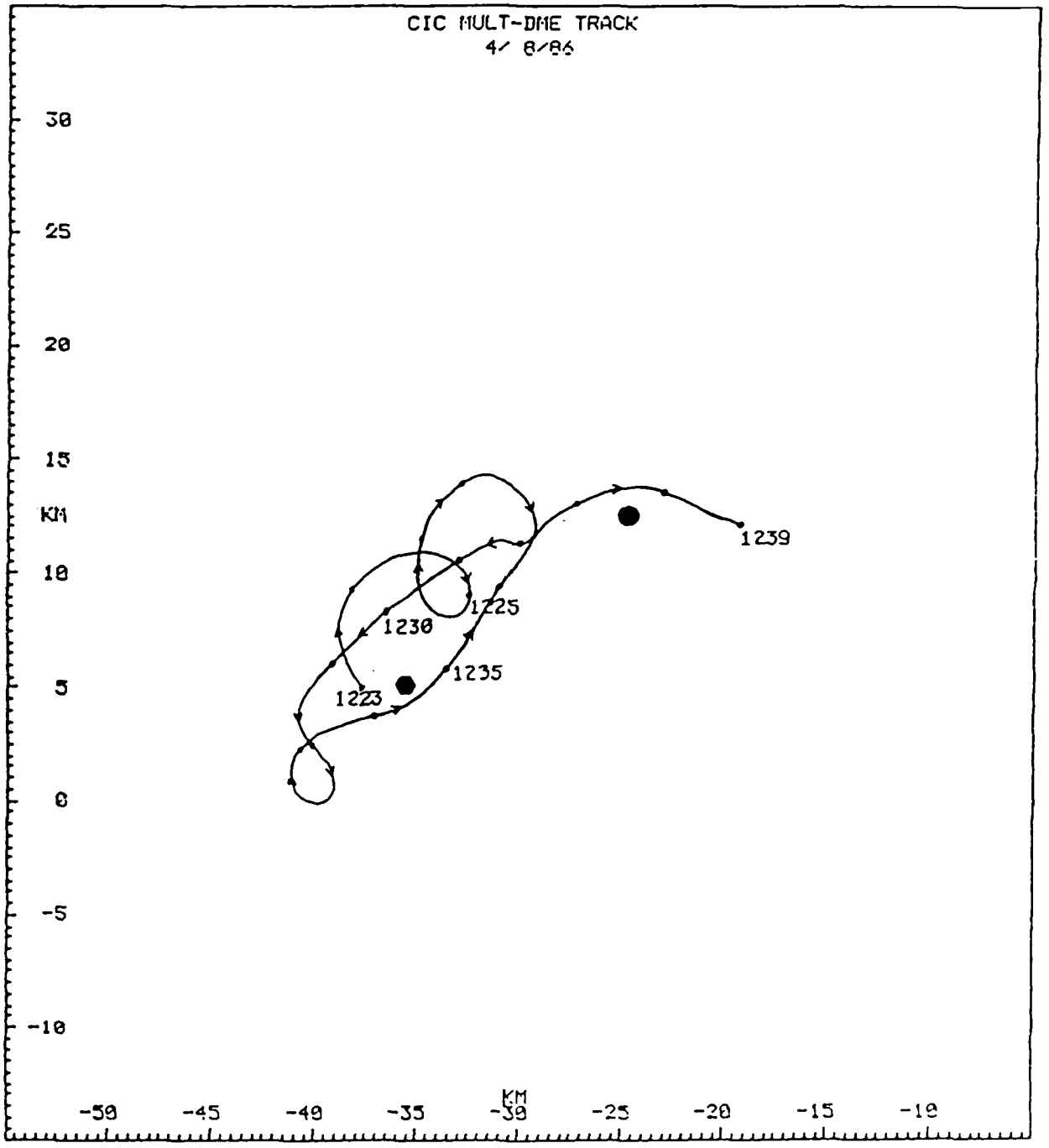
CIC MULT-DME TRACK
4/ 8/86
30
25
20
15
KM
10
5
0
-5
-10
1239
1225
1230
1235
1223
-50
-45
-40
-35
-30
KM
-25
-20
-15
-10

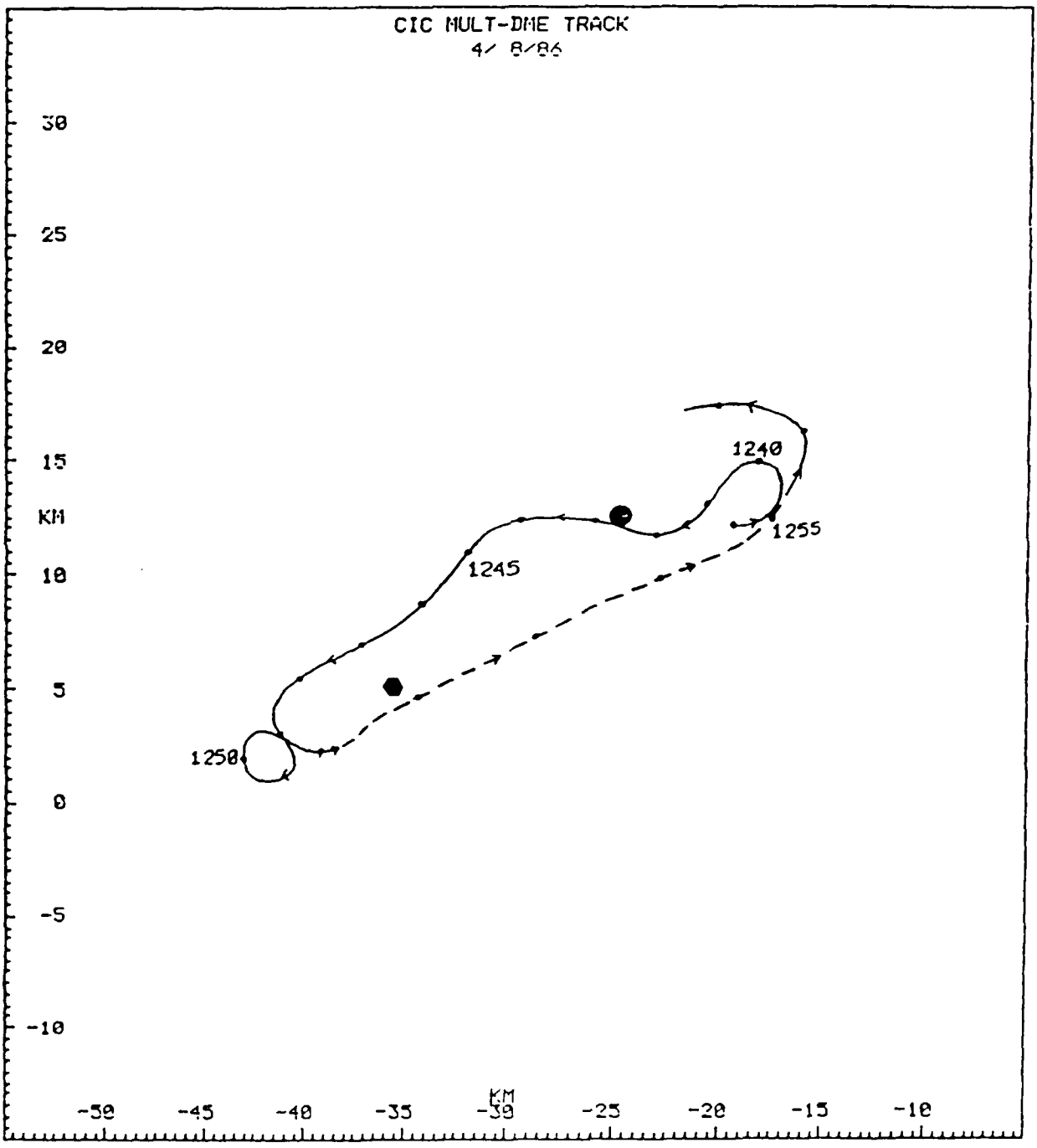
CIC MULT-DME TRACK
4/ 8/86
30
25
20
15
KM
10
5
0
-5
-10
1240
1255
1245
1250
-50
-45
-40
-35
-30
KM
-25
-20
-15
-10

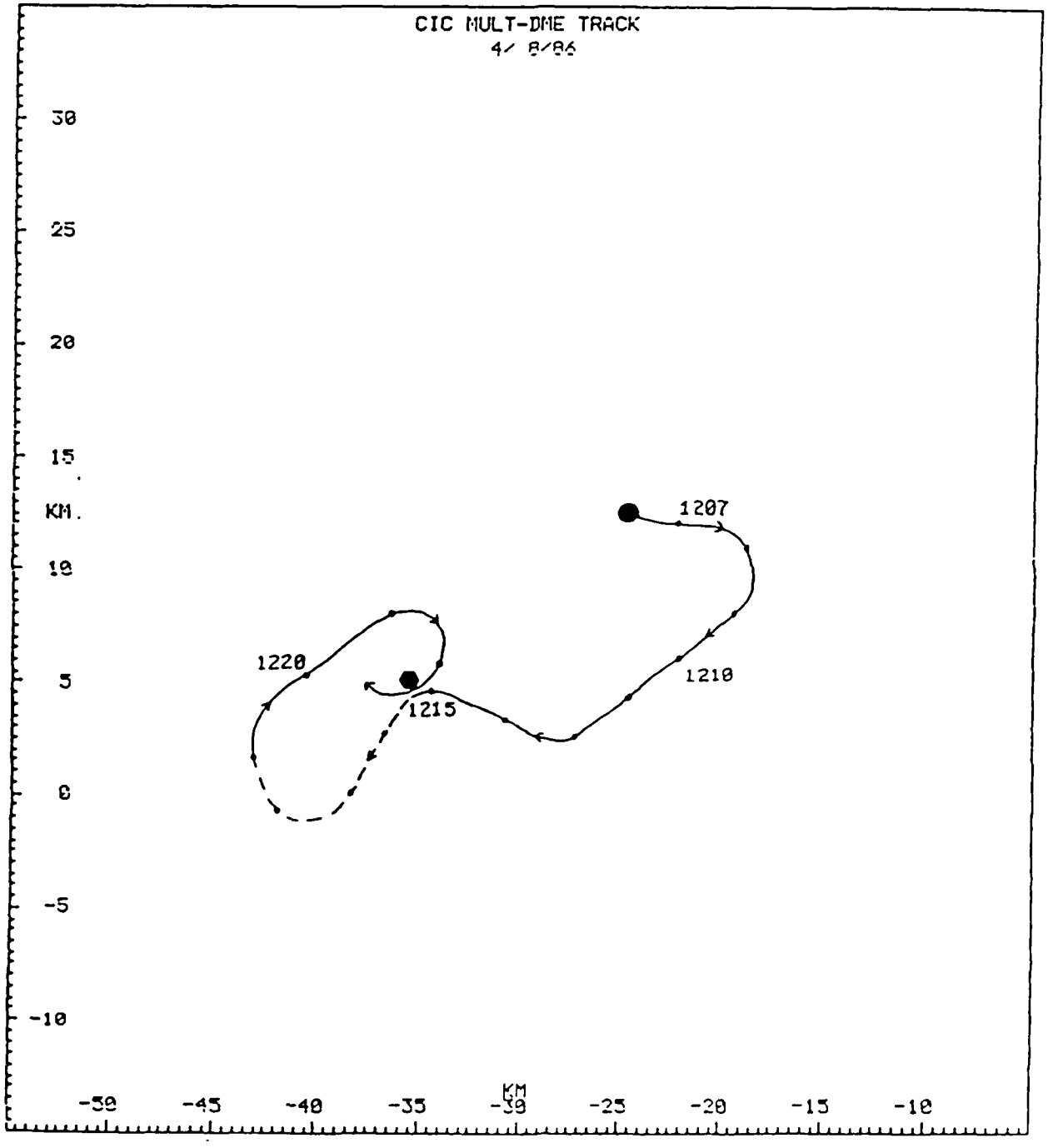
CIC MULT-DME TRACK
4/ 8/86
30
25
20
15
KM.
10
5
0
-5
-10
1207
1210
1215
1220
-50
-45
-40
-35
-30
KM
-25
-20
-15
-10

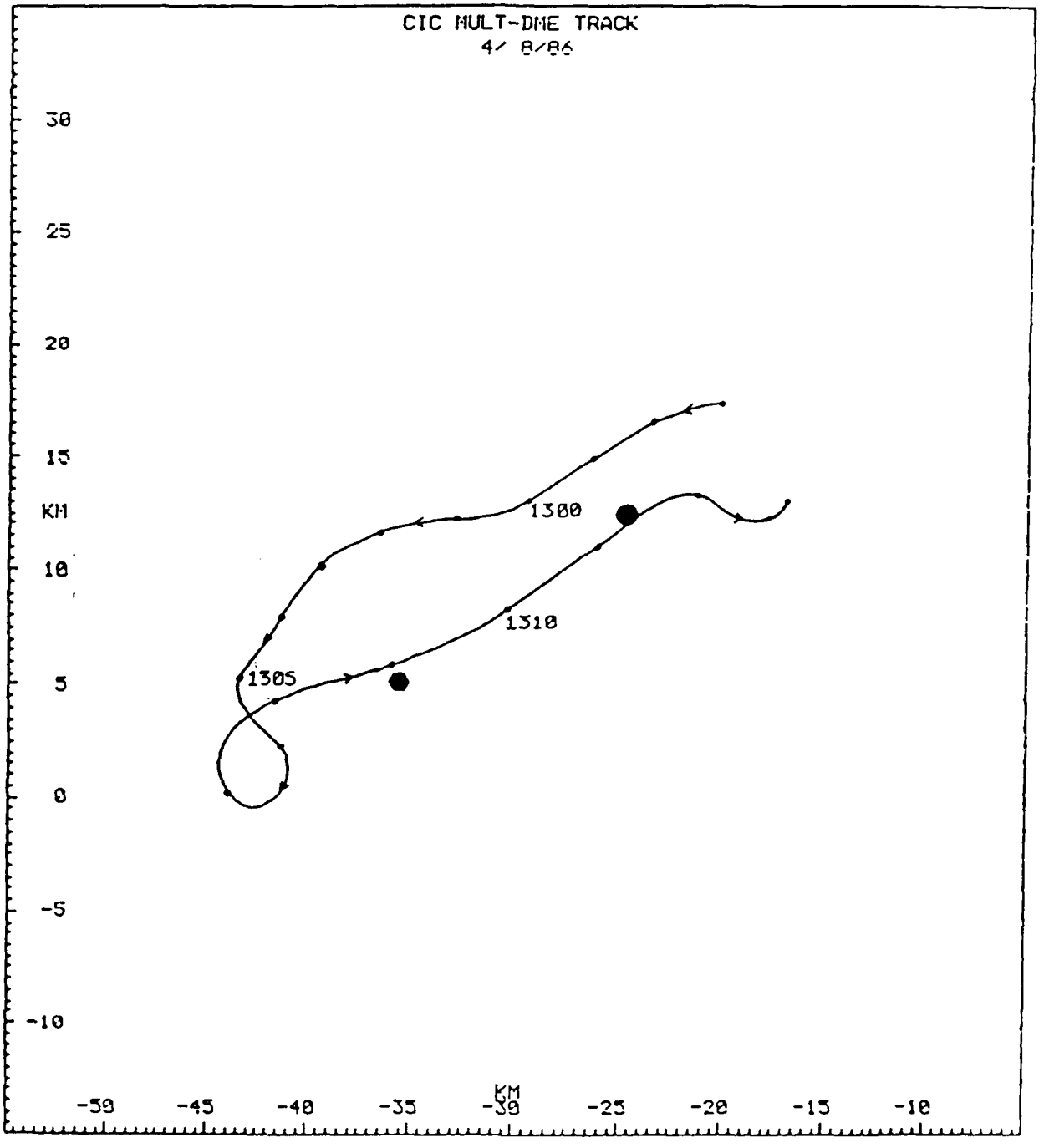
CIC MULT-DME TRACK
4/ 8/86
30
25
20
15
KM
10
5
0
-5
-10
1300
1310
1305
-50
-45
-40
-35
-30
KM
-25
-20
-15
-10

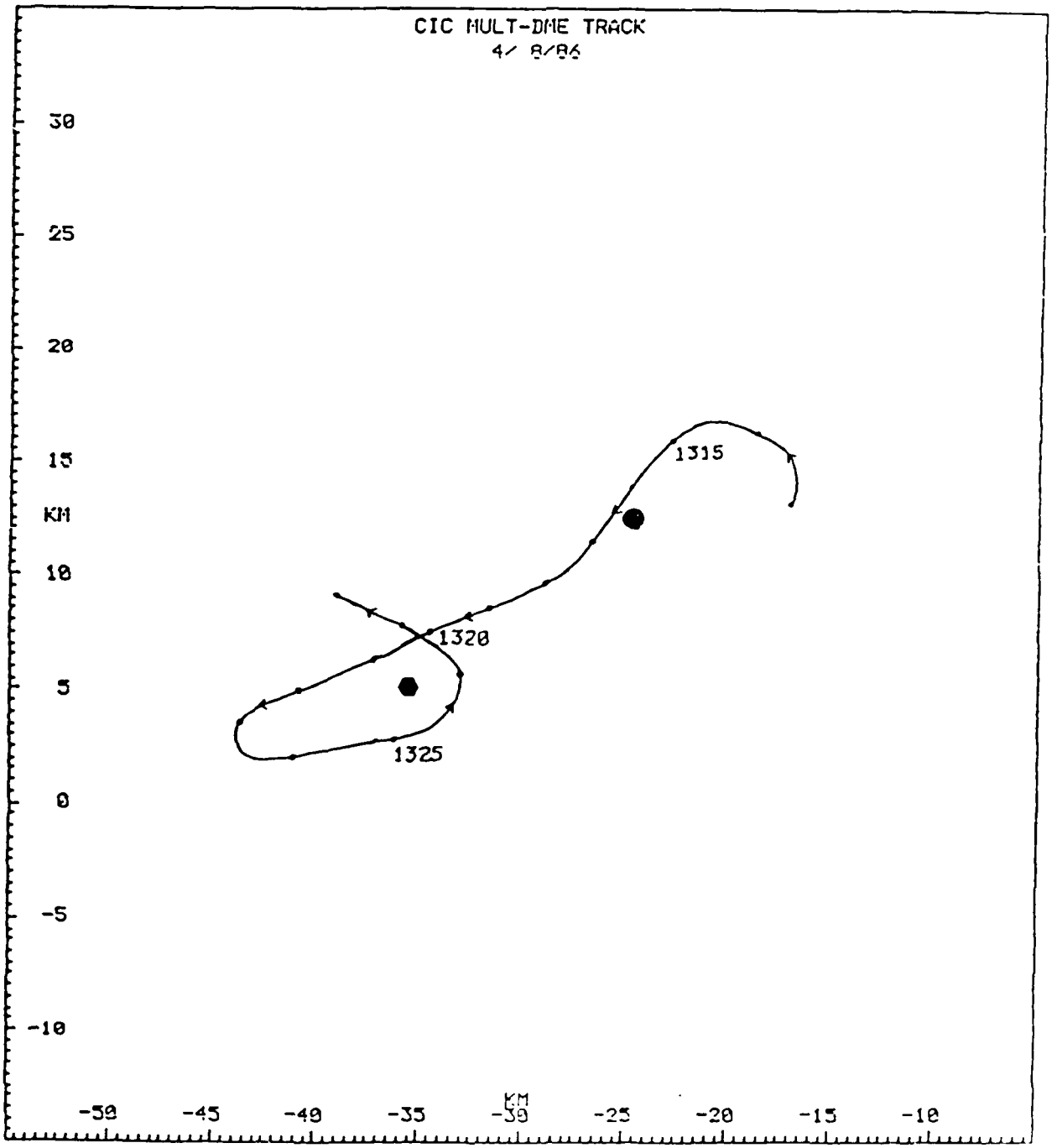
CIC MULT-DME TRACK
4/ 8/86
30
25
20
15
KM
10
5
0
-5
-10
1315
1320
1325
-50
-45
-40
-35
-30
-25
-20
-15
-10
KM

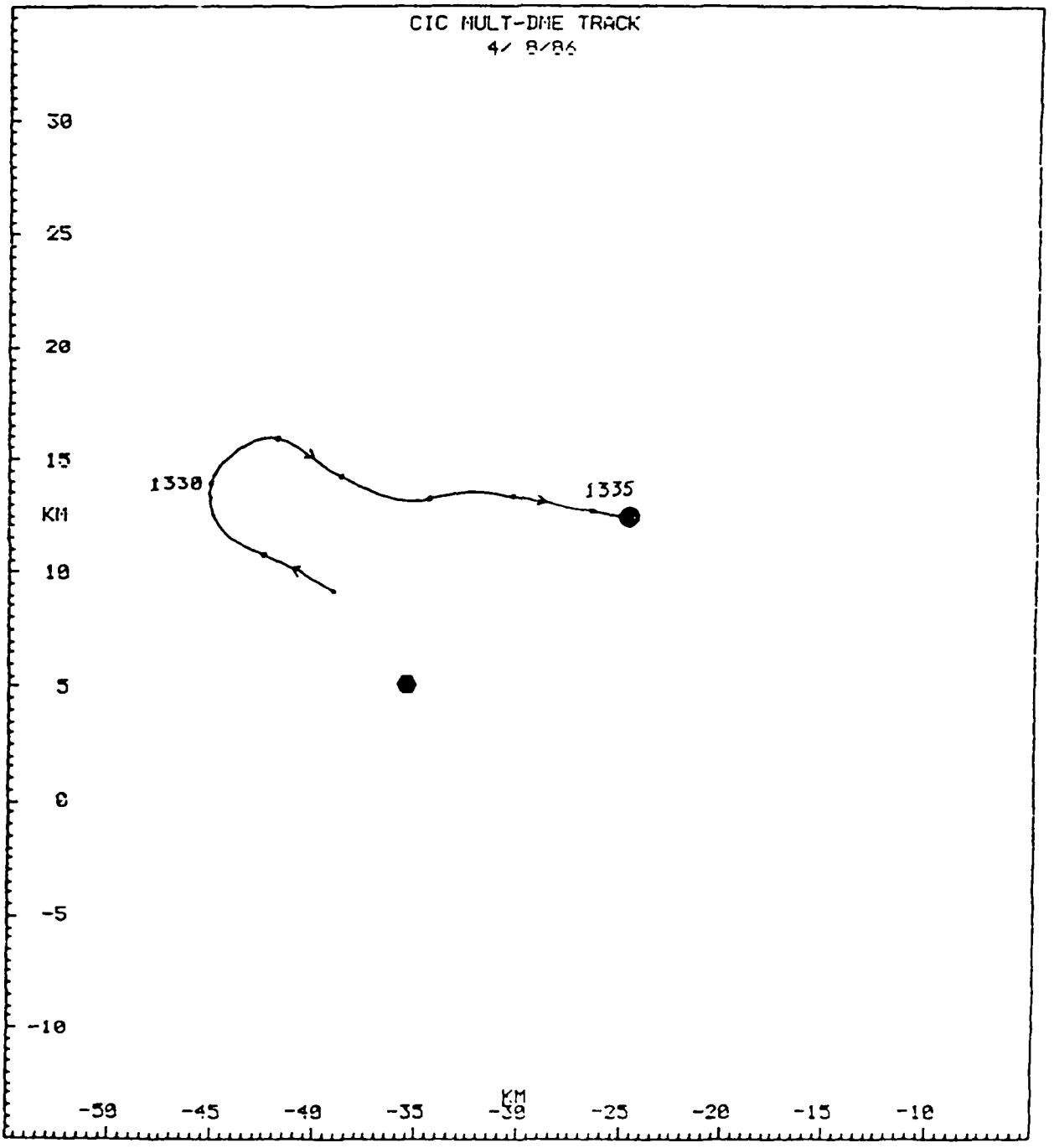
CIC MULT-DME TRACK
4/ 8/86
30
25
20
15
KM
10
5
0
-5
-10
1330
1335
-50
-45
-40
-35
-30
-25
-20
-15
-10
KM

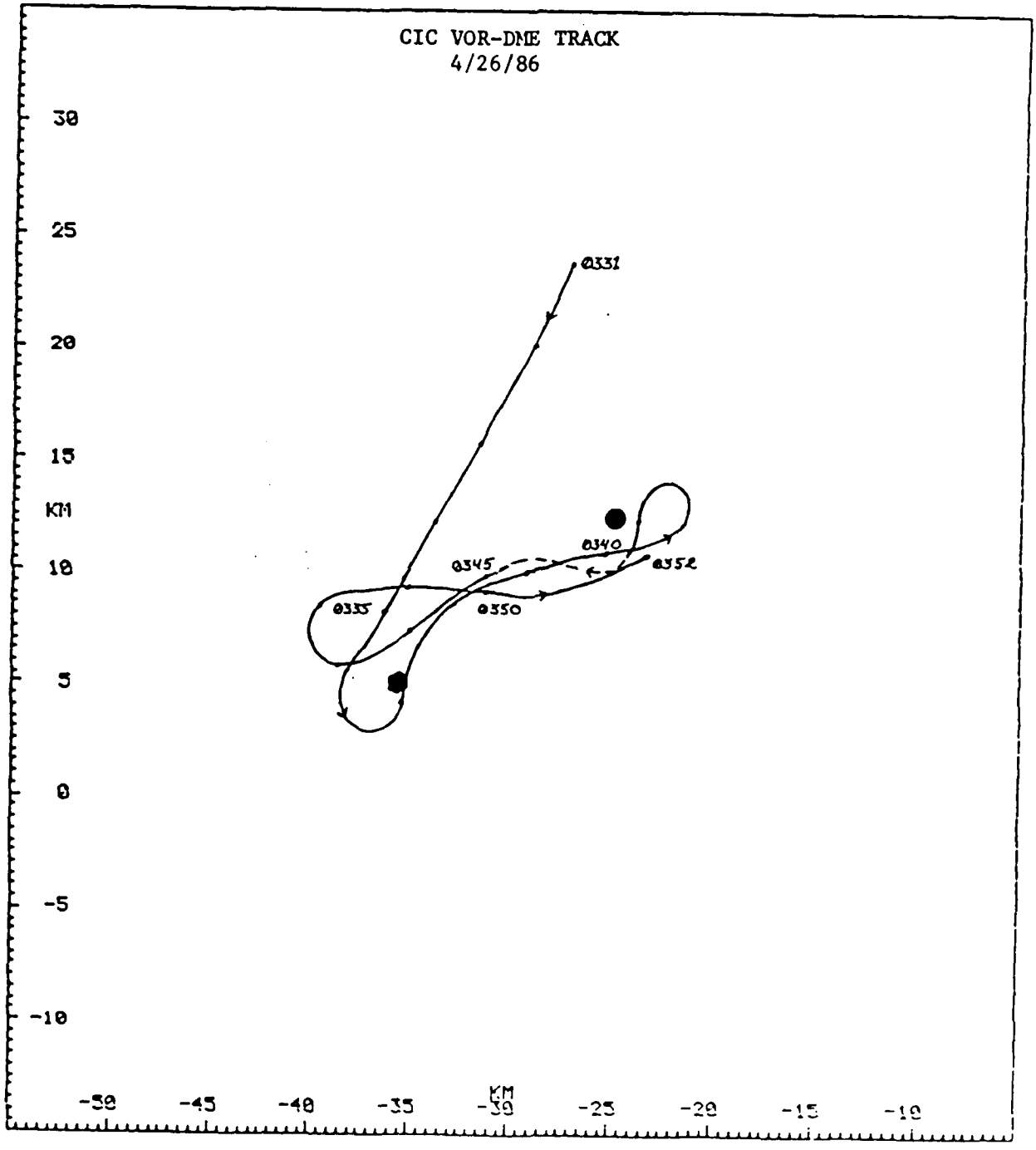
CIC VOR-DME TRACK
4/26/86
30
25
20
15
KM
10
5
0
-5
-10
-50
-45
-40
-35
-30
KM
-25
-20
-15
-10
0331
0340
0345
0352
0335
0350

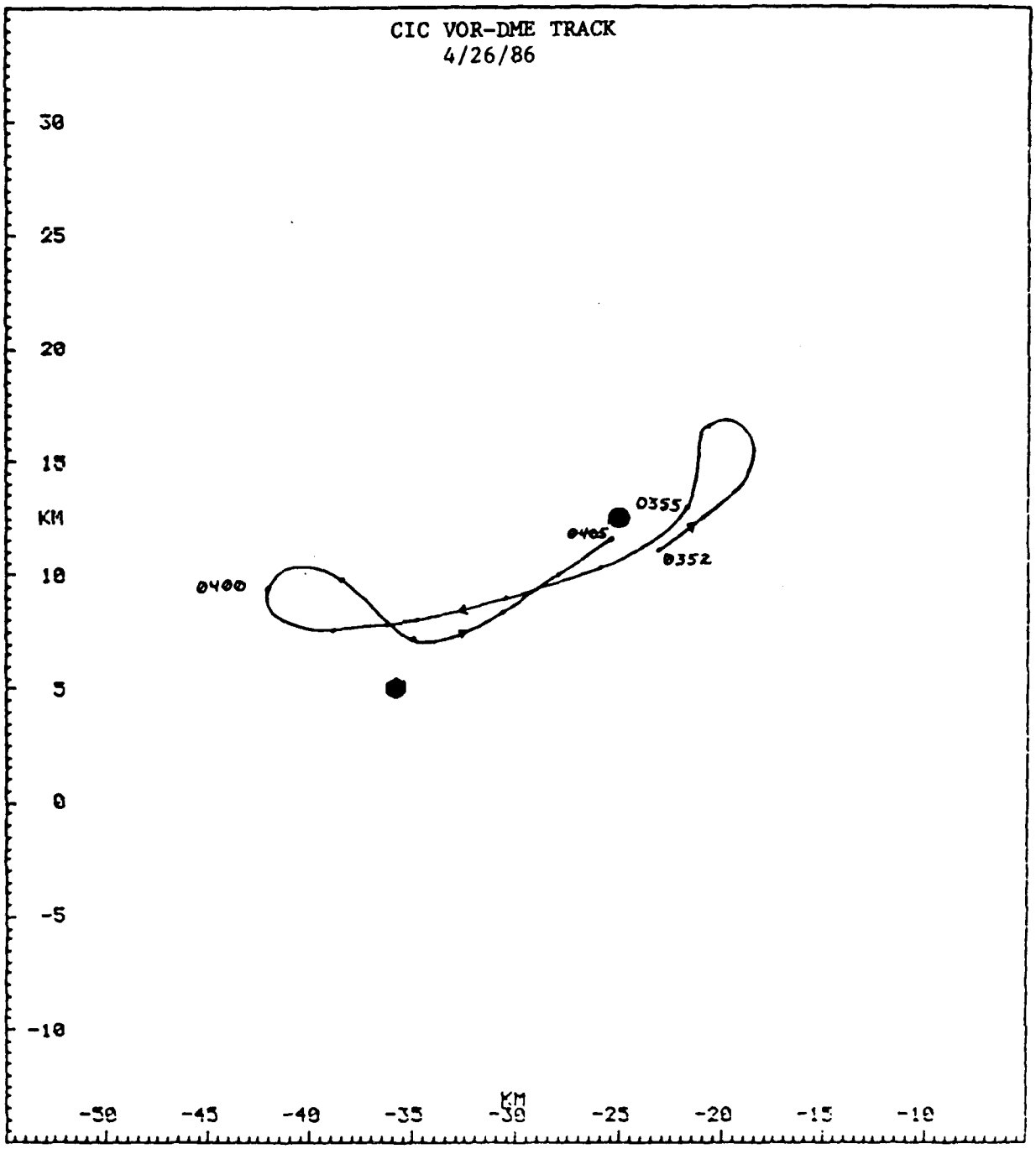
CIC VOR-DME TRACK
4/26/86
30
25
20
15
KM
10
5
0
-5
-10
0355
0405
0352
0400
-50
-45
-40
-35
KM
-30
-25
-20
-15
-10

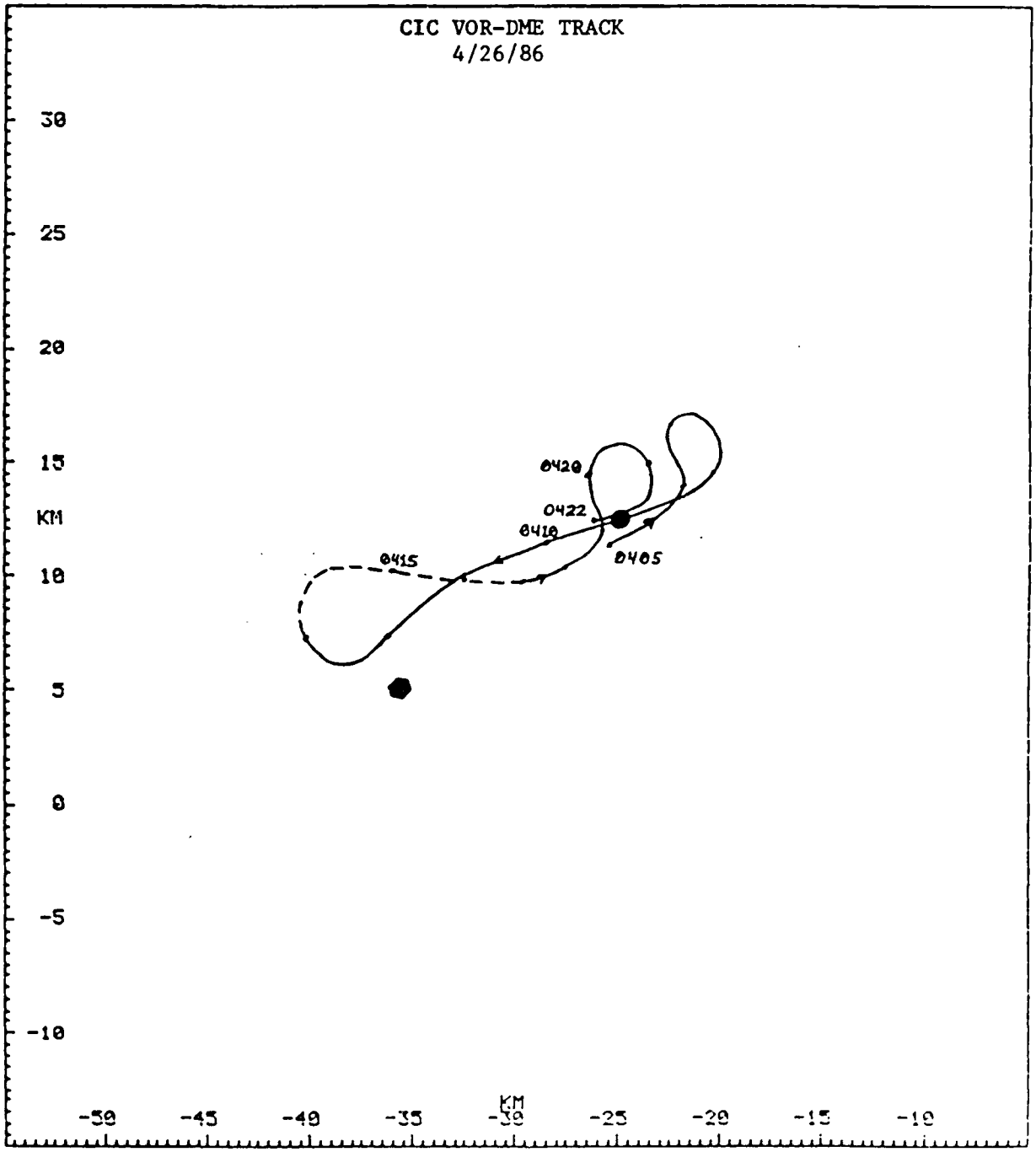
CIC VOR-DME TRACK
4/26/86
30
25
20
15
KM
10
5
0
-5
-10
0420
0422
0410
0415
0405
-50
-45
-40
-35
-30
-25
-20
-15
-10
KM

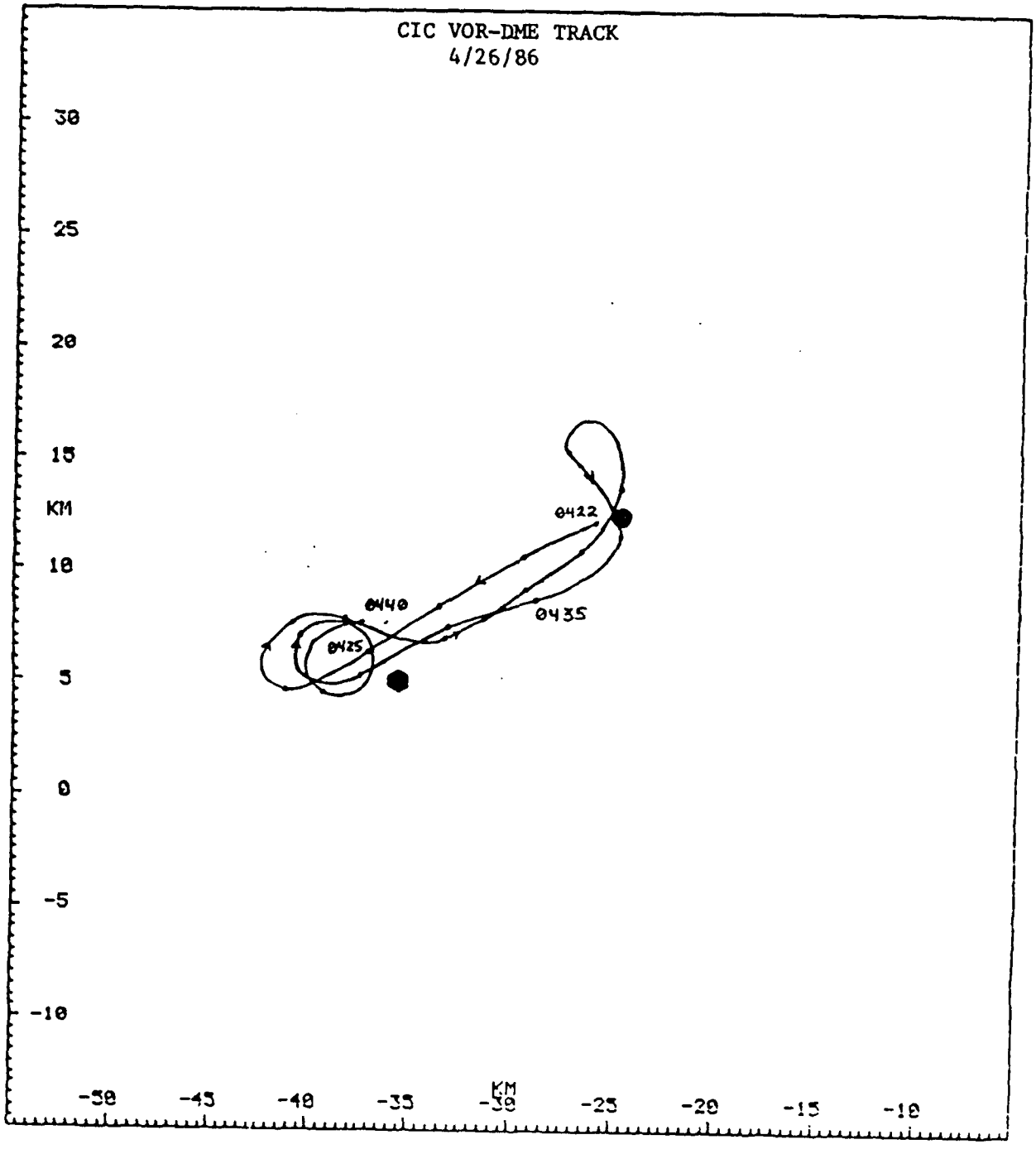
CIC VOR-DME TRACK
4/26/86
30
25
20
15
KM
10
5
0
-5
-10
0422
0440
0435
0425
-50
-45
-40
-35
KM
-30
-25
-20
-15
-10

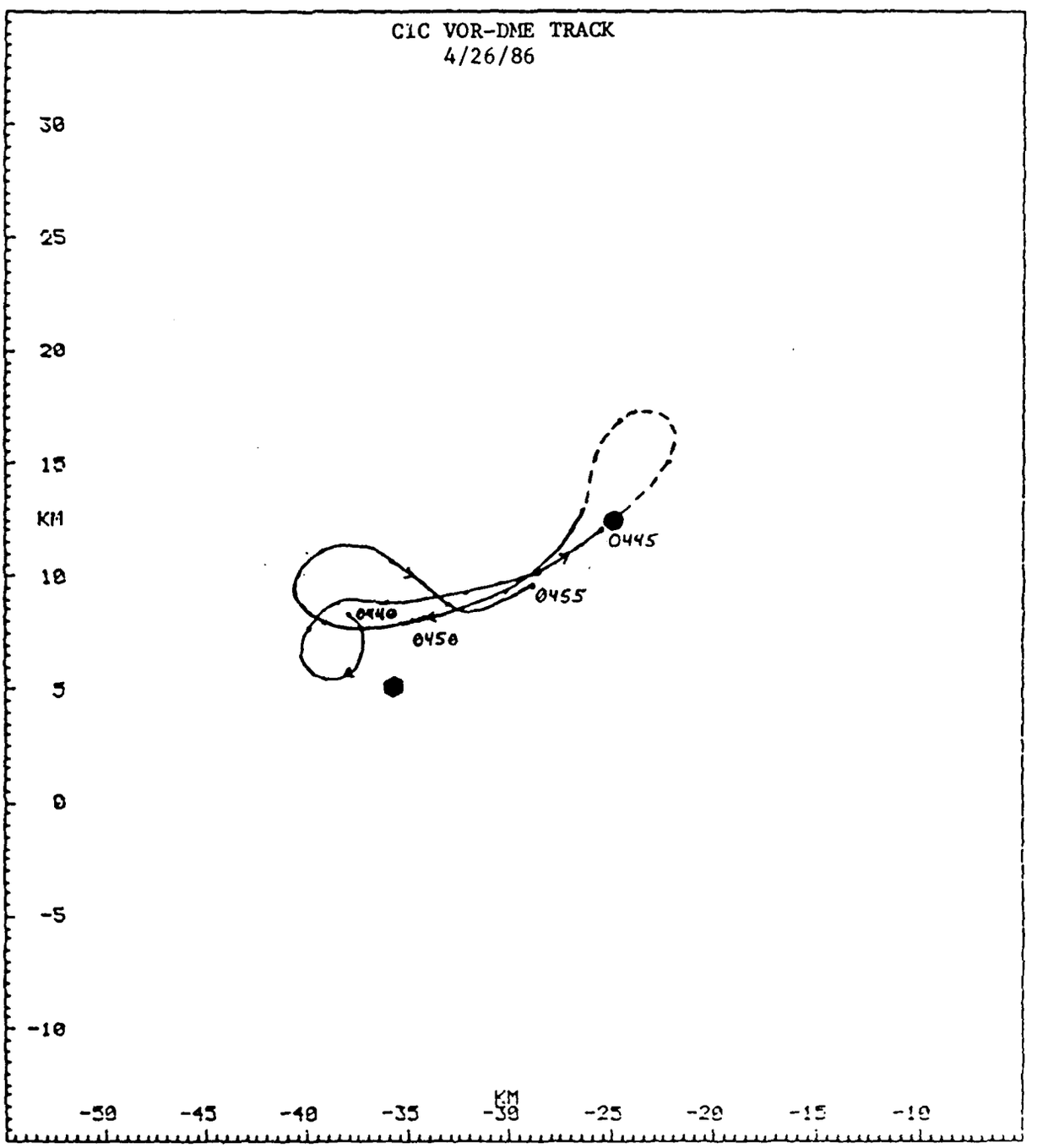
C1C VOR-DME TRACK
4/26/86
30
25
20
15
KM
10
5
0
-5
-10
-50
-45
-40
-35
-30
KM
-25
-20
-15
-10
0445
0455
0440
0450

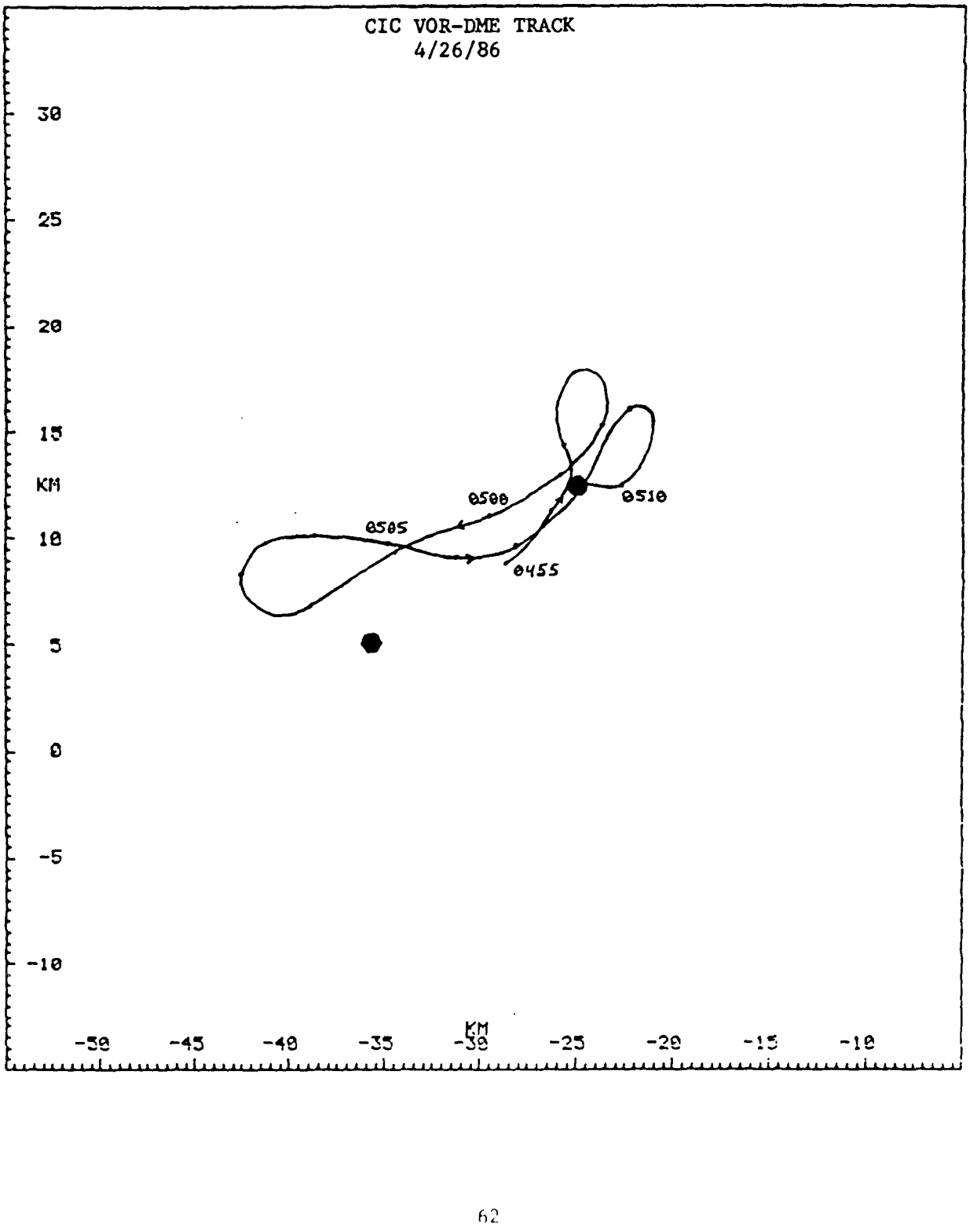
CIC VOR-DME TRACK
4/26/86
30
25
20
15
KM
10
5
0
-5
-10
0500
0505
0510
0455
-50
-45
-40
-35
-30
KM
-25
-20
-15
-10

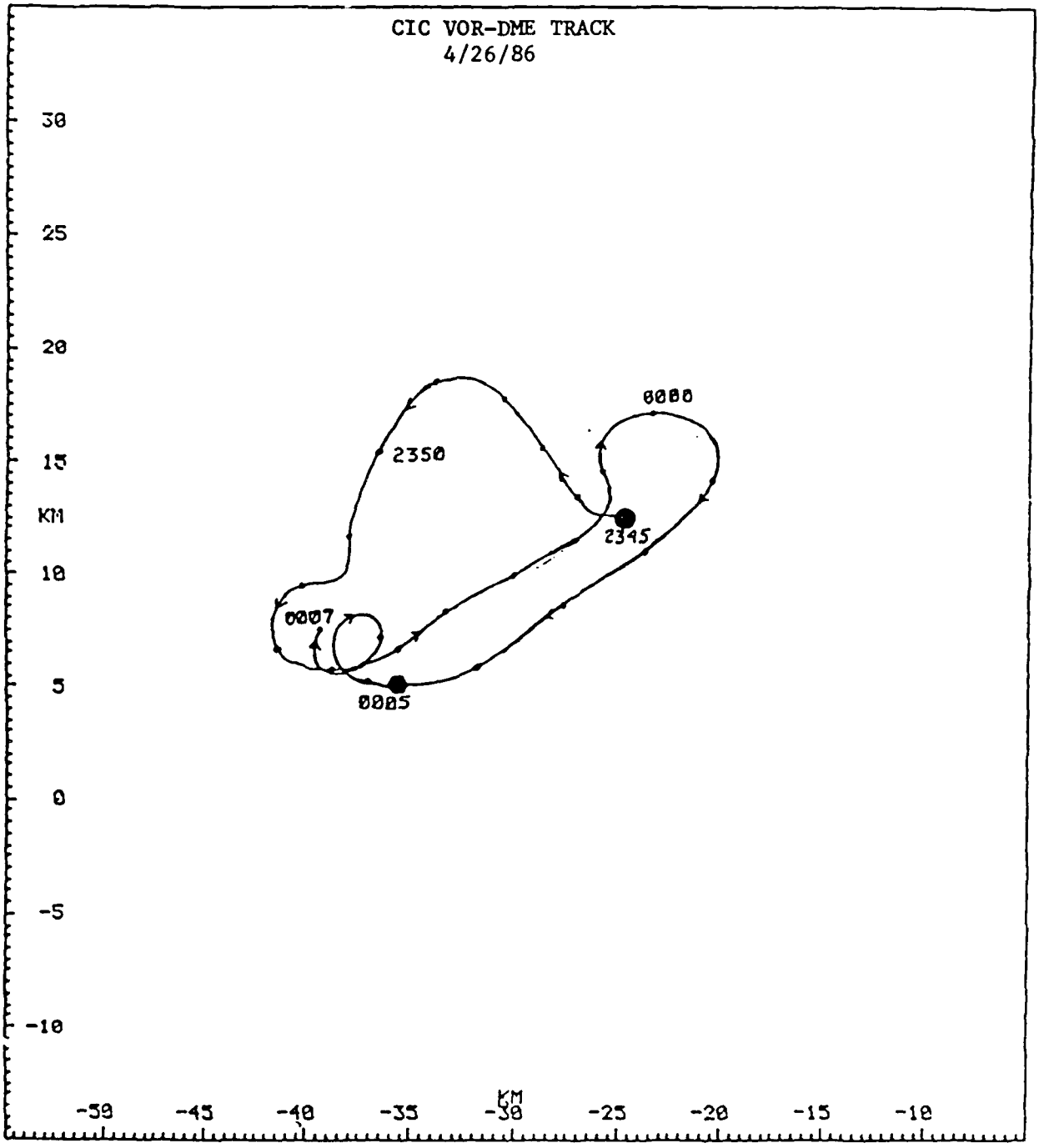
CIC VOR-DME TRACK
4/26/86
30
25
20
15
KM
10
5
0
-5
-10
0000
2350
2345
0007
0005
-50
-45
-40
-35
-30
-25
-20
-15
-10
KM

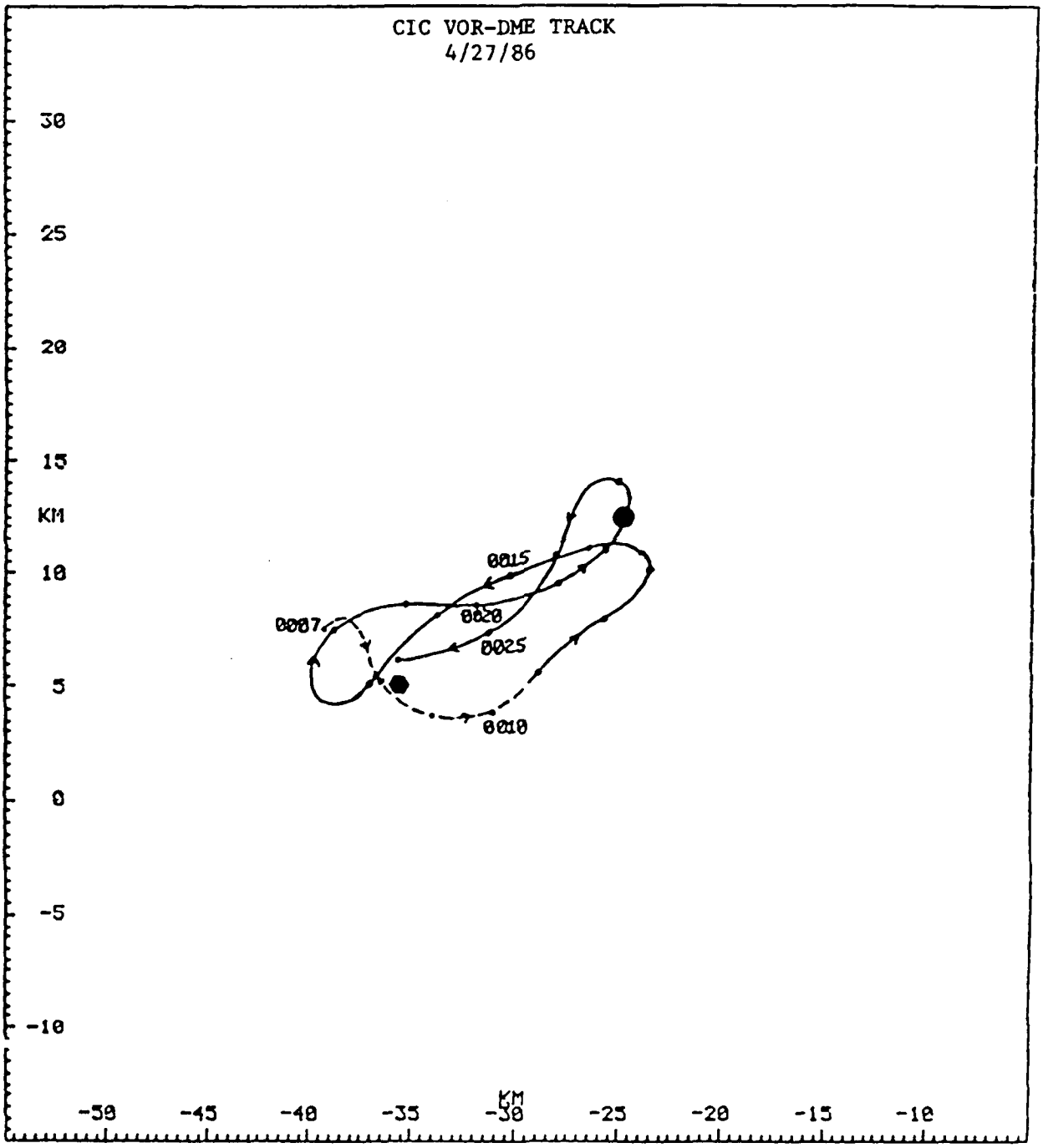
CIC VOR-DME TRACK
4/27/86
30
25
20
15
KM
10
5
0
-5
-10
0015
0020
0007
0025
0010
-50
-45
-40
-35
-30
-25
-20
-15
-10
KM

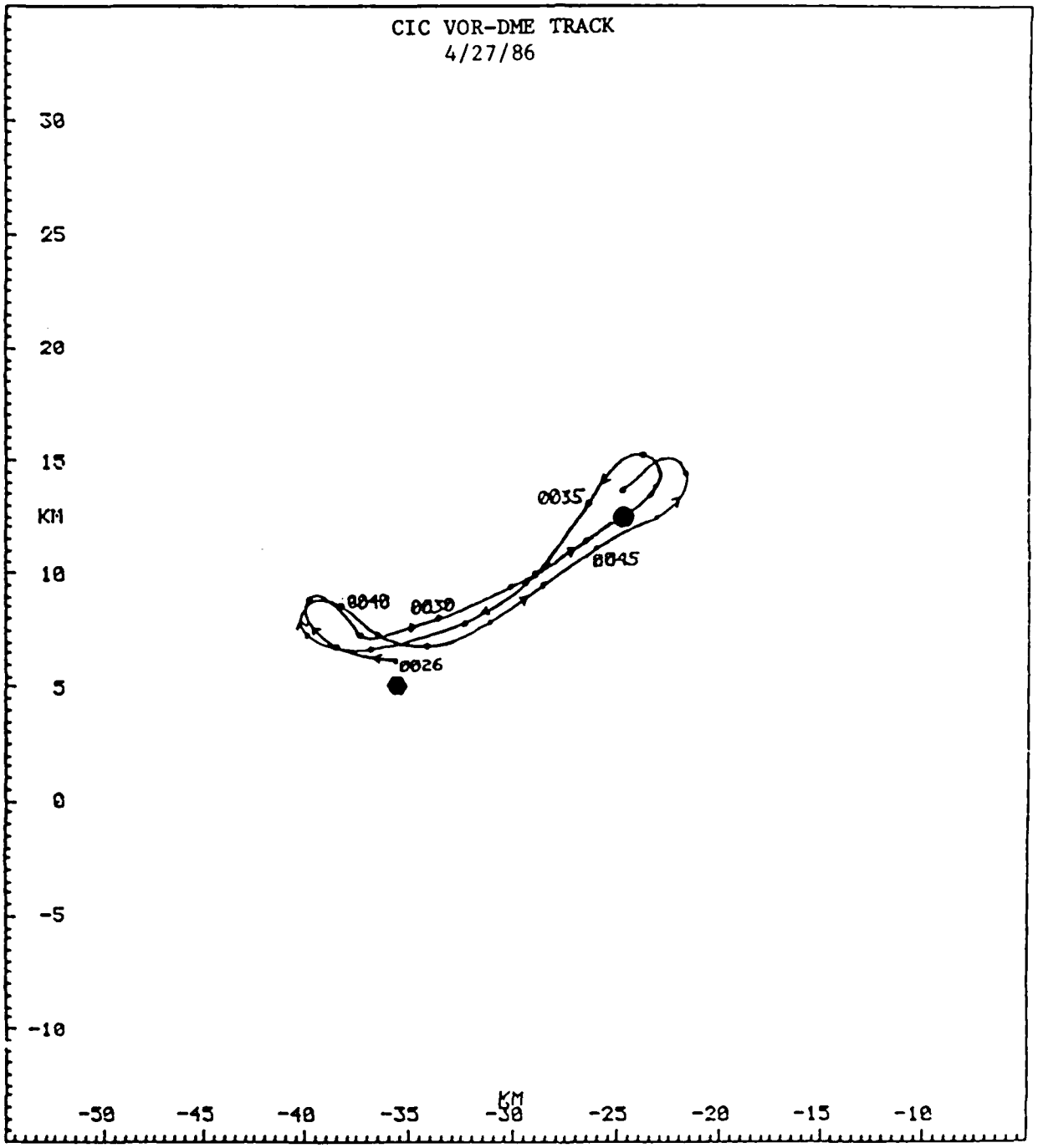
CIC VOR-DME TRACK
4/27/86
30
25
20
15
KM
10
5
0
-5
-10
0035
0045
0040
0030
0026
-50
-45
-40
-35
-30
-25
-20
-15
-10
KM

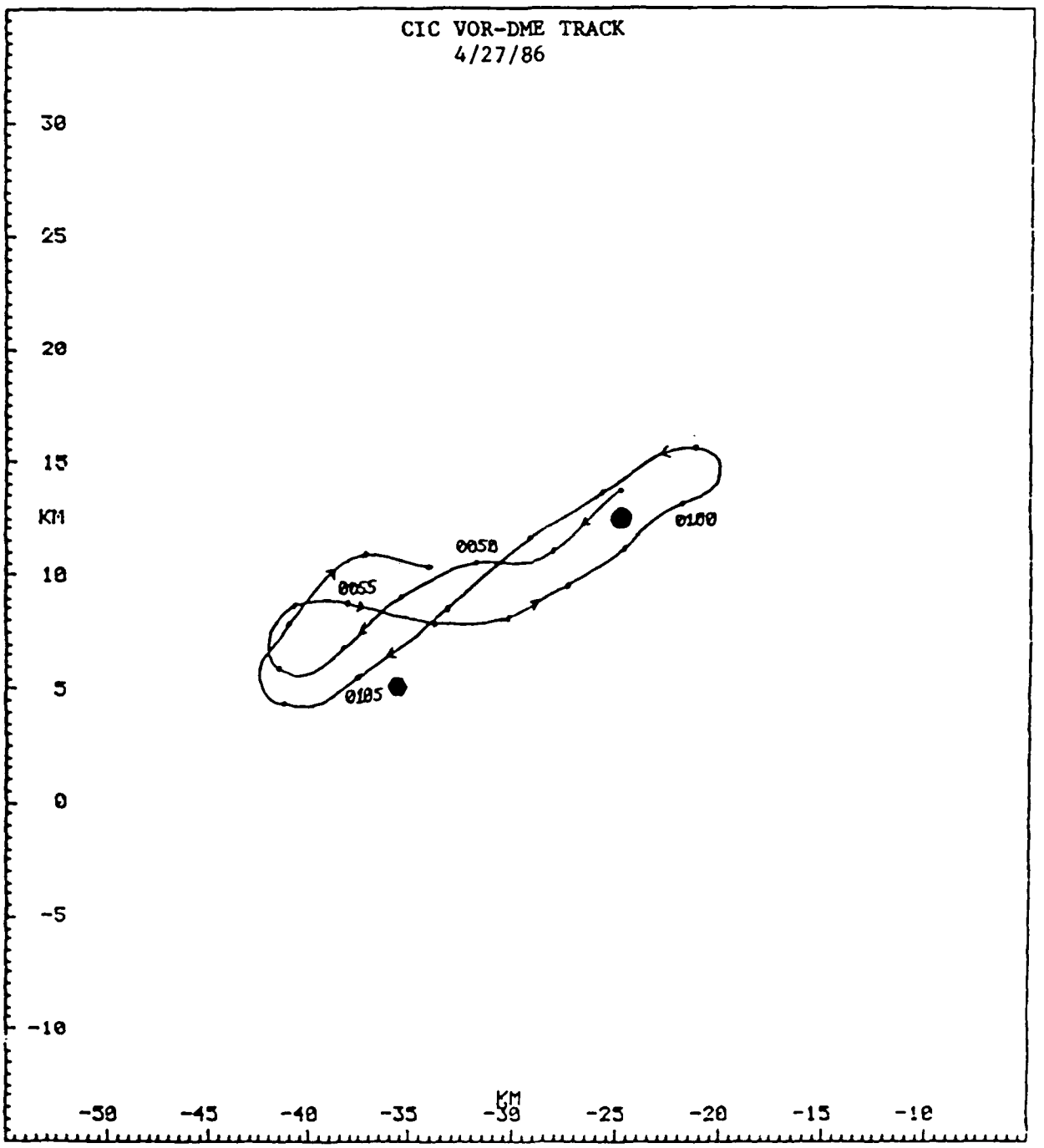
CIC VOR-DME TRACK
4/27/86
30
25
20
15
KM
10
5
0
-5
-10
0058
0055
0100
0105
-50
-45
-40
-35
-30
KM
-25
-20
-15
-10

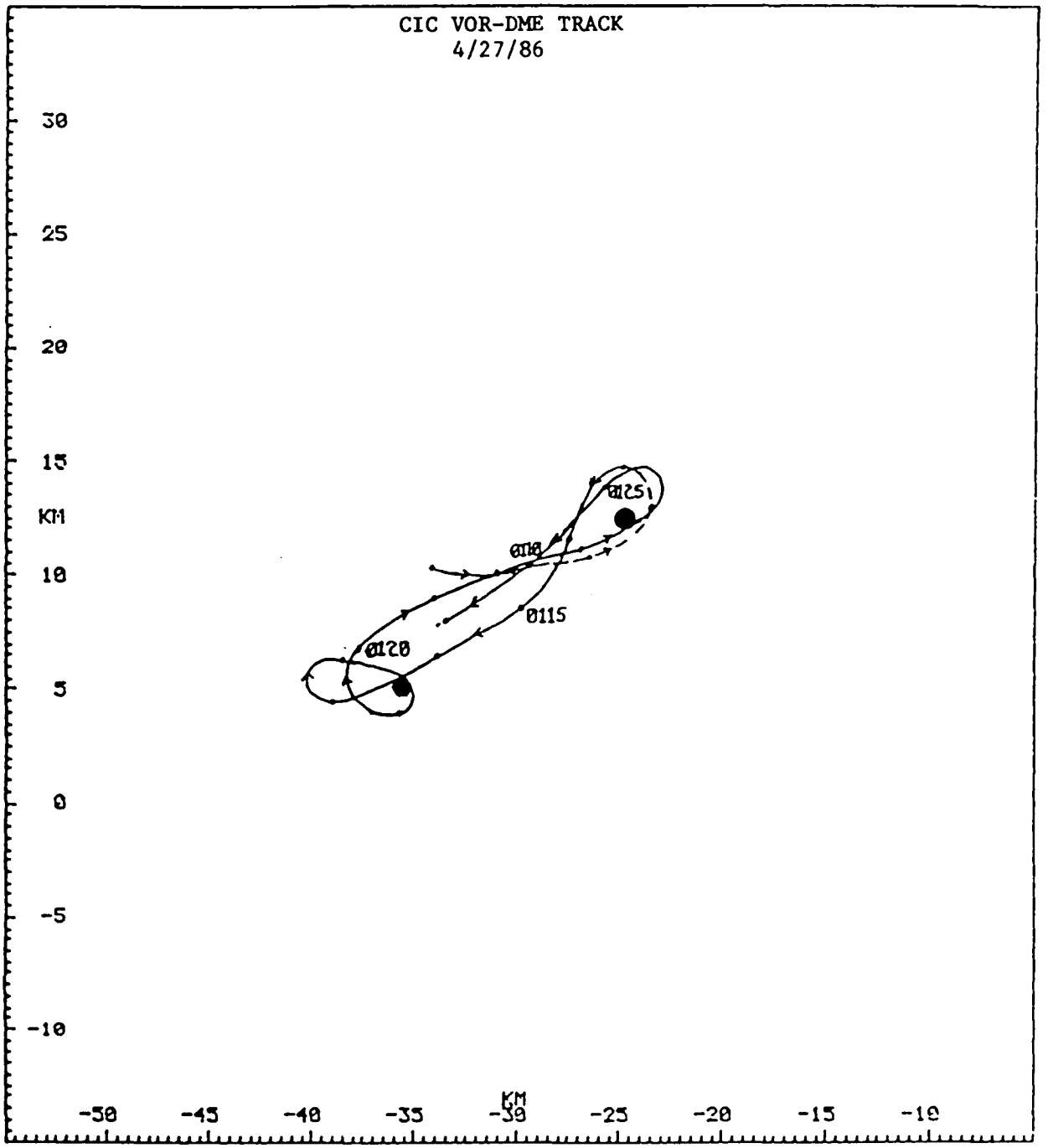
CIC VOR-DME TRACK
4/27/86
30
25
20
15
KM
10
5
0
-5
-10
-50
-45
-40
-35
-30
-25
-20
-15
-10
KM
0125
0110
0115
0120

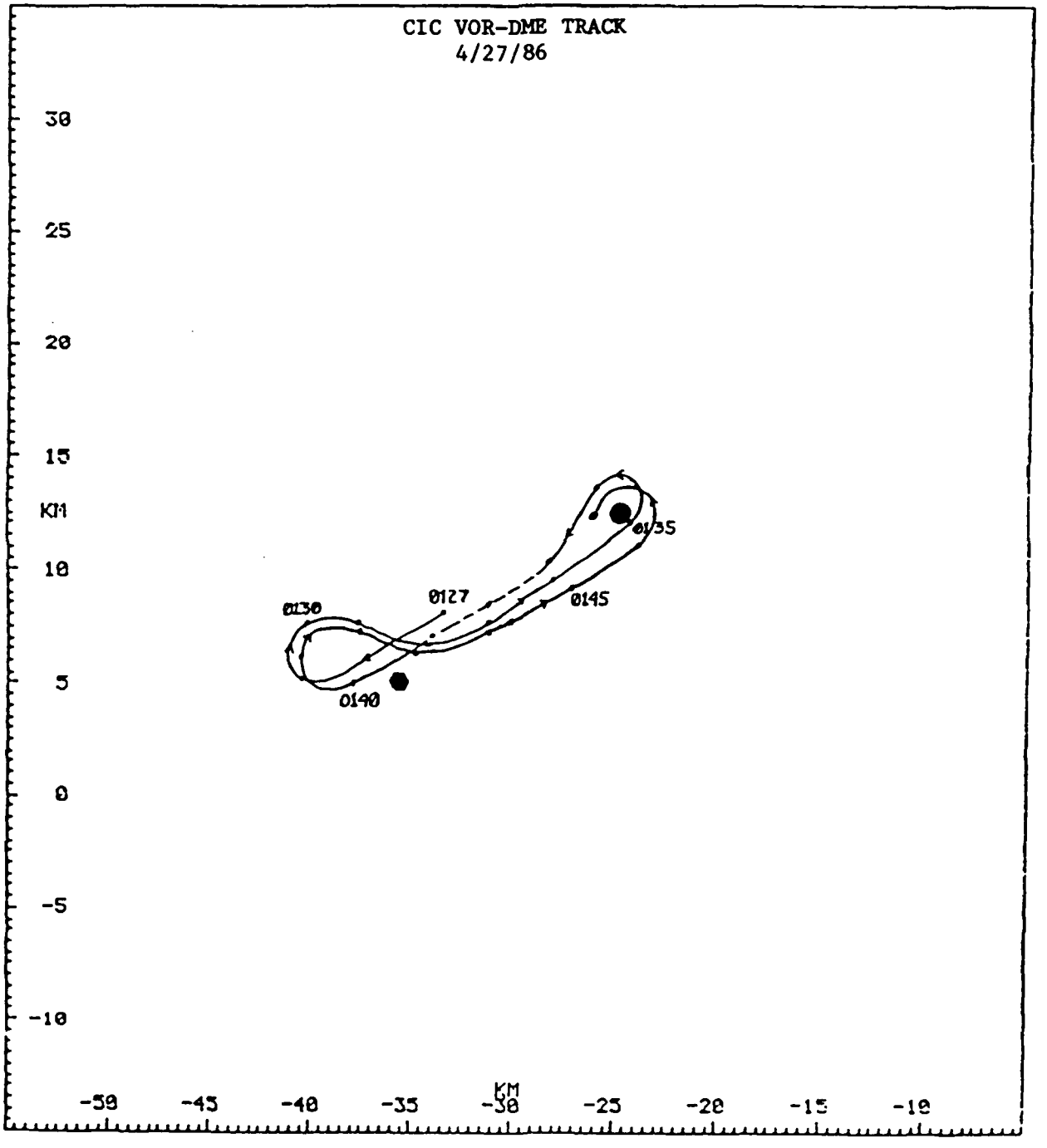
CIC VOR-DME TRACK
4/27/86
30
25
20
15
KM
10
5
0
-5
-10
0135
0127
0130
0145
0140
-50
-45
-40
-35
-30
KM
-25
-20
-15
-10

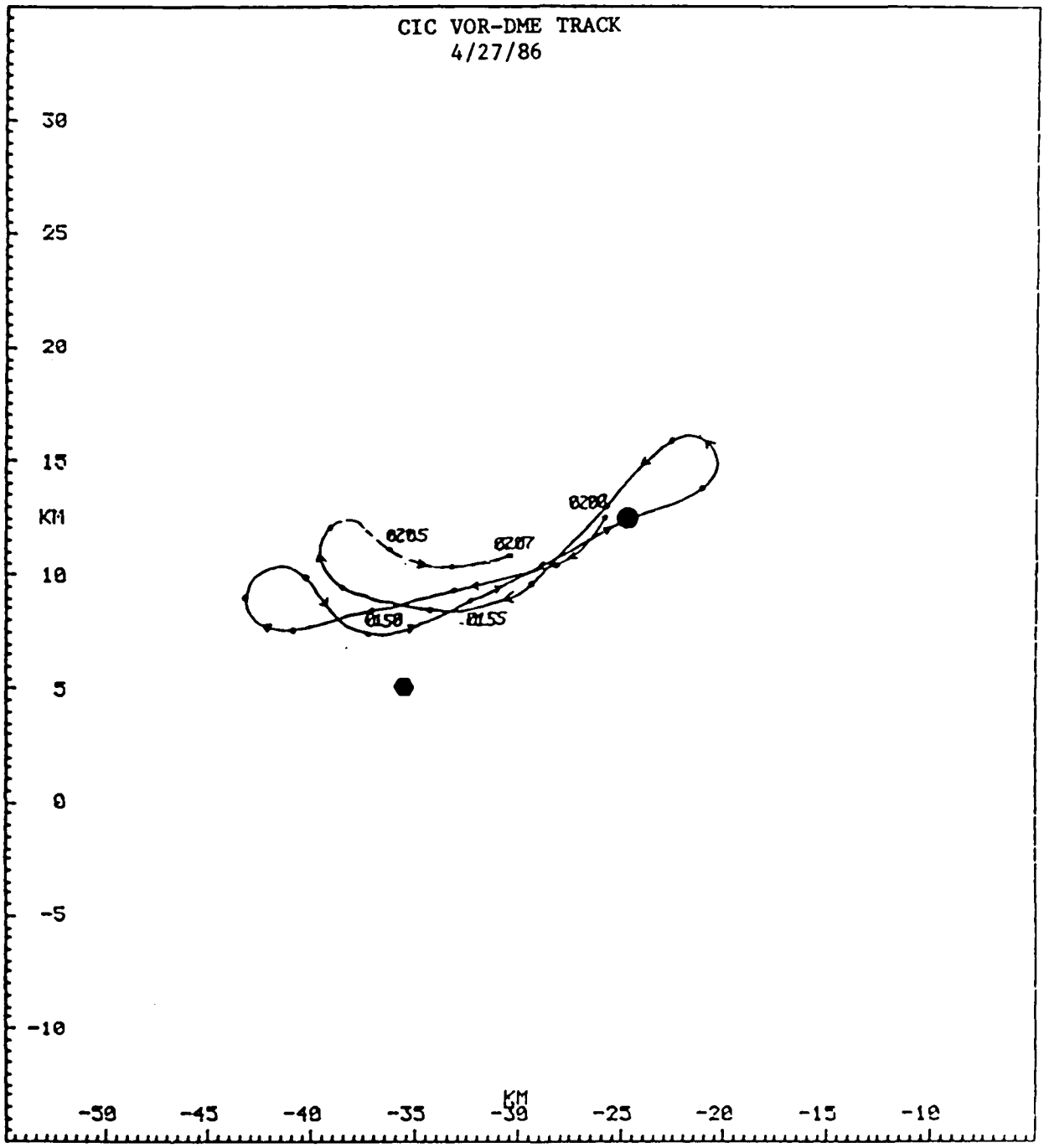
CIC VOR-DME TRACK
4/27/86
30
25
20
15
KM
10
5
0
-5
-10
0200
0205
0207
0150
0155
-50
-45
-40
-35
-30
KM
-25
-20
-15
-10

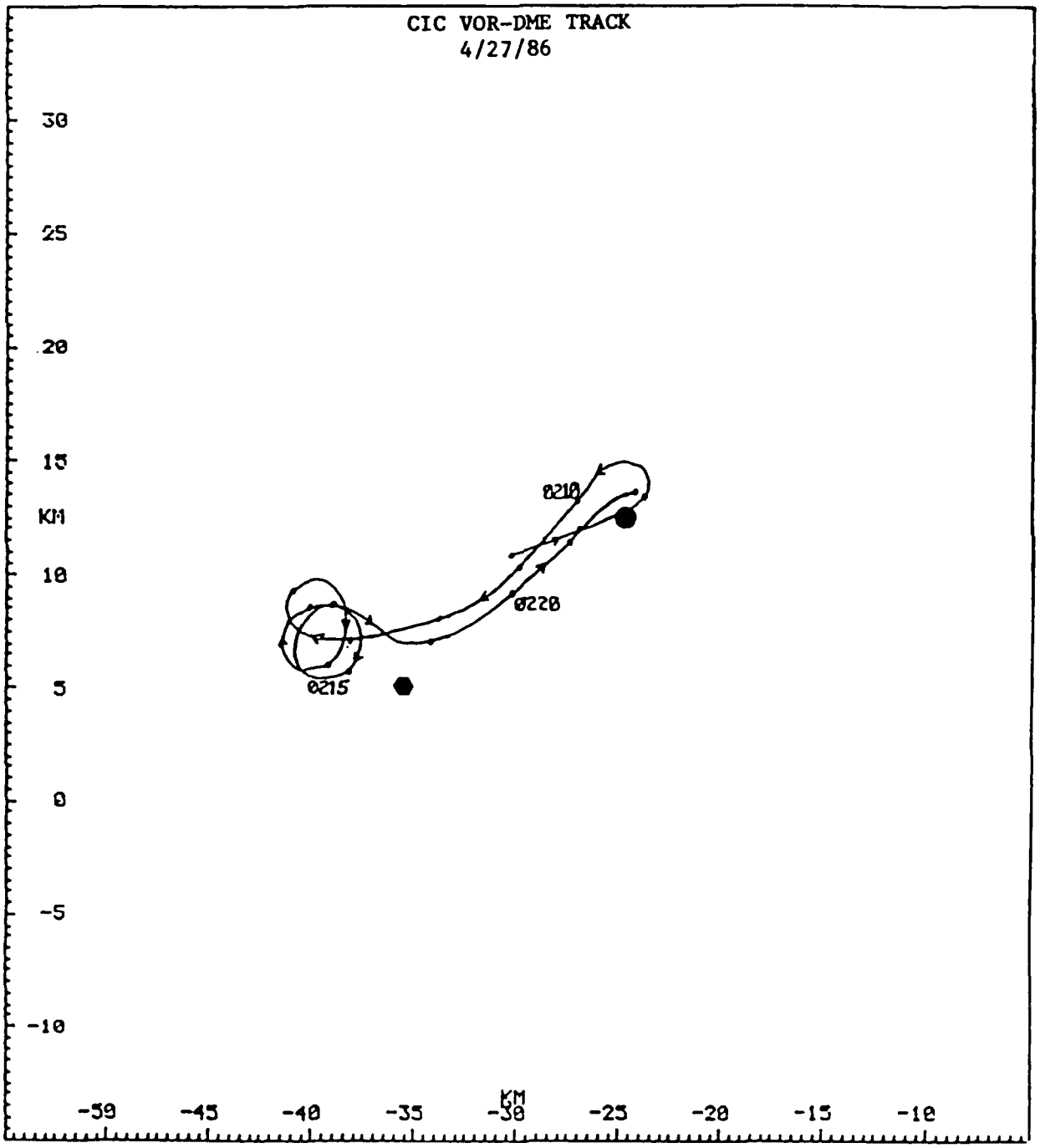
CIC VOR-DME TRACK
4/27/86
30
25
20
15
KM
10
5
0
-5
-10
0210
0220
0215
-50
-45
-40
-35
KM
-30
-25
-20
-15
-10

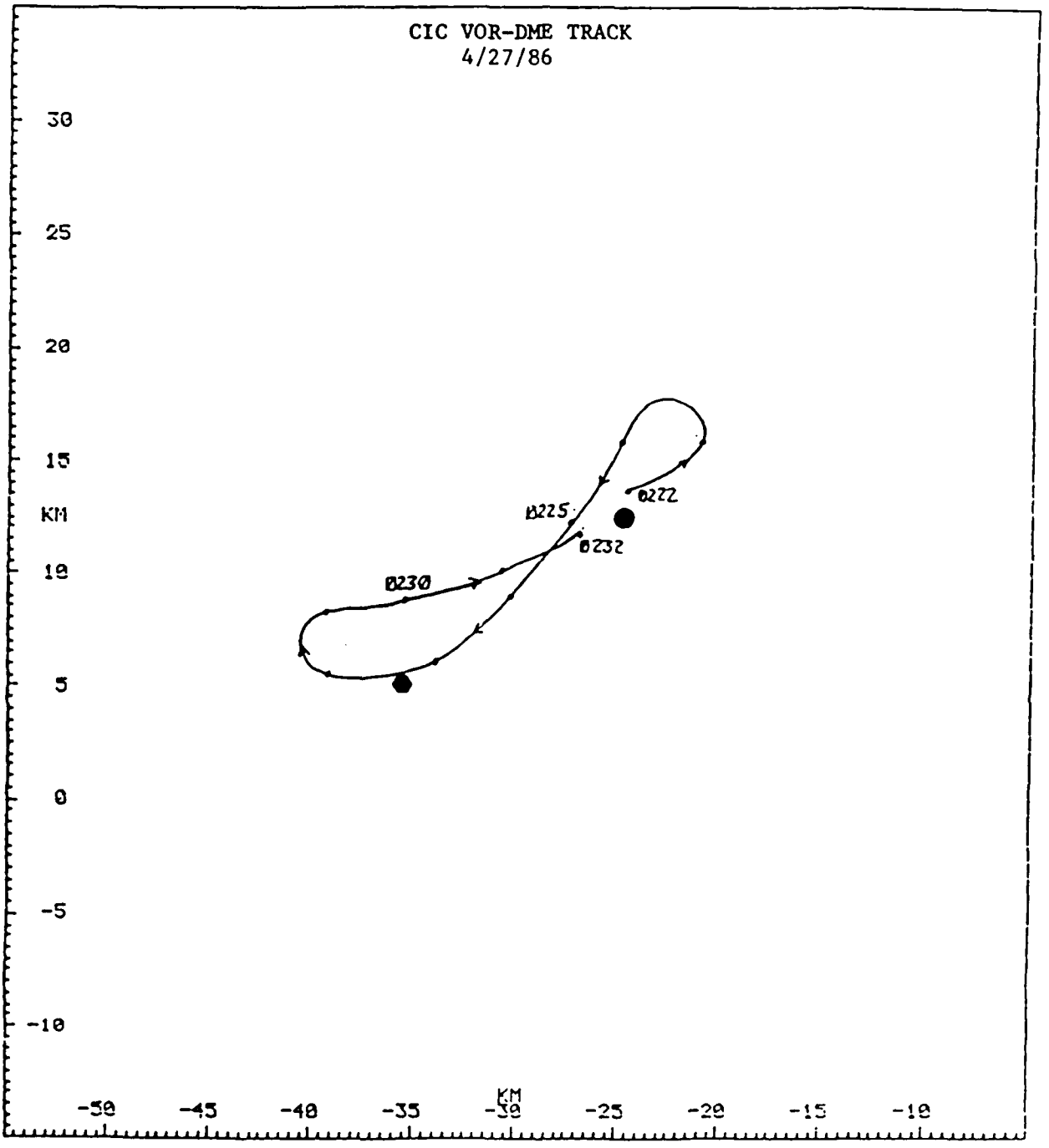
CIC VOR-DME TRACK
4/27/86
30
25
20
15
KM
10
5
0
-5
-10
-50
-45
-40
-35
-30
-25
-20
-15
-10
KM
0222
0225
0232
0230

## APPENDIX B

## ITEMIZATION OF SOFTWARE DELIVERED TO AFGL

| Program Name | Description |
|---|---|
| AFGL | Reads 9-track tape, prints data listings |
| TAPE | Subroutine to read mag tape from IBM PC |
| AFGL2D | Reads 9-track tape, draws PMS images |
| DRW2D | Subroutine to draw PMS 2d images on Toshiba Printer |
| TRKPL | Plots track from Multi-DME position |
| MLDMT | Computes Multi-DME position |
| MDSR | Subroutine |
| SNSR | Subroutine |
| CPMS | Performs artifact rejection of PMS images and computes liquid water content, equivalent dBZ and other statistics (written for HP-1000) |
| TWOD | Assembler subroutine to process image data |
| FFT | Performs spectral analysis of selected parameters, including de-trending, tapering, power spectra, coherence and phase (written for the HP-1000) |

END

DATE

FILMED

MARCH

1988

DTIC